Contrast Media Research Symposium 2022

Akif, R.; Dekkers, I.; Molen, A.J. van der

Molecular Imaging and Biology (2022) 24 (Suppl 1):S1–S61
https://doi.org/10.1007/s11307-022-01785-3

ABSTRACTS

Contrast Media Research Symposium 2022

Published online: 29 November 2022

Date: August 21st-25th, 2022

Location: Annapolis, Maryland

Sponsorship: Publication of this supplement was sponsored by the World Molecular Imaging Society. All content was reviewed and selected by the CMR Review Committee, which held full responsibility for the abstract selections.

001-Prevention of Post-contrast Acute Kidney Injury in Patients with Advanced Kidney Disease

Raman Akif, Ilona Dekkers, Aart J. van der Molen

Leiden University Medical Center, Leiden, The Netherlands

Background

Post-contrast acute kidney injury (PC-AKI) guidelines have relied on expert opinion and (sub)analyses conducted in large studies with patients with an estimated glomerular filtration rate (eGFR) > 30 m^{l}/min/1.73m^2. To contribute to the advancement of more appropriate, patient-centered decision-making in the field of PC-AKI prevention, our study provides an evaluation of the implementation of PC-AKI guidelines in patients with severely decreased renal function or renal failure (*i.e.*, an eGFR 15–29 mL/min/1.73m^2 and < 1 5 mL/min/1.73m^2, respectively). We intended to assess the degree of protocol adherence in cases of IV contrast medium (CM) administration in CT based on quality indicators as described in the Dutch PC-AKI guidelines.

Methods and Materials

A single-center observational cohort study was conducted. Primary analysis evaluated protocol adherence outcomes related to contrast administration such as per-protocol kidney function assessment (KFA), adherence to hydration protocols, and the incidence of PC-AKI, defined as an increase in serum creatinine (sCr) of 25% or an absolute increase >0.5 mg/dL related to contrast administration. All included cases and related variables were verified by manual case review. A combination of propensity score matching and conditional logistic regression was used to evaluate the efficacy of hydration in the prevention of PC-AKI.

Results

Seven hundred thirteen CT-scans from 500 patients were included for primary analysis regarding protocol adherence. Measures in the period preceding CM administration (*i.e.*, pre-contrast KFA and intravenous volume expansion on the day of CM administration) largely adhered to guideline recommendations. Among 713 cases, 556 (78%) received intravenous hydration on the day of contrast administration, of which 347 cases involved hydration with 250ml sodium bicarbonate 1.4% (70% of hydrated cases). Notably, evaluation of post-contrast KFA revealed a significant difference in adherence between the outpatient and inpatient cohort (34% (N = 64 / 190) versus 94% (N = 355 / 377), respectively [P = <0.001]). Of the 27/117 cases in which PC-AKI was deemed related to CM administration, only one involved an outpatient as opposed to 26 inpatients (P = 0.010).

Conclusions

We showed a strict adherence to aspects related to the period prior to CM administration in contrast to KFA 2–7 days after CM. The incidence of PC-AKI further suggests that sCr is not an adequately specific indicator of PC-AKI in this patient population. A critical shift similar to that of PC-AKI in patients with GFR >30 ml/min/1.73m2 might be inevitable in response to our growing understanding in patients with advanced kidney injury.

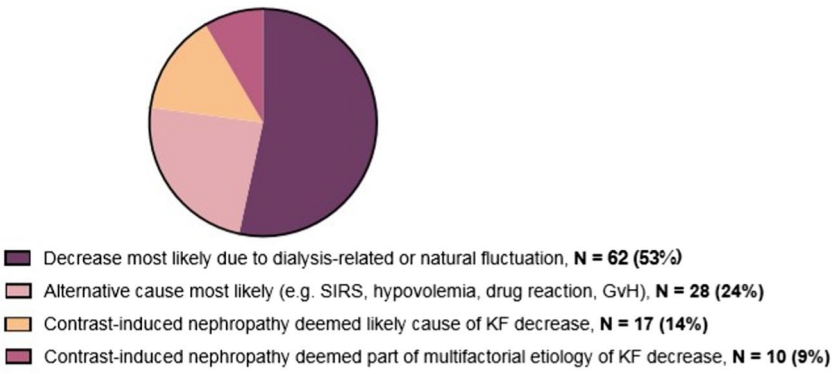

Figure 1. *Further analysis of cases deemed potential PC-AKI based on Serum Creatinine criteria.*
No. of included cases = 117. SIRS = systemic inflammatory response syndrome, GvH = graft-versus-host, KF = kidney function.

Declarations

Conflict of Interest

The authors declare no competing interests.

002- Enzymatic Activity Monitoring Through Dynamic Nuclear Polarization in the Earth Magnetic Field, the PRIMOGAIA Project

Elodie Parzy[1], Dahmane Boudries[1], Samuel Jacoutot[2], Muriel Albalat[3], Nicolas Vanthuyne[3], Jean-Michel Franconi[1], Philippe Mellet[1], Eric Thiaudiere[1], Gérard Audran[2], Sylvain R.A. Marque[2], Philippe Massot[1], Robert N. Muller[4], Sarah Garifo[4], Dimitri Stanicki[4], Sophie Laurent[4,5]

[1]University of Bordeaux-CNRS Bordeaux, France
[2]Aix Marseille Univ, CNRS, Marseille, France
[3]Aix Marseille University, CNRS, Marseille, France
[4]University of Mons, Mons, Belgium
[5]Center for Microscopy and Molecular Imaging (CMMI), Gosselies, Belgium

Background

Cost-effective and portable MRI systems operating at Earth-field would be helpful in poorly accessible areas or in developing nations. Furthermore, Earth-field MRI can provide new contrasts opening the way to the observation of pathologies at the biochemical level. However, low-field MRI suffers from a dramatic lack in detection sensitivity even worsened for molecular imaging purposes where biochemical specificity requires detection of dilute compounds. In a preliminary approach, it is proposed here to detect protease-driven hydrolysis of a nitroxide probe through electron-nucleus Overhauser enhancement in a home-made double resonance system at earth-field. Besides, another system based on nitroxides grafted on targeted nanosystems is also proposed to afford specific detection.

Methods and Materials

The nitroxide probe is a six-line nitroxide which lines are shifted according to its substrate/product state, upon catalysis by Neutrophil Elastase (1). Related to the other system, the three-line nitroxide grafted on nanoparticles is a permanent signal to set with specificity. Quantum mechanical calculations were carried out to predict EPR line frequencies and Overhauser enhancements at Earth field (43 μT). The NMR system is equipped with a 13-mT prepolarization coil, a 153-MHz EPR coil and a 2-kHz NMR coil.

Results

Theoretical calculations predicted the occurrence of 20 EPR lines. Either prepolarized NMR or DNP-NMR without prepolarization provided NMR spectra within 3 min. The frequency dependence of Overhauser enhancement (around 150 and −150 at 149 MHz and 153 MHz, respectively for 1.2

mM nitroxide in water) was in agreement with theoretical calculations. Protease-mediated catalysis of the nitroxide probe was measured through Overhauser effect with 5 min time resolution. As a result of preliminary characterizations, nitroxide-based systems were more appropriate than the first initial system with intrinsic capabilities (*e.g.*, nanodiamonds) and showed promising efficiency since nitroxides are associated to convenient electronic-nucleus coupling factor.

Conclusions

Nitroxide conversion though proteolysis was observable within minutes using DNP-enhanced NMR at earth field, paving the way of molecular imaging in cost-effective systems.

References

1. Jugniot N., Duttagupta I., Rivot A., Massot P., Cardiet C., Pizzoccaro A., Jean M., Vanthuyne N., Franconi J.M., Voisin P., Devouassoux G., Parzy E., Thiaudiere E., Marque S.R.A., Bentaher A., Audran G., Mellet P. An elastase activity reporter for Electronic Paramagnetic Resonance (EPR) and Overhauser-enhanced Magnetic Resonance Imaging (OMRI) as a line-shifting nitroxide. Free Radic. Biol. Med.126 (2018) 101-112. https://doi.org/10.1016/j.freeradbiomed.2018.08.006

Declarations

Conflict of Interest

The authors declare no competing interests.

003- Prostate-Specific Membrane Antigen Targeted Gold Nanoparticles for PCa Radiotherapy and MR Imaging

Dong Luo[1], Xinning Wang[1], Sophia Zeng[1], Gopalakrishnan Ramamurthy1, Clemens Burda[1], Thomas J. Meade[2], James P. Basilion[1]

[1]Case Western Reserve University, Cleveland, OH, USA
[2]Northwestern University, Evanston, IL, USA

Background

X-Rays were first discovered in 1896 by Dr. Roentgen and were first tried as a cancer therapy shortly after in 1899 and remain a main component of the radiotherapeutic approaches to treat prostate cancer. Although radiosensitizers have been developed to increase the efficacy of radiotherapy, no radiosensitizer has been developed to selectively target prostate cancer. The purpose of this work is to develop a prostate cancer selective radiosensitizer to improve radiotherapy of prostate cancer.

Methods and Materials

Gold is a strong absorber of X-ray radiation and can be used to amplify the therapeutic efficacy of X-ray therapy. Here we have targeted gold-nanoparticles (AuNPs) and gold nanoclusters (AuNCs) and utilized them to sensitize tissues to X-ray therapy. For the first time, we systematically investigate both AuNP size and a new targeting ligand on cell uptake, tumor targeting and radiotherapy efficacy. AuNPs and AuNCs were conjugated with a ligand highly selective for prostate specific membrane antigen (PSMA) and their uptake and ability to increase radiosensitivity measured both *in vitro* and *in vivo*. AuNPs ranging in size from 2-19 nm core diameter and AuNCs (1.7 nm diameter) were investigated. Additonally, we have chelated Gd(III) to the PSMA-targeted AuNP/NC enabling their dual use as MR contrast agents and radiosensitizers.

Results

With increasing AuNP size, the total amount of gold internalized was slightly improved. However, enhancement of radiotherapy was significantly more pronounced by internalization of smaller PSMA targeted-AuNPs. The smaller AuNPs that were targeted with PSMA-1 also showed a high degree of selectivity for tumors that overexpressed the PSMA receptor. Interestingly, the AuNPs showed significant uptake and clearance through the RES and liver while the much smaller AuNCs showed primarily renal clearance with much less RES excretion, but still remained effective as radiosensitizers. By conjugating Gd(III)complexes and prostate-specific membrane antigen (PSMA) targeting ligands to AuNP surfaces, we found enhanced uptake of AuNPs by PSMA-expressing cancer cells with excellent MR contrast and radiation therapy outcome *in vitro* and *in vivo*. The AuNPs binding affinity and r1 relaxivity were dramatically improved and the combination of Au and Gd(III) provided better tumor suppression after radiation.

Conclusions

These data suggest that small targeted AuNPs may be more effective radiosensitizers and serve as MR contrast agents allowing for MR-LINAC approaches to be more precise. Further reduction of the size of the nanoparticles, *i.e.*, gold nanoclusters, significantly altered their excretion profile. The more rapid excretion of the AuNCs may serve to reduce off target radiosensitivity and also, due to reduced gold deposition in non-targeted tissues, a reduction in elemental gold toxicity.

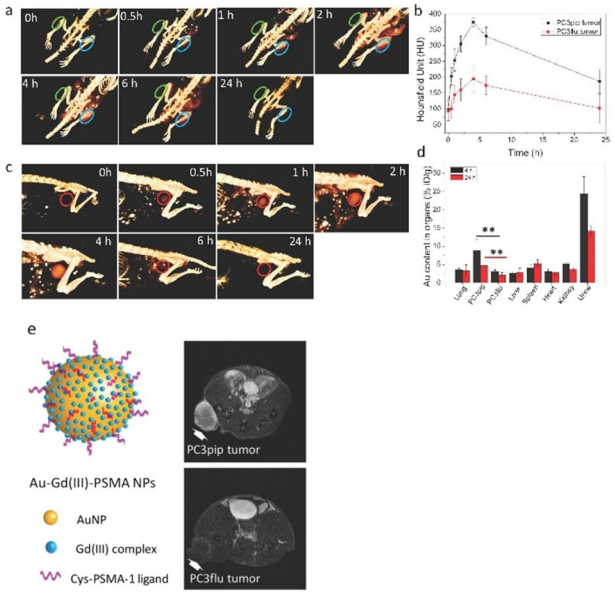

Figure caption: Tumor uptake and biodistribution of PSMA-targeted AuNCs. a *In vivo* 3D CT images of the PSMA-expressing PC3pip (right, blue) and PSMA-negative PC3flu (left, green) tumor-bearing mice (indicated by blue and green ovals) before and at 0.5 h, 1 h, 2 h, 4 h, 6

Declarations

Conflict of Interest

The authors declare no competing interests.

004- Detecting Zinc in Biological Samples with Hyperpolarized 15N MRS

Eul Hyun Suh[1], Jae Mo Park[1], Lloyd Lumata[2], A. Dean Sherry[1,2], Zoltan Kovacs[1*]

[1]University of Texas Southwestern Medical Center, Dallas, TX, USA
[2]University of Texas at Dallas, Richardson, TX, USA

Background

The 15N nucleus has several favorable properties for hyperpolarized (HP) NMR studies including narrow linewidths, relatively long T1 values, and a much larger chemical shift range compared to 13C. HP-15N labeled compounds are particularly well suited for the design of newer types of sensors. Zn2+ is an important target for imaging because it participates in various biochemical processes. The tripodal ligand tris(2-pyridylmethyl)amine (TPA) has excellent selectivity for Zn2+ over other common biological cations. The goal of this project was to develop hyperpolarized 15N probes based on TPA to monitor tissue Zn2+ levels [1].

Methods and Materials

15N-labeled and 15N labeled, deuterated TPA derivatives were synthesized using standard organic reactions. The 15N probes were hyperpolarized by microwave driven dynamic nuclear polarization (DNP) using a HyperSense commercial polarizer [2]. 15N NMR spectroscopy and chemical shift imaging (CSI) were performed at 9.4 T on an Agilent (Varian) vertical bore microimager.

Results

The 15N labeled, deuterated version of TPA (15N-TPA-d6) was synthesized in 4 steps starting from 15N-ammonium acetate and chloromethyl-d2 pyridine with an overall yield of 61%. The TPA derivatives polarized well under standard DNP conditions with OX063 trityl radical to a level of 6–8%. The 15N spin-lattice (T1) relaxation time of the label was calculated from the decay of the hyperpolarized magnetization and was found to be 26 s for 15N-TPA and 71 s for 15N-TPA-d6 at 9.4 T. Large upfield shift (20 ppm) in the 15N resonance of the central 15N atom was observed upon binding to Zn2+ ion. Hyperpolarized [15N-]TPA-d6 was tested as a Zn2+ sensor in human prostate epithelial (PNT1A) cells and human benign prostate hyperplasia (BPH) homogenates freshly prepared from biopsy samples. ICP-MS measurements of the Zn-concentration verified that HP-[15N]-TPA-d6 could accurately report Zn2+ levels in these biological samples. The feasibility of 15N spectroscopic imaging of Zn2+ was demonstrated in phantoms containing HP-[15N]-TPA-d6 in the absence and presence of Zn2+.

Conclusions

15N labeled TPA displays a large chemical shift change upon Zn2+-binding. The deuterated, 15N labeled ligand has favorable properties as a hyperpolarized 15N zinc sensor including long T1 value and sharp 15N resonance. HP-[15N]-TPA-d6 can detect Zn2+ in the low micromolar range with no interference from protons or other endogenous metal ions. The probe was successfully used to detect and quantify free Zn-levels in human prostate tissue homogenate and intact human prostate epithelial cells.

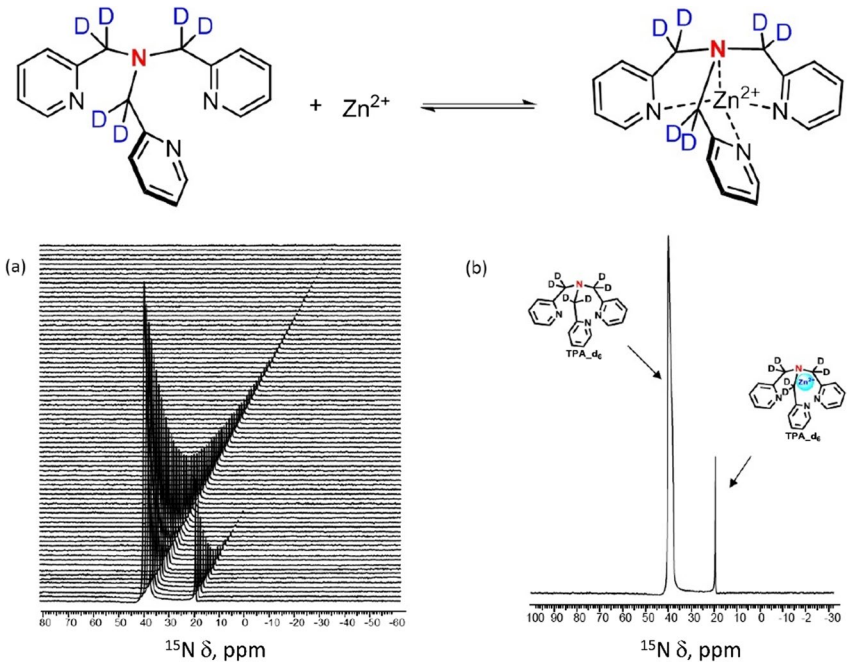

Figure caption: Zn-detection with HP-15N-TPA-d6 in a tissue sample; (a) decay of 15N signal; (b) the first spectrum.

References

1. Suh EH, Park JM, Lumata L, Sherry AD, Kovacs Z. Hyperpolarized 15N-labeled, deuterated tris(2-pyridylmethyl)amine as an MRI sensor of freely available Zn2+ in tissues. Communications Chemistry (Nature) 2020; 3; 185.
2. Ardenkjaer-Larsen JH, Fridlund F, Andreas Gram A, Hansson G, Hansson L, Lerche MH, Servin R, Thaning M,. Golman K. Increase in signal-to-noise ratio of > 10,000 times in liquid-state NMR. Proc Natl Acad Sci U S A 2003; 100; 10158-10163.

Declarations

Conflict of Interest

The authors declare no competing interests.

005- PEGylated Magnetic Nanoparticles as a Theranostic Agent

Indiana Ternad[1], Dimitri Stanicki[1], Thomas Vangijzegem[1], Sebastien Penninckx[3], Robert Muller[1,2], Stephane Lucas[3], Sophie Laurent[1,2]

[1]University of Mons (UMONS), Mons, Belgium

[2]Center for Microscopy and Molecular Imaging (CMMI), Gosselies, Belgium

[3]Namur Research Institute for Life sciences (NARILIS), University of Namur, Namur, Belgium

Background

Since 2004, there has been growing interest in high-Z nanoparticles (NPs) as radiosensitizing compounds. Up to now, reports have highlighted the ability of these nanoparticles to increase tumor cell death upon irradiation, improving thus, the radiation treatment efficiency. Despite some extensive studies led in the field (especially focused on golds NPs (GNPs)), the mechanism(s) responsible for the radiosensitization effect of GNPs remains poorly understood, and mainly focused on physical effects. Recent studies suggest the central role of some biochemical mechanisms on the observed radiosensitizing effect [1]. A significant correlation has been made between the inhibition of the detoxification enzyme in GNP-treated cells and the magnitude of radiosensitizing effect [2]. In view of these elements, we were interested to study if such inhibition behavior could be demonstrated for other kind of NPs. Because of their biocompatibility and superparamagnetic properties, iron oxide nanoparticles (IONPs) were selected.

Methods and Materials

Inhibition of the thioredoxin reductase enzyme (TrxR) by IONPs was assessed by measuring its activity as previously

described [2] (with a commercial kit). For this purpose, the lung carcinoma cell line (A549) was incubated without and with PEGylated IONPs for 24h at 50 µg Fe/mL. Cells were irradiated with 225kV X-rays at a dose rate of 2 Gy/min (X-Rad 225 XL, PXi Precision x-ray, USA). Longitudinal relaxation rates (R1) of the previously synthesized PEGylated IONPs were extracted from the Nuclear Magnetic Dispersion (NMRD) profiles carried out with a field cycling relaxometer (STELAR, Italy). MR images of phantom and mice were acquired in a Biospec 9,4T (Bruker, Germany). IONPs were intravenously injected at 70 µmoles Fe/Kg in CD1 mice.

Results

Superparamagnetic properties of PEGylated iron oxide nanoparticles were evaluated by recording relaxometric parameters and phantom MR images. *In vivo* magnetic resonance imaging (MRI) experiments demonstrated circulation times exceed 7 hours by observing the signal of the cardiac left ventricle. A549 cells preincubated with IONPs showed a 26% inhibition of TrxR activity. To attest that such inhibition can give rise to a radiosensitizing effect, A549 cells were irradiated with X-ray beam. IONPs showed a radiosensitizing effect at 2 Gy to induce a 12% increase in cell death in IONPs treated cells compared to untreated cells.

Conclusions

To conclude, the radiosensitizing properties of IONPs and their detection by MRI were demonstrated. These elements make them good candidates as a theranostic agents.

References

1. S. Penninckx, et.al. « Gold Nanoparticles as a Potent Radiosensitizer: A Transdisciplinary Approach from Physics to Patient ». Cancers 12, 2020: 2021.
2. S. Penninckx et al.« Thioredoxin Reductase Activity Predicts Gold Nanoparticle Radiosensitization Effect ». Nanomaterials 9, 2 : 295.

Declarations

Conflict of Interest

The authors declare no competing interests.

006-Near Infrared Photoimmunothrapy of Cancer: Targeting Immune Suppressor Cells for Enhancing Immunity

Hisataka Kobayashi

Molecular Imaging Branch, NCI/NIH, Bethesda, USA

Background

Near-infrared (NIR) photoimmunotherapy (NIR-PIT) is a new cancer therapy, which utilizes a monoclonal antibody-photoabsorber, IRDye700DX (IR700), conjugate (APC) and NIR light to kill cancer cells. After APC is injected intravenously, NIR light exposure causes photo-induced ligand release reactions in IR700, resulting in cell membrane disruption and selective immunogenic cell death on APC-bound cancer cells with minimal damage to surrounding normal tissues (1). A fast-tracked global phase III clinical trial of NIR-PIT using cetuximab-IR700 (ASP-1929) targeting epidermal growth factor receptor (EGFR) in patients with inoperable and recurrent head and neck cancer began in 2019 (https://clinicaltrials.gov/ct2/show/NCT03769506) and the first clinical use of NIR-PIT was approved in Japan in September 2020. Together with cancer cell killing, immune suppressor cells can be simultaneously targeted with NIR-PIT to further enhance host immune response (2).

Methods and Materials

By employing CD25, CTLA-4, and VISTA as targets for regulatory T cell (Treg), Treg/myeloid derived suppressor cell (MDSC), and MDSC, respectively, we synthesized APCs using respective monoclonal antibodies. Then immune suppressive cell-targeted NIR-PIT studies with or without combining cancer-targeting NIR-PIT were performed in syngeneic mouse models with MC38, LL2, MOC1, and MOC2 tumors. Accumulation of APC was monitored with IR700 fluorescence imaging.

Results

All three APCs accumulated in tumor beds that validated with IR700 fluorescence imaging. With a single immune suppressive cell-targeted NIR-PIT, 0-30% of mice showed complete response (CR) by targeting CD25, 40–80% of mice showed CR by targeting CTLA-4, and no mouse showed CR by targeting VISTA. However, when combined with cancer targeting NIR-PIT against CD44 or EGFR, CR rate of CD25 targeting NIR-PIT increased to 40–87%, and that of VISTA targeting NIR-PIT increased to 40%. Once NIR-PIT treated mice cured tumors completely, all mice rejected the growth of the same tumor cells, even when 5,000,000 tumor cells were re-injected. When CTLA4 targeting NIR-PIT combined with CD44 targeting NIR-PIT in four MC38 tumor bearing mice, treatment of a single tumor resulted in CR of all four tumors in 60% of mice after a single NIR-PIT.

Conclusions

Immune suppressive cell-targeted NIR-PIT enhanced anti-tumor host immunity. When immune suppressive cell-targeted NIR-PIT combined with cancer-targeted NIR-PIT, large proportions of mice completely cured with a single treatment and acquired long term immunity against cured cancer cells.

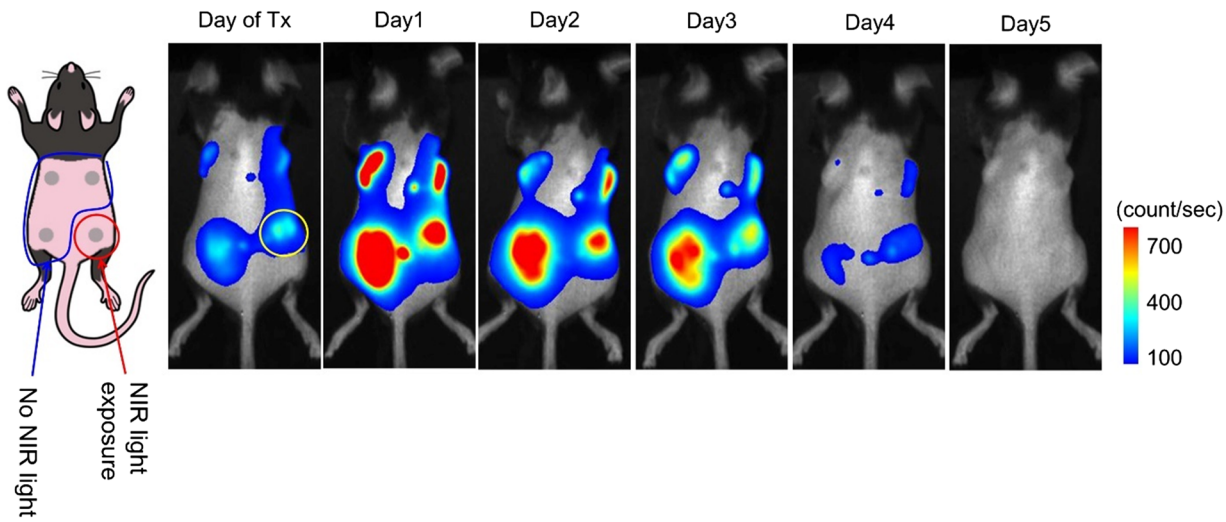

Fig. 1 Serial bioluminescence images of four MC38 bearing mice treated with combination of CD44-targeting NIR-PIT with CTLA4-targeting NIR-PIT are shown. After a single tumor was treated with NIR-PIT, all tumors decreased in size and disappeared on Day 5

References

1. Mitsunaga M, Ogawa M, Kosaka N, Rosenburm LT, Choyke PL, Kobayashi H. Cancer Cell-Selective *In Vivo* Near Infrared Photoimmunotherapy Targeting Specific Membrane Molecules. Nature Medicine 2011; 17: 1685-1691.
2. Kobayashi H, Choyke PL. Near infrared photoimmunotherapy of cancer. Accounts of Chemical Research 2019; 52: 2332-2339.

Declarations

Conflict of Interest

The author declares no competing interests.

007-Oligo(ethylene glycol) Bisphosphonate Dendrons in Fluorocarbon-Stabilized Biomedical Microbubbles

Da Shi[1], Justine Wallyn[1], Benjamin Ayela[2], Delphine Felder-Flesch[2], Marie Pierre Krafft[1]

[1]Institut Charles Sadron (CNRS), University of Strasbourg, Strasbourg, France [2]SUPERBRANCHE, Strasbourg, France

Background

Microbubbles (MBs) focus marked interest in biomedical imaging and therapy. In combination with ultrasound technologies, MBs are used in the clinic for cardiovascular imaging and early detection of cancer. Other applications of MBs under preclinical and clinical evaluation concern molecular and multimodal imaging, cell therapies, treatment of neurodegenerative diseases and potentiation of oxygen-dependent cancer therapies [1]. Phospholipid-shelled MBs are typically stabilized by a perfluorocarbon gas. It is notable that the formulation of the MB shells has hardly changed for decades. There is a shortage of well-defined, biocompatible and versatile amphiphilic shell components for multifunctional MB design [1]. Our current efforts focus on exploring the benefits of newly developed oligo(ethylene glycol) bisphosphonate dendrons in MB formulations [2,3]. The dendrons were shown to increase the colloidal stability and bioavailability of iron oxide nanoparticles [4]. Such dendronized Iron oxide nanoparticles (DIONPs) can be effectively encapsulated within phospholipid MB shells [5].

Methods and Materials

The MBs were generated with a Vialmix shaker and characterized by optical microscopy, static light scattering, and an acoustic attenuation method. The morphology and structure of the MB shell were assessed by electron microscopy and atomic force microscopy. The magnetism of the hybrid nanoparticle-containing MBs was investigated by relaxometry.

Results

Grafting fluorinated moieties (CF3, C2F5, or C4F9) at the end of OEG chains was found to accelerate the diffusion of the dendrons to the air/water interface and to enhance Gibbs film formation. This was assigned to potent fluorine-fluorine interactions with the MB's inner

perfluorohexane gas, thus facilitating MB formation. The newly developed oligo(ethylene glycol) bisphosphonate dendrons proved miscible with the MB phospholipid shells. Gibbs film kinetic adsorption studies also demonstrated that the perfluorohexane MB core strongly enhances the adsorption of the DIONPs at the gas/water interface. Small (1-2 μm in radius) and stable (half-life 5-10 h) MBs were obtained. The adsorption of DIONPs was supported by atomic force microscopy, which showed their incorporation in the phospholipid shell. The magnetism of the embedded IONPs remained unchanged, as demonstrated by relaxometry.

Conclusions

Based on their numerous assets (biocompatibility, bioavailability profile, versatility for grafting targeting ligands or bioactive molecules), oligo(ethylene glycol) bisphosphonate dendrons constitute promising candidates for the development of functional MBs for multimodal (ultrasound, MR or magnetic particle) imaging.

References

1. Krafft, M.P.; Riess, J.G. Therapeutic oxygen delivery by perfluorocarbon-based colloids. Adv. Colloid Interface Sci. 2021, in press.
2. Nguyen, D.-V.; Hugoni, L.; Filippi, M.; Perton, F.; Shi, D.; Voirin, E.; Power, L.; Cotin, G.; Krafft, M.P.; Scherberich, A., et al. Mastering bioactive coatings of metal oxide nanoparticles and surfaces through phosphonate dendrons. New J. Chem. 2020, 44, 3206-3214.
3. Shi, D.; Nguyen, D.-V.; Maaloum, M.; Gallani, J.-L.; Felder-Flesch, D.; Krafft, M.P. Interfacial behavior of oligo(ethylene glycol) dendrons spread alone and in combination with a phospholipid as Langmuir monolayers at the air/water interface. Molecules 2019, 24, 4114.
4. Parat, A.; Bordeianu, C.; Dib, H.; Garofalo, A.; Walter, A.; Bégin-Colin, S.; Felder-Flesch, D. Dendrimer nanoparticle conjugates in nanomedicine. Nanomedicine (Lond.) 2015, 10, 977-992.
5. Shi, D.; Wallyn, J.; Nguyen, D.-V.; Perton, F.; Felder-Flesch, D.; Bégin-Colin, S.; Maaloum, M.; Krafft, M.P. Microbubbles decorated with dendronized magnetic nanoparticles for biomedical imaging. Effective stabilization via fluorous interactions. Beilstein J. Nanotechnol. 2019, 10, 2103-2115.

Declarations

Conflict of Interest

The authors Benjamin Ayela and Delphine Felder-Flesch would like to disclose financial interest in this abstract.

008-A Nephroprotective Iodinated Contrast Agent with Cardioprotective Properties: a Pilot Study

Elizabeth Rowe[1,2], Vernon Rowe[1,2], John Hunter[1,2], Michael R. Gralinski[3], Liomar Neves[3]

[1]Neurrow Pharmaceuticals, Inc, Shawnee, KS, USA
[2]MidAmerica Neuroscience Research Foundation, Shawnee, KS, USA
[3]CorDynamics, Inc., Chicago, IL, USA

Background

Evaluation and treatment of acute ischemic syndromes, in the heart and the brain, require vessel visualization by iodinated X-ray contrast agents. However, these contrast agents can induce injury, in both the kidneys, as they are cleared form the body, and the target organs themselves. Contrast agents are known to be toxic to cardiomyocytes and neurons, and can be associated with encephalopathy in the absence of known target tissue damage. A recent report found 13% of patients undergoing diagnostic coronary angiography had elevated troponin T levels, with the volume of contrast agent used being one of the independent predictors of cardiomyocyte damage. Sulfobutylether beta cyclodextrin (SBECD) added to iohexol (SBECD-iohexol)(CE-iohexol, Ligand Pharmaceuticals) is currently in clinical trials in cardiovascular procedures, to determine its relative renal safety in high risk patients. Preclinical studies showed that SBECD-iohexol reduced contrast-induced acute kidney injury (CI-AKI) in rodent models by blocking apoptosis (1). The current study was undertaken to determine whether SBECD-iohexol is also cardioprotective, in the male rat ischemia-reperfusion model, compared to iohexol alone.

Methods and Materials

After anesthesia, the left coronary artery was ligated for 30 min and the ligation released and reperfusion followed for two hours prior to sacrifice. Groups 1–4 were injected in the tail vein ten minutes prior to ischemia with 1) vehicle; 2) iohexol; 3) SBECD; and 4) SBECD-iohexol. Infarct size, hemodynamics, and serum markers were measured.

Results

An eight-fold increase in serum creatine kinase (CPK) in the iohexol-alone group was observed, compared with no increase in the SBECD-iohexol and other groups. The mean arterial pressure and rate pressure product were depressed in the iohexol-alone group, but not in the SBECD-iohexol group or the control groups. No difference in infarct size or serum creatinine among the groups was observed.

Conclusions

The results of this study suggest that SBECD-iohexol is superior to iohexol alone, for both the preservation of cardiomyocyte integrity, and for preservation of myocardial function in myocardial ischemia. Further studies of this new contrast agent in additional tissues, particularly in neuronal tissue, are warranted. If the current clinical trials of SBECD-iohexol (CE-iohexol, Ligand Pharmaceuticals) are successful and this new contrast agent is approved, it may contribute to improved outcomes, not only in cardiovascular procedures, but also in neurointerventional procedures.

References

1. Rowe ES, Rowe VD, Biswas, S., Mosher, G., Insisienmay, L., Ozias, M.K., Gralinski, M., Hunter, J., Barnett, J., Preclinical studies of a kidney safe iodinated contrast agent. J Neuroimaging 2016;26:511-8.

Declarations

Conflict of Interest

The authors declare no competing interests.

009-Acid, Base, and Autocatalyzed Proton Exchange as an Additional Route to Enhance the Relaxivity of Par

Zsolt Baranyai

Bracco Imaging Spa, Trieste, Italy

Background

GdIII complexes enhance the nuclear relaxation rate of solvent water protons through the modulation of the dipolar interaction between the unpaired electrons of the metal ion and the nuclear spins of protons via three processes: i) outer-sphere—r1os; ii) inner-sphere—r1is; iii) proton exchange reactions between functionalities coordinated to the metal center and the bulk water molecules—r1pr.1,2. Actually, Gd(HP-DO3A) (ProHance®, Bracco Imaging S.p.a, Scheme 1) contains a coordinated -OH moiety that acts as a source of proton exchange enhanced relaxivity, however, at pH values higher than the patho-physiological ones. In order to tune the proton exchange contribution close to the physiological condition, the acid-, base-, and autocatalyzed exchange of -OH proton of GdIII-complexes formed with several HP-DO3A derivative ligands (Scheme 1) have been examined in detail.

Methods and Materials

The protonation constant (logKiH) of the functional groups in GdIII-complexes has been determined by pH-potentiometry and spectrophotometry. Relaxivity values of Gd(HP-DO3A) derivatives were studied as a function of pH and buffer composition by 1H NMR relaxometry at 20 and 400 MHz and 298 K. Relaxation parameters (T1PH, kH, kOH, and kB) characterizing the proton exchange reactions of Gd(HP-DO3A) derivatives were calculated from the relaxivity values obtained in the presence and absence of buffers in the pH range 3.0–12.5.

Results

The proton exchange of -OH proton is acid- and base-catalyzed and, upon comparing different buffer compositions, it was concluded that the proton exchange increases with the decrease of the difference between the protonation constant (logKiH) of the -OH moiety and the considered buffer component. The exchange of the -OH proton can also be autocatalyzed by an appropriate donor group attached to the Gd(HP-DO3A) derivatives. Such an internal catalysis requires the vicinity of the -OH moiety and the donor group acts as a general acid or base in the proton exchange process.

Conclusions

Results reported here indicate that a coordinated donor group with exchangeable proton(s) may have a significant contribution to the relaxivity of GdIII-complexes. When the coordinated hydroxyl functionality is the source of the proton exchange contribution, T1PH is about 50% shorter than the corresponding relaxation time of the coordinated water protons due to the shorter GdIII - H distance. Based on these evidences a new generation of GBCAs can be produced with enhanced relaxometric properties that will allow to tackle the challenges of reduced CA doses without compromising their clinical performance.

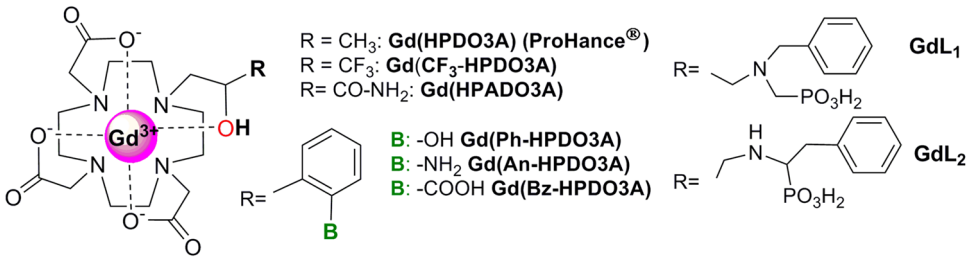

Scheme 1 Structure of the Gd(HP-DO3A) derivatives

References
1. Peters JA., Huskens J., Raber DJ. Lanthanide induced shifts and relaxation rate enhancements. Prog. NMR Spectrosc. 1996, 28, 283-350.
2. Aime S., Barge A., Botta M., Parker D., De Sousa AS., Prototropic vs Whole Water Exchange Contributions to the Solvent Relaxation Enhancement in the Aqueous Solution of a Cationic Gd3+ Macrocyclic Complex. J. Am. Chem. Soc.1997, 119, 4767-4768.

Declarations

Conflict of Interest
The author declares no competing interests.

010-SUPERSPIO®: a Functional Magnetic Platform for Active Tumor Targeting

Benjamin Ayela[1], Geoffrey Cotin[1], Michael Claron[2], Claire Bernhard[2], Jean-Michel Chezal[3,4], Elisabeth Miot-Noirault[3,4], Delphine Felder-Flesch[1*]

[1]Superbranche, Strasbourg, France
[2]ICMUB, Dijon, France
[3]Institut national de la santé et de la recherche médicale (INSERM), Clermont-Ferrand, France
[4]Laboratoire dimagerie moléculaire et thérapie vectorisée, Clermont-Ferrand, France

Background
Designing theranostic nanoparticles (NPs) for molecular diagnosis and targeted therapy is of the utmost importance. The specifications of such systems are numerous: they should selectively home in on the cells and organs of the body that are involved in the disease process, specifically targeting their potent healing effects on these cells and organs, while sparing cells not involved in the disease process. They should be completely non-toxic, biodegradable or capable of natural excretion, not be recognized or eliminated by the body's own immune system before they have reached their target, and not induce any allergic reactions. Ideally, they are generic, *i.e.*, they can be "programmed" to combat a wide variety of diseases by docking onto any target structures one chooses and being capable of carrying any medicines. To improve active tumour targeting and obtain better *in vivo* MR imaging properties, our studies explored the multivalency effect of a dendritic surface functionalization of superparamagnetic iron oxides (SPIOs).1-3

Methods and Materials
SPIOs synthesized by thermal decomposition were coated with COOH or N3-functional oligo(ethylene) glycol dendron to improve colloidal stability, graft chelating agents and specific ligands (Fab HER2+ or a melanocyte targeting ligand (TL)). The size distribution, colloidal stability, and biodistribution properties were studied. Both *in vivo* MR contrast and tumor targeting studies after intravenous injection of SUPERSPIO® were conducted.4

Results
DLS and zeta potential measurements assessed the functionalization of SUPERSPIO® with the different molecules of interest: the changes in hydrodynamic volume were in correlation with the added functionalities and showed the preservation of a monomodal size distribution. Transverse relaxation rates (r2) vary considerably between the samples. Consequently, grafting of Melanocyte TL caused an r2 relaxivity decrease of 30% attributed to the ligand hydrophobicity. Biodistribution studies showed highest tumour uptake at 6h post injection (pi) (3,43 ± 1,06 %ID/g) for SUPERSPIO@MelanocyteTL_177Lu. Renal excretion was evidenced by the increase of bladder signal at 6h pi. At 24h pi, the signal decreased in liver and increased in lungs, emphasizing the probe metabolization or degradation process over time. Considering the ratio tumour /muscle (T/M) uptake, higher values were obtained for SUPERSPIO@MelanocyteTL_177Lu as compared to SUPERSPIO@177Lu, as reflect of *in vivo* targeting.

Conclusions
The unique properties of dendritic structures which can be tuned to reach ideal biodistribution combined to efficient targeting make SUPERSPIO® a versatile construct for the simultaneous presentation of receptor binding ligands or radioactive probes to achieve active targeting of tumor.

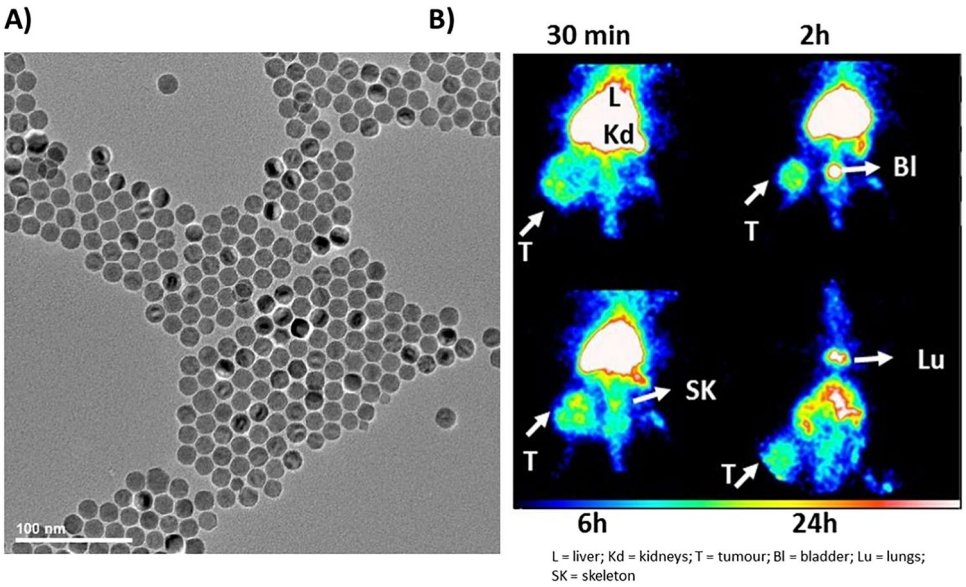

Figure caption: A) Transmission electron microscope (TEM) image of SUPERSPIO®. B) Planar scintigraphy images of B16F0 melanoma bearing nude mice injected with SUPERSPIO@177Lu (top) and SUPERSPIO@ melanineLigand_177Lu (bottom) at various times post intravenous injection.

References

1. Walter A, Garofalo A, Ulhaq C, Lefèvre C, Taleb J, Laurent S, Vander Elst L, Muller RN, Lartigue L, Gazeau F, Billotey C, Felder-Flesch D, Begin-Colin S. Mastering shape and composition to tailor MRI and hyperthermia properties of dendronized iron oxide nanoparticles. Chem. Mater. 2014; 26(18); 5252-5264.
2. Walter A, Garofalo A, Parat A, Taleb J, Bonazza P, Jouhannaud J, Pourroy G, Voirin E, Billotey C, Laurent S, Vander Elst L, Muller RN, Begin-Colin S, Felder-Flesch D. Validation of a dendron concept to tune colloidal stability, MRI relaxivity and bioelimination of functional nanoparticles. J. Mater. Chem. B 2015; 3; 1484-1494.
3. Bordeianu C, Parat A, Affolter-Zbaraszczuk C, Muller RN, Boutry S, Begin-Colin S, Meyer F, Laurent S, Felder-Flesch D. How a grafting anchor tailors unspecific cellular uptake and *in vivo* fate of dendronized iron oxide nanoparticles. J. Mater. Chem. B 2017; 5; 5152-5164.
4. Bordeianu C, Parat A, Piant S, Walter A, Zbaraszczuk-Affolter C, Meyer F, Begin-Colin S, Boutry S, Muller RN, Jouberton E, Chezal JM, Labeille B, Cinotti E, Perrot JL, Miot-Noirault E, Laurent S, Felder-Flesch D. Evaluation of the active targeting of melanin granules after intravenous injection of dendronized nanoparticles. Molecular pharmaceutics 2018; 15; 536-547.

Declarations

Conflict of Interest

The authors Benjamin Ayela, Geoffrey Cotin, and Delphine Felder-Flesch would like to disclose financial interest in this abstract.

011- Nanobubbles for Contrast Enhanced Ultrasound Imaging of Prostate Cancer in a Large Animal Model

Agata Exner[1], Eric Abenojar[1], Jinning Wang[1], Sid Tavri[1], Andy Milkowski[2], James Basilion[1]

[1]Case Western Reserve University, Cleveland, OH, USA
[2]Ultrasound Division, Siemens Healthcare, Issaquah, WA, USA

Background

The long-term goal of our work is to develop a nanoscale ultrasound contrast agent (nanobubble, NB) targeted to the prostate specific membrane receptor (PSMA) for improved delineation of prostate tumors. Prostate biopsies are routinely performed using transrectal ultrasound guidance for prostate gland orientation. However, targeting of the biopsy using ultrasound to sample specific regions of interest has not improved the sensitivity or specificity of disease detection. Parametric dynamic contrast enhanced ultrasound (CEUS) has the potential to improve delineation of suspect lesions in the prostate, but neither standard nor targeted microbubbles used in this application have improved outcomes. Herein we describe CEUS imaging orthotopic human prostate cancer in rabbits using PSMA-targeted NBs.

Methods and Materials

Tumors were initiated in New Zealand White rabbits (6–12 months old) immunosuppressed with cyclosporine, using PC3pip human prostate cancer cells (modified to express PSMA). C3F8 PSMA-NBs were prepared, as previously described1. Lumason® microbubbles (MBs) were used for comparison. Nonlinear CEUS and B-mode scans were acquired weekly using a clinical US with custom research protocol (Siemens Acuson S3000, 18 MHz, CPS at 8 MHz, 0.1 MIF, and 1 fps). To confirm tumor location, magnetic resonance imaging (MRI) scans were performed (Siemens Magnetom Vida 3T). Normalized time intensity curves (TIC) were determined for selected regions of interest, and were used to extract the prostate to tumor ratios. Parametric map analysis of CEUS signals was performed using the Siemens Contrast Dynamics software.

Results

PSMA-NBs showed extended enhancement and delayed washout in tumors compared to normal prostate (Fig. 1A–B). Tumor enhancement with Lumason (Fig. 1C-D) showed typical kinetics, with washout after ~2 min. At week 3–5 of tumor growth, significantly higher signal was observed in the tumor compared to the prostate for PSMA-NBs at 300-500 s post NB injection, with a maximum CTR (contrast to tissue ratio) of 4.8 at 400 s at week 3. At 5 weeks parametric maps of the peak intensity show clearer delineation of tumor using NBs, as compared to histology.

Conclusions

We have shown that PSMA-NBs improve the CTR of prostate tumors within a background of normal prostate. The progression can be eventually be used for real-time guidance of prostate biopsies using transrectal CEUS.

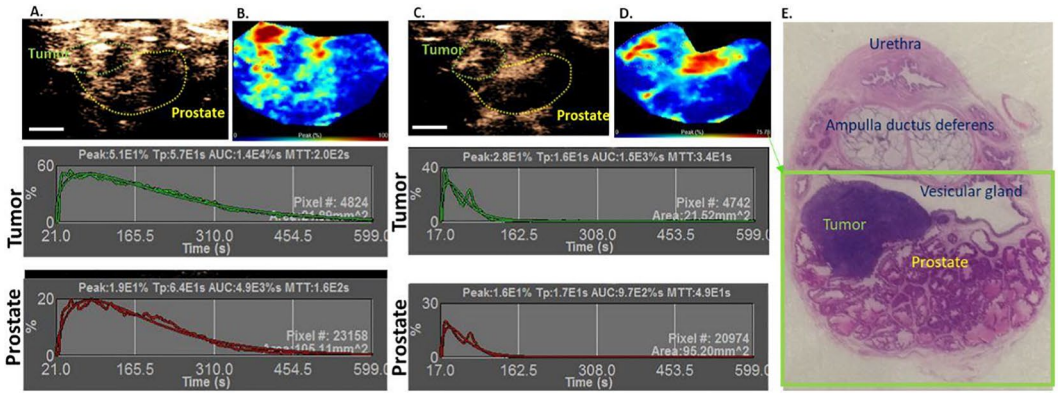

Figure 1: Representative nonlinear contrast images, time intensity curves and parametric maps of normalized peak intensity shown for PSMA-NB (A, B) and Lumason (C, D) in rabbit tumor at week 5 after cell injection. Histology of the same tumor is shown in panel (E). Green box delineates area shown on US images.

References

1. Perera RH, Wang X, Wang Y, Ramamurthy G, Peiris P, Abenojar E, Basilion JP, Exner AA. Real time ultrasound molecular imaging of prostate cancer with PSMA-targeted nanobubbles. Nanomedicine: Nanotechnology, Biology and Medicine. 2020 1;28:102213.

Declarations

Conflict of Interest

The authors declare no competing interests.

012-Pass the Aspirin: Self-assembled Nanotheranostics for CEST MRI, Raman Imaging, and Cancer Therapy

Yue Yuan[1], Piyush Raj[2], Soumik Siddhanta[2], Jia Zhang[1,3], Guanshu Liu[1,3], Ishan Barman[2], Michael T. McMahon[1,3], Jeff W.M. Bulte[1,3]

[1]Institute for Cell Engineering, the Johns Hopkins University School of Medicine, Baltimore, USA
[2]Hopkins University Whiting School of Engineering, Baltimore, USA

[3]F.M. Kirby Center, Hugo W. Moser Institute, Kennedy Krieger Inc., Baltimore, MD, USA

Background

Overall, the field of cancer nanotheranostics has seen few clinical applications due to unfavorable pharmacokinetic profiles and non-specific biodistribution. Our objective was to achieve tumor-selective uptake of theranostic nanoparticles by rational design of a small molecular probe that undergoes a tumor-specific enzymatic reaction, resulting in the formation of nanoparticles which cannot be pumped out of the cell. We have chosen olsalazine (Olsa), a clinically used aspirin-derivative and broad-spectrum anti-cancer agent as small molecule, as it can be detected by chemical exchange saturation transfer (CEST) MRI [1] and Raman imaging (RI) [2].

Methods and Materials

Olsa was conjugated to 2-cyano-6-aminobenzothiazole and the cell-penetrating peptide RVRR, a substrate specific for the tumor-overexpressed enzyme furin. Following cleavage by furin in the presence of glutathione, Olsa self-assembles into nanoparticles (Olsa-NPs) (Fig. 1a,b). HCT116 and LoVo cells were used as high and low furin-expressing colon cancer cells, respectively. Tumor-carrying NU/J nude mice were subjected to 11.7T MRI and Raman imaging after intravenous injection of 0.2 mmol/kg Olsa-RVRR or Olsa alone as control.

Results

In vivo studies using HCT116 and LoVo murine xenografts showed that the OlsaCEST signal and anti-tumor therapeutic effect were 6.5-fold and 5.2-fold increased, respectively, compared to olsalazine without RVRR. (Fig 1c), with an excellent "theranostic correlation" (R^2=0.97) between the imaging signal and therapeutic response (normalized tumor size). The tumor-catalyzed olsalazine nano-assemblies could also be detected with high specificity by RI with a distinct scattering signature *in vitro* and *in vivo* (Fig. 1d).

Conclusions

Reduced effusion and prolonged retention of Olsa-NPs enabled their use as a specific multimodal CEST MRI/RI theranostic contrast agent. These two imaging modalities are complementary: CEST MRI can be performed first to determine gross tumor localization and Olsa drug uptake, followed by RI during image-guided surgery to precisely delineate tumor margins during and after resection in real-time, which is not possible with CEST MRI.

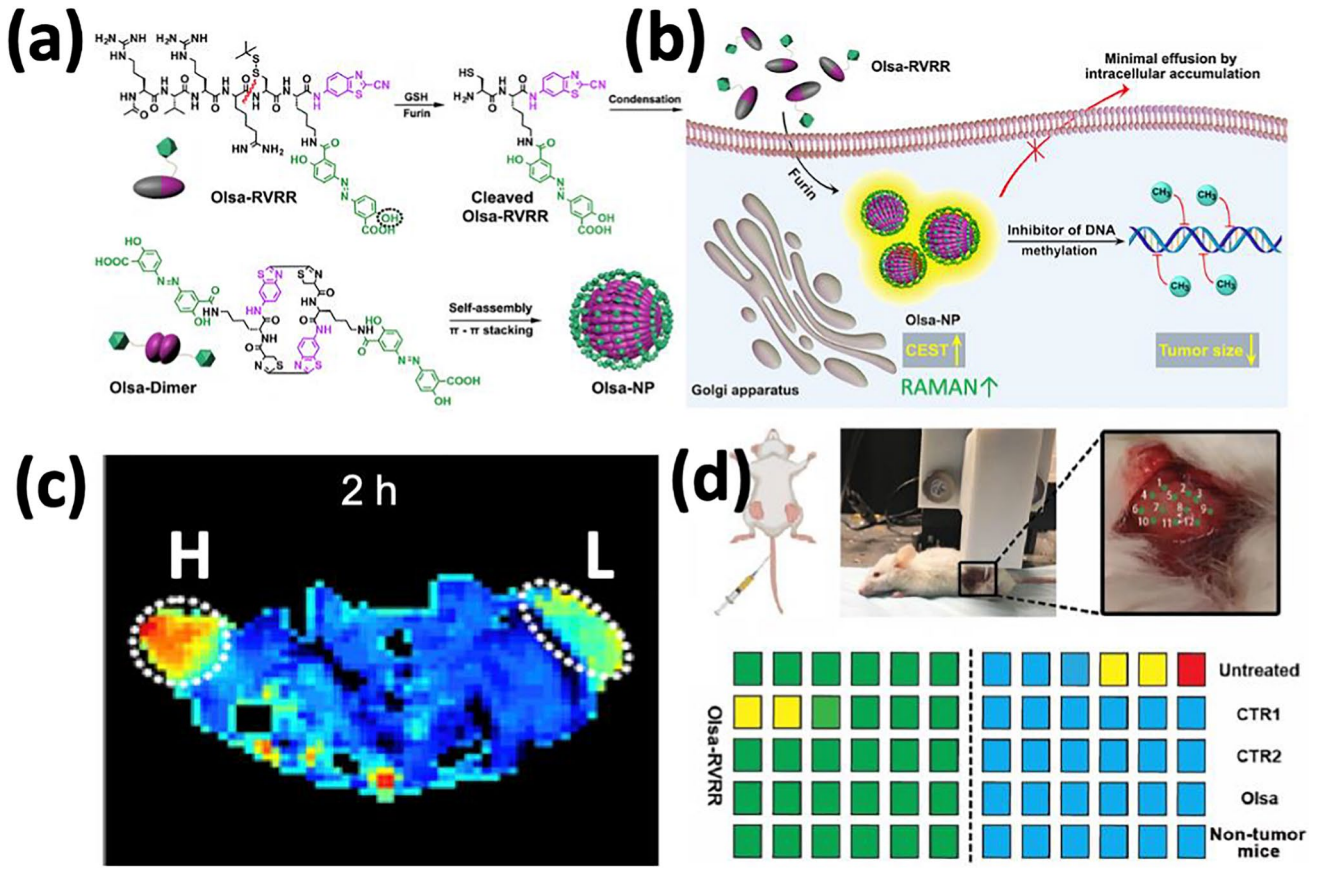

Figure caption: Formation of Olsa NPs by furin-mediated intracellular reduction and condensation of Olsa-RVRR peptide. *In vivo* (c) CEST MRI and (d) RI of furin high-expressing (HCT116, left) and low-expressing (LoVo, right) tumors 2 hours after Olsa-RVRR injection.

References

1. Yue Y, Zhang J, Qi X, Li S, Liu G, Siddhanta S, Barman I, Song X, McMahon MT, Bulte JWM. Furin-mediated intracellular self-assembly of olsalazine nanoparticles for enhanced MR imaging and tumor therapy. Nat. Mater. 2019; 18; 1376-1383.
2. Yuan Y, Raj P, Zhang J, Siddhanta S, Barman I, Bulte JWM. Furin-mediated self-assembly of olsalazine nanoparticles for targeted Raman imaging of tumors. Angew. Chem. Int. Ed. 2021; 60; 3923-3927.

Declarations

Conflict of Interest

The authors declare no competing interests.

013-Preclinical Assessment of MT218 for Accurate Diagnosis of Invasive Prostate Cancer with MRMI

Zheng-Rong Lu, Amita Vaidya, Nadia Ayat, Aman Shankardass

Case Western Reserve University, Cleveland, OH, USA

Background

Tumor heterogeneity is a hallmark of prostate cancer and drives its dynamic progression towards invasion and drug resistance. Accurate differential diagnosis using robust biomarkers of these aggressive tumor populations is imperative, to facilitate risk-stratification and timely adaptive interventions. To address this unmet clinical need, we explored the potential of leveraging the abundant extracellular matrix oncoprotein, extradomain-B fibronectin (EDB-FN), as a biomarker for MR molecular imaging (MRMI) of invasive prostate tumors.

Methods and Materials

LNCaP-CXCR2 and drug-resistant C4-2-DR and PC3-DR cells were generated by stable overexpression of the pro-tumorigenic IL-8 receptor CXCR2 and acquired drug resistance to 20 μM enzalutamide, respectively. EDB-FN expression, invasion, and 3D cell growth were evaluated using qRT-PCR, transwell assays, and matrigel culture, respectively. Athymic nude mice were subcutaneously implanted with the prostate xenografts, and MRMI was performed with ZD2-targeted macrocyclic contrast agent MT218 [ZD2-N3-Gd(HP-DO3A)] on 3T MRS 3000 scanner. T1-weighted MR images were obtained before and 20 min after injection of MT218 (0.04 mmol/kg) using mouse short quad coil and axial fast spin-echo sequence (TR=305 ms, TE=11 ms, FA=90°, FOV=40 mm × 40 mm, slice thickness=1 mm, slice number=15, Nav=2, matrix = 256×256) with respiratory gating. Contrast-to-noise ratios (CNRs) were calculated as (mean tumor intensity - mean muscle intensity)/standard deviation of noise. Image and CNR analysis was performed using FIJI.

Results

Compared to the relatively indolent LNCaP and C4-2 cells, their invasive counterparts, LNCaP-CXCR2 and C4-2-DR cells, demonstrate significant upregulation of EDB-FN at mRNA and protein levels in 2D and 3D cultures. In xenograft mouse models, differential contrast enhanced MRMI with MT218 results in stronger signal enhancement in the invasive LNCaP-CXCR2, C4-2, and C4-2-DR tumors, compared to the low-grade LNCaP tumors. Additionally, the C4-2-DR tumors also demonstrate robust signal enhancement over the non-resistant C4-2 tumors. This is reflected in the nearly 3-fold increase of CNR in the LNCaP-CXCR2 and C4-2 tumors and 6-fold increase in C4-2-DR tumors at 20 min post-injection, while the low-grade LNCaP tumors demonstrate negligible increase in their CNR. These results indicate that EDB-FN is strongly upregulated in low-risk tumors that evolve into invasive tumors.

Conclusions

EDB-FN is a promising diagnostic marker of high-risk aggressive prostate tumors. MRMI of EDB-FN using significantly lower doses of MT218 highlights its potential for non-invasive diagnostic imaging and continued surveillance of aggressive drug-resistant prostate neoplasms.

Declarations

Conflict of Interest

The authors declare no competing interests.

014-Gadolinium Speciation in Tissues: a General Review on the Current Strategies and Perspectives

Cécile Factor[1], Izabela Strzeminska[1], Uwe Karst[2], Ryszard Lobinski[3], Stefanie Fingerhut[2], Lukas Schlatt[2], Sabrina Funke[2], Claire Corot[1], Joanna Szpunar[3], Marlène Rasschaert[1], Philippe Robert[1]

[1]Guerbet, Research and Innovation, Cedex, France
[2]University of Münster, Institute of Inorganic and Analytical Chemistry, Münster, Germany

[3]The Institute of Analytical Sciences and Physico-Chemistry for Environment and Materials (IPREM-UMR) CNRS, Cedex, France

Background
Nowadays, about 30% of MRI procedures involve injections of contrast media. Until recently, it was admitted that of gadolinium-based contrast agents (GBCAs) did not cross the blood brain barrier. In early 2014, following administration of several GBCAs on patients with normal renal functions, T1 hyperintensities in dentate nucleus and globus pallidus were associated with gadolinium (Gd) accumulation [1]. This finding prompted scientists to investigate the fate of Gd in brain and the risk of adverse neurological effects.

Methods and Materials
NA

Results
Spatial distribution of Gd provides information on its accumulation in specific areas (such as deep cerebellar nuclei, choroid plexus, …) as well as at cellular level, depending on the spatial resolution of the techniques, therefore giving insights on retention and wash out mechanisms [2]. However, according to the sample preparation (frozen tissue, FFPE tissue, ...), only a fraction of the total Gd can be detected. Also, despite some of these techniques can simultaneously measure endogenous elements (such as iron, phosphorous, …), only hypothesis on Gd species can be provided (*i.e.*, phosphate-Gd precipitates) and the status of Gd (intact GBCAs or dechelated) cannot be proven. Several methods for Gd speciation have been described by analyzing extracts using either size-exclusion chromatography (SEC) or hydrophilic interaction liquid chromatography/reversed phase chromatography (HILIC/RP) associated with inductively coupled plasma or electrospray ionization/mass spectrometry (ICP or ESI/MS) [3,4]. In rat cerebellums, Gd is detected only as soluble small molecules including the intact GBCA for macrocyclic GBCAs even 12 months after the last injection whereas a fraction of Gd is also found as bound to macromolecules associated to reduced wash out for linear GBCAs. These observations have also been described following a single injection of a clinically relevant dose of GBCA [5]. Limitations of these approaches will be discussed, including extraction efficiency, as well as strategies to overcome them. Recent works on other matrix such as the kidney (organ of elimination) and bone (organ of long-term storage) will also be discussed, particularly a method that allows the quantification of both total Gd and intact GBCA in bones within one analysis for the first time.

Conclusions
Investigations include sensitive quantification of the Gd content in different brain structures, localization up to cellular level and identification of its molecular forms. Several approaches are therefore necessary to provide a comprehensive picture of Gd. Further investigations on other organs will certainly be useful for a better understanding of Gd retention, especially in the context of new GBCAs.

References
1. Kanda T, Kawaguchi H, Kitajima K, Takenaka D. High signal intensity in the dentate nucleus and globus pallidus on unenhanced T1-weighted MR images: Relationship with increasing cumulative dose of a gadolinium-based contrast material. Radiology 2014; 270; 834-841
2. Rasschaert M, Weller RO, Schroeder JA, Brochhausen C, Idée JM. Retention of gadolinium in brain parenchyma: Pathways for speciation, access and distribution. A critical review. JMRI 2020; 52; 1293-1305
3. Frenzel T, Apte C, Jost G, Schöckel L, Lohrke J, Pietsch H. Quantification and assessment of the chemical form of residual gadolinium in the brain after repeated administration of gadolinium-based contrast agents. Invest Radiol 2017 ; 52 ; 396-404
4. Gianolio E, Bardini P, Arena F, Stefania R, Gregorio E, Iani R, Aime S. Gadolinium retention in the rat brain: Assesment of the amounts of insoluble gadolinium-containing species and intact gadolinium complexes after repeated administration of gadolinium-based contrast agents. Radiology 2017; 285; 839-849
5. Strzeminska I, Factor C, Robert P, Grindel AL, Comby PO, Szpunar J, Corot C, Lobinski R. Long term evaluation of gadolinium retention in rat brain after single injection of a clinically relevant dose of gadolinium-based contrast agents. Invest Radiol 2020; 55; 138-143

Declarations

Conflict of Interest
The authors Cécile Factor, Izabela Strzeminska, Marlène Rasschaert, Philippe Robert, Claire Corot, Uwe Karst, Ryszard Lobinski, and Joanna Szpunar would like to disclose financial interest in this abstract. The other authors disclosed no financial interest.

015-Toxicity and Behavioural Assessment in Mice Following GBCA Exposure in Utero or in Juveniles

Clemens Guenther[1], Simona Bussi[2], Alessandra Coppo[2], Paul A. Jones[3], Ella Hirani[3], Nathalie Fretellier[4], Alan Hoberman[5], Elise Lewis[5]

[1]Bayer AG, Leverkusen, Germany
[2]Bracco Imaging Spa., Milan, Italy
[3]GE Healthcare Ltd., Chicago, USA
[4]Guerbet, Villepinte, France
[5]Charles River Laboratories Inc., Wilmington, USA

Background

Khairinisa et al. reported that Gd retention in the brain of F1 generation pups during postnatal development may lead to impaired brain development and subsequent impacts on behavior. In December 2017, FDA requested additional post-marketing data from the 4 GBCA (Gadolinium Based Contrast Agents) manufacturers leveraging GBCA exposure during pregnancy and post-partum as a highly sensitive model to further understand potential adverse effects of long-term Gd brain retention on offspring growth and development. To fulfill this request, 2 separate studies in mice have been conducted with repeated administrations of each GBCA to evaluate potential effects of a) prenatal and b) early postnatal exposure on behavioral, neurological, and histopathological changes during postnatal development and in adult mice.

Methods and Materials

Seven linear and macrocyclic GBCAs (Figure 1) were investigated in pre- & postnatal (PPN) and juvenile toxicity studies in CD1 mice to provide safety data assessing standard parameters based on ICH S5 and S11 guidelines. Clinical observations, body weight, food consumption, sexual maturity, full histopathology, and behavioral/neurological parameters including learning and memory were assessed. Studies also examined the pharmacokinetics of GBCAs including Gd presence in brain and other selected organs/tissues. Study designs were essentially similar and aligned with FDA prior to execution. PPN studies were designed to evaluate ICH S5 stages C–E of the reproductive process. F0 generation female mice (N?22/group) received daily intravenous doses from implantation throughout the fetal period (Gestation Day 6–17). Observations, including neurobehavioral testing (functional observational battery, locomotor activity, Morris Water Maze), were continued through sexual maturity of F1 generation mice until Postnatal Day 70. In juvenile toxicity studies, animals were intravenously dosed on Postnatal Days (PND) 9, 12, 15, 18, and 21 (main: 10/sex/group; recovery: 10/sex/group). Observations (analogous to the PPN studies) continued until PND 70.

Results

No GBCA-related adverse effects were observed in PPN F1 pups post-weaning or juvenile mice including histopathology or for any neurobehavioral endpoints investigated in all studies at all dose levels despite presence of low Gd levels in brain and other tissues.

Conclusions

Gd levels observed in brain tissue of mice after prenatal or juvenile exposure to multiples of clinical doses of all GBCAs did not correlate with any morphological or functional findings. The extensive study programs did not suggest that exposure to GBCA during development presents a potential risk for long-term effects such as behavioral, neurological or histopathological findings in the brain, and/or impaired learning or memory of developing offspring in mice.

Figure 1: GBCA and dose levels investigated

		Dose level (mmol Gd/kg)	Concentration (mmol Gd/mL)
Linear	Gadodiamide (Omniscan, GE Healthcare)	0, 0.6, 1.2, 2.5	0.5
	Gadopentetate dimeglumine (Magnevist, Bayer)	0, 0.6, 1.2, 2.5	0.5
	Gadoxetate disodium (Eovist, Bayer)	0, 0.15, 0.3, 0.63	0.25
	Gadobenate dimeglumine (MultiHance, Bracco Imaging)	0, 0.6, 1.2, 2.5	0.5
Macrocyclic	Gadobutrol (Gadavist, Bayer)	0, 0.6, 1.2, 2.5	1.0
	Gadoterate meglumine (Dotarem, Guerbet)	0, 0.6, 1.2, 2.5	0.5
	Gadoteridol (ProHance, Bracco Imaging)	0, 0.6, 1.2, 2.5	0.5

Fig. 1 GBCA and dose levels investigated

References
1. Khairinisa MA, Takatsuru Y, Amano I, Erdene K, Nakajima T, Kameo S, Koyama H, Tsushima Y, Koibuchi N. The Effect of Perinatal Gadolinium-Based Contrast Agents on Adult Mice Behavior. Invest Radiol 2018; 53(2); 110-118.

Declarations

Conflict of Interest
All authors are employees and own shares on their respective affiliation. Bayer AG, Bracco Imaging Spa., GE Healthcare Ltd. & Guerbet sponsored the conduct of the studies which were performed at Charles River Laboratories Inc.

016-Ultrasound Mediated Cavitation for the Treatment of Alzheimer's Disease

Maria F. Acosta[1], Dillon Hanrahan[1], Devin P. Murphy[2], Christine Howison[2], Theodore P. Trouard[2], Emmanuelle J. Meuillet[1], Evan C. Unger[1]

[1]Microvascular Therapeutics, LLC., Tucson, AZ, USA
[2]Medical Imaging, University of Arizona, Tucson, AZ, USA

Background
5.5 million Americans age 65 and older may have Alzheimer's disease (AD), ranked as the sixth leading cause of death in the USA. There is clearly an urgent need for novel, safe, and reliable diagnostic tools to detect and treat AD. A hallmark of AD is the accumulation of extracellular plaques containing extracellular Amyloid ?-protein (A?) and intracellular neurofibrillary tangles (NFTs) containing tau proteins in the brain. Furthermore, the blood brain barrier (BBB) prevents delivery of therapeutics such as growth factors and nucleotide-based agents, which might have utility for treating Alzheimer's disease (AD). Safe, targeted, and locally concentrating and delivering therapeutics could have great utility for the diagnostic and treatment of AD.

Methods and Materials
In this study, we developed a novel safe and stable lipid-based nanodroplet (ND) formulation with acoustic properties. Moreover, these ND are targeted for tau and A? plaques in the brain using a specific ligand conjugated to the lipid surface. Owing to their small size, the targeted ND (tND) may be able to permeate through the BBB without additional BBB opening tools, which can be invasive and unsafe.

Results
Our hypothesis is that once in the brain, ultrasound mediated cavitation of the ND can trigger the disruption of NFTs and A? plaques. We indeed have recently showed *in vitro* the concept that ultrasound (US) can be used with tND to disrupt Tau and A? aggregates.

Conclusions
Ongoing studies in a 3xTg-AD mouse model are being carried out to establish the *in vivo* utility of this multifunctional nanoplatform as a novel approach for the treatment of AD.

Declarations

Conflict of Interest
MVT is a minor corporate sponsor of CMR. Dr. Evan Unger is the founder and CEO of MVT. The other authors disclosed no financial interest.

017-A Novel Microbubble Platform for Cancer Immunotherapy: Using MUSIC to Activate the STING Pathway

Sina Khorsandi[1], Xuefeng Li[2], Yifan Wang[2], Robert F. Mattrey[1], Wen Jiang[2], Jacques Lux[1]

[1]University of Texas Southwestern Medical Center, Dallas, TX, USA
[2]MD Anderson Cancer Center, Houston, TX, USA

Background
The innate immune sensor cyclic GMP-AMP synthase-stimulator of interferon genes (cGAS-STING) has recently emerged as a potential therapeutic target to boost antitumor immune responses. However, STING is a cytoplasmic protein, and its natural activator cGAMP is a negatively charged dinucleotide that is difficult to deliver intracellularly. Since microbubbles (MBs) can deliver payloads in the cytoplasm using sonoporation, we have developed a new platform called Microbubble-assisted UltraSound (US)-guided Immunotherapy of Cancer (MUSIC) to activate STING with spatio-temporal control to treat cancer.

Methods and Materials
To maximize cGAMP loading and target macrophages, spermine-modified dextran (SpeDex) and anti-CD11b antibodies were thiolated and conjugated onto the surface of maleimide-bearing MBs. Both THP-1 human macrophages and mouse bone-marrow derived macrophages were sonoporated with cGAMP-loaded Spe-Dex-aCD11b MBs (MUSIC) to deliver cGAMP directly into the cell cytosol and activate STING *in vitro*. Sonoporation was performed at 1 MHz for 60 s (Sonitron GTS) using 1 W/cm2, 20% duty cycle. Western blot, fluorescence microscopy, qRT-PCR, and ELISA were used to confirm STING activation and downstream effects. For *in vivo* studies, C57Bl/6 and Balb/c mice were implanted with E0771 and Luc-4T1 breast cancer cells respectively. Primary tumors were treated locally with MUSIC when they were large enough

(E0771) or when they metastasized to the lungs (Luc-4T1). Tumor volumes and bioluminescence were measured over time to assess therapeutic responses. After treatment, tumor-free C57Bl/6 mice that were rechallenged with the same E0771 cancer cells. STING-/- mice were used as controls.

Results

MUSIC showed greater STING activation compared to cGAMP alone *in vitro*. In murine models, MUSIC showed dramatic tumor growth inhibition and increased survival in both syngeneic breast cancer models (see Figure). The absence of antitumor immune responses in STING-/- mice shows that MUSIC action is STING-dependent. Furthermore, 6/10 MUSIC-treated mice were tumor-free vs. 2/10 cGAMP-treated mice. All of the rechallenged MUSIC-treated mice remained tumor-free 30 days after rechallenge. MUSIC also resulted in a 7-fold decrease in metastatic burden when compared to cGAMP alone.

Conclusions

MUSIC showed efficient STING activation *in vitro*. In addition, local MUSIC treatment of primary tumors produced systemic antitumor immune responses *in vivo* as well as anticancer immune memory preventing tumor growth upon rechallenge. We are now exploring the use of nanobubbles for systemic administration. This work was supported in part by the Cancer Prevention and Research Institute of Texas (CPRIT) Grants RR150010 and RP190233. R.F.M. is a CPRIT Established Investigator.

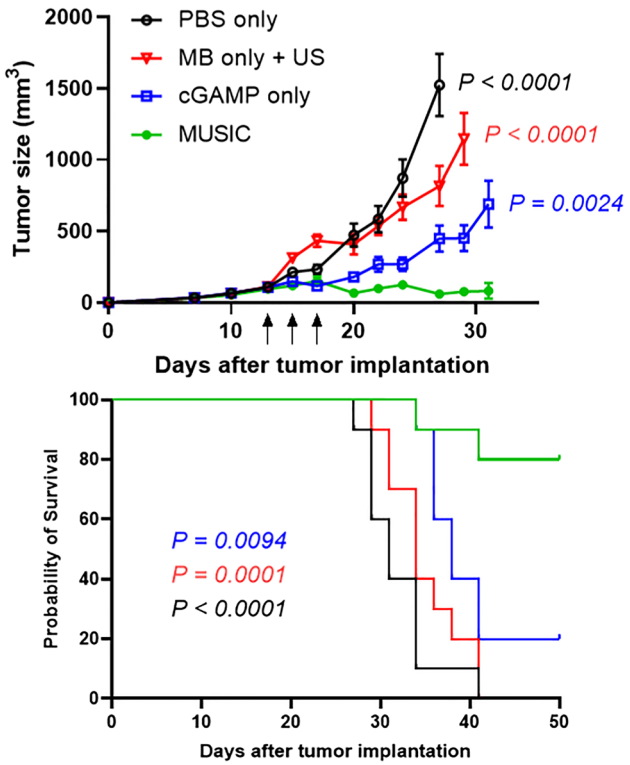

Figure caption: Tumor growth (top) and Kaplan-Meier survival plot (bottom) of C57Bl/6 mice treated with MUSIC and control groups (n=10 for each).

Declarations

Conflict of Interest

The authors declare no competing interests.

018-Improving Tumor Cell Clusters Retrieval from Blood Through Increased Buoyancy with Targeted Microbubbles and Nanodroplets

Lalit Chudal, Caroline de Gracia Lux, Jacques Lux, Robert Mattrey

University of Texas Southwestern Medical Center, Dallas, USA

Background

Isolation of circulating tumor cells (CTCs) using anti-EpCAM labeled magnetic beads is the only FDA approved CTC enumeration technique1. We introduced CTC targeted microbubbles (MBs) as a buoyancy-based retrieval method2. Unfortunately, CTC enumeration has failed to impact patient management that requires tumor molecular profiling. CTC clusters are shed directly from tumors, are longer lived, and carry a 100-fold greater metastasis potential. Early data suggest that they can be cultured and analyzed to provide the primary tumor's molecular and drug sensitivity profiles. Retrieving CTC clusters, however, is very challenging because they are heavy, large and extremely rare in circulation. Last CMR we showed that perfluorobutane (PFB) vapor-filled MBs increase their diameter by up to 100-fold when exposed to liquid PFB nanodroplets (NDs)3. Since buoyancy force increases linearly with MB volume, 100-fold expansion increases buoyancy a million-fold to lift heavy particles to the surface. This report describes the improvement in CTC cluster retrieval when NDs are added.

Methods and Materials

Using FITC-labeled 12–50-μm silica beads—130 times heavier than CTCs, we optimized the technique to maximize retrieval using anti-FITC labeled MBs and MB-targeted NDs. We created CTC cluster surrogates using H2122 non-small cell lung cancer that are EpCAM positive and form grape-like clusters in suspension4. We compared the retrieval rates of these clusters with targeted MBs before and after adding NDs when 1, 2, 30, or 300

clusters were spiked in 3-mL whole blood. Using a metastatic model of breast cancer in mice, we assessed the impact of adding NDs on the retrieval of naturally occurring CTC clusters.

Results

Comparing particle size distribution of FITC-labeled silica beads to the distribution retrieved after adding FITC-targeted MBs or after adding targeted MBs and MB-targeted NDs showed that 50-µm beads could only be retrieved with NDs and the addition of NDs markedly skewed the distribution towards large particle sizes. When cluster surrogates were spiked in 3 mL whole blood, the addition of NDs dramatically increased the retrieval rate without the need for centrifugation. While targeted MBs alone retrieved 2 out of the 30 clusters, the addition of NDs lifted nearly all spiked clusters to the surface. 4T1 cell clusters were only retrieved from mice when using both targeted MBs and NDs.

Conclusions

Conventional MB-based buoyancy cell retrieval was enhanced by the addition of MB-targeted NDs, which dramatically increased the retrieval rate of heavy particles and CTC clusters from whole blood regardless of their weight and without the need for centrifugation. Study supported by CPRIT RR150010. RFM is a CPRIT Established Investigator.

References

1. Alix-Panabières, C. & Pantel, K. Clinical Applications of Circulating Tumor Cells and Circulating Tumor DNA as Liquid Biopsy. Cancer Discovery 6, 479-491, doi:10.1158/2159-8290.Cd-15-1483 (2016).
2. Simberg, D. & Mattrey, R. Targeting of perfluorocarbon microbubbles to selective populations of circulating blood cells. Journal of Drug Targeting 17, 392-398, doi:10.1080/10611860902902797 (2009).
3. Brambila, C. J. et al. Bubble Inflation Using Phase-Change Perfluorocarbon Nanodroplets as a Strategy for Enhanced Ultrasound Imaging and Therapy. Langmuir, doi:10.1021/acs.langmuir.9b03647 (2020).
4. May, A.N., B.D. Crawford, and A.M. Nedelcu, *In Vitro* Model-Systems to Understand the Biology and Clinical Significance of Circulating Tumor Cell Clusters. Front Oncol, 2018. 8: p. 63.

Declarations

Conflict of Interest

The authors declare no competing interests.

019-Acoustic Vaporization of Internalized Perfluorobutane Nanodroplets for Imaging and Immunotherapy

Lalit Chudal, Caroline de Gracia Lux, Jacques Lux, Robert F. Mattrey

University of Texas Southwestern Medical Center, Dallas, TX, USA

Background

Ultrasound (US) can detect and interact with its contrast agents, allowing perfluorocarbon-based nanodroplets (NDs) or microbubbles (MBs) to detect and treat tumors in deep tissues. Although easily functionalized for targeting, even nanoscale particles are limited in targeting extravascular sites. Since NDs given IV passively accumulate in tumor macrophages, we aimed to determine whether phagocytosed perfluorobutane (PFB) NDs that boil at −2°C can be vaporized *in vivo* using a clinical scanner. Should that be possible, PFB NDs can then be used to deliver drugs or genes to modulate macrophage function.

Methods and Materials

We formulated stable PFB NDs and used confocal microscopy to optimize and validate their internalization into THP-1 macrophages. Z-stack images were collected using 63× objective of Zeiss Airyscan LSM880 confocal microscope and processed with ImageJ. PFB ND loaded macrophages were then infused into nude rats and US imaging (low MI US imaging, 18H6 transducer) of the liver and spleen performed *in vivo* using a Siemens Sequoia clinical scanner before and after applying microbubble destruction pulses (at 1.4 MI, 10L4 transducer), a commonly used tool to assess tissue perfusion.

Results

Cy5-labeled PFB NDs (red/orange) were visible intracellularly in DAPI (blue) and Calcein-AM stained cells (green) indicating cell viability (Fig. 1A). Internalized PFB NDs were stable at 37°C *in vitro* and *in vivo*. *In vitro*, they vaporized into MBs at 0.58 MI. *In vivo*, PFB ND-loaded macrophages were not visible using low MI imaging, before applying MB destruction pulses (Fig, 1B left). They immediately vaporized into US visible microbubbles when destruction pulses were applied (Fig. 1B middle) over the liver and remained visible for many minutes after vaporization (Fig. 1B right).

Conclusions

PFB NDs were successfully loaded into macrophages and stable *in vitro* as well as *in vivo*. Thirty min after IV infusion of ND-loaded macrophages, intracellular NDs could be converted into detectable microbubbles *in vivo* using

MI lower than the FDA limit of 1.9. Our goal is to assess ND-loaded macrophage function before and after ND activation to determine the feasibility of modulating immune function. Study supported by CPRIT RR150010. RFM is a CPRIT Established Investigator. Siemens ACUSON Sequoia Ultrasound System provided as a loan by Siemens Medical Solutions, USA.

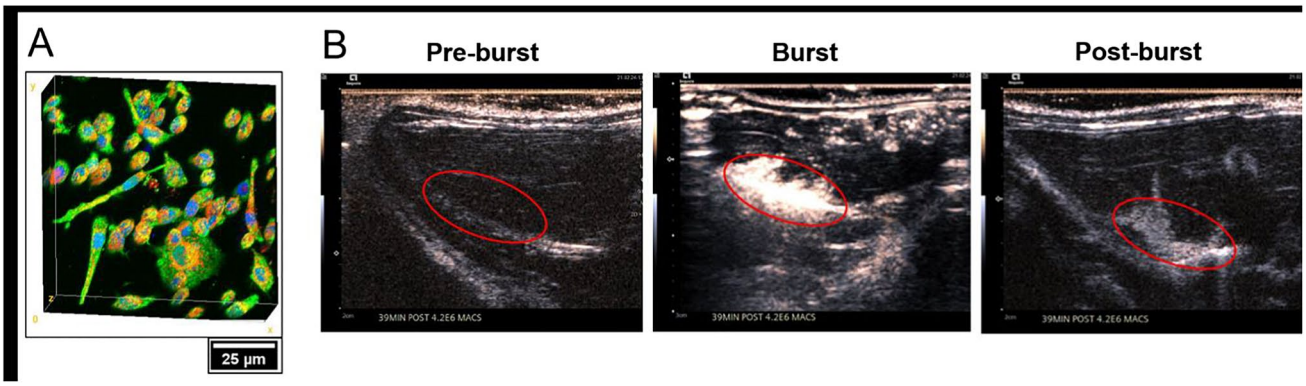

Figure caption: Validation of *in vitro* THP-1 differentiated macrophage labeling with PFB NDs (A) and *in vivo* vaporization of internalized PFB NDs in the liver (B)

Declarations

Conflict of Interest

The authors declare no competing interests.

020- Engineering Prostate Tumors with Targeted Photodynamic Therapy for Enhanced Nanoparticle Delivery

Ethel Ngen[1], Ying Chen[1], Babak Behnam Azad[1], Srikanth Boinapally[1], Desmond Jacob[1], Ala Lisok[1], Chentian Shen[1], Mir S. Hossain[1], Jiefu Jin[1], Zaver Bhujwalla[1,2], Martin Pomper[1,2], Sangeeta Banerjee[1,2,3]

[1]Johns Hopkins University School of Medicine, Baltimore, USA
[2]The Sidney Kimmel Comprehensive Cancer Center, Johns Hopkins University School of Medicine, Baltimore, USA
[3]The F. M. Kirby Research Center for Functional Brain Imaging, Kennedy Krieger Research Institute, Baltimore, USA

Background

Magnetic nanoparticle-induced hyperthermia (MNP-IH) is a less morbid focal therapy being explored for prostate cancer (PC). However, the delivery of nanoparticles (? 100 nm) to tumors, after intravenous administration is still a challenge 1. Current practices to deliver magnetic nanoparticles (MNPs) for MNP-IH, involve direct tumor injections. This is invasive and can cause treatment-related morbidity, which negatively impacts patient quality of life. Thus, there is a need for nanoparticle delivery systems capable of increasing tumor-specific accumulation, after intravenous administration 2,3. Enhanced vascular permeability plays an essential role in nanoparticle delivery to tumors, through the enhanced permeability and retention (EPR) effect. However, the EPR effect varies greatly within tumors and between patients 1. Consequently, tumor engineering approaches to specifically enhance the EPR effect and nanoparticle delivery, are being explored 4. Prostate-specific membrane antigen (PSMA) is overexpressed on aggressive PCs and has been targeted for imaging and therapy 2,3. Here, we evaluated the feasibility of using low-dose PSMA-targeted photodynamic therapy (PDT), to enhance the EPR effect and the delivery of PSMA-targeted MNPs to human PSMA(+) PC tumor xenografts, in a preclinical mouse model.

Methods and Materials

PSMA(+) PC3 PIP tumor-bearing NSG mice (Group 1) were intravenously administered a PSMA-targeted photosensitizer and treated with fluorescence image-guided PDT, 4 h after. The mice were then intravenously administered 50 mg/kg of a PSMA-targeted MNP, immediately after PDT and monitored with both fluorescence imaging and T2-weighted MRI for 66 h.5 PSMA(+) PC3 PIP tumor-bearing NSG mice, not pretreated with PDT and only intravenously administered the PSMA-targeted MNP, were used as

negative controls (Group 2). Additional control groups were also used to investigate the specificity of the PDT-mediated EPR enhancement effect.

Results

An 8-fold increase in the delivery of PSMA-targeted MNPs was detected in the tumors of Group 1 mice compared to Group 2 mice, 42 h after PDT. Additionally, T2-W MRIs revealed enhanced peripheral intra-tumoral delivery of the PSMA-targeted MNPs. This is in keeping with two-photon microscopy results which revealed higher vascular densities at the tumor periphery.

Conclusions

These results suggest that PSMA-targeted PDT enhances the delivery of PSMA-targeted MNPs to PSMA(+) PC3 PIP tumors by enhancing the EPR effect. Thus, PDT can be used synergistically with MNP-IH for effective PC treatment.

Fig. 1 A) Experimental design. B) *In vivo* fluorescence images of nanoparticle delivery. C) Fluorescence quantification of nanoparticle delivery. D) *In vivo* T2W MRI of nanoparticle delivery. E) T2W MRI quantification of nanoparticle delivery

References

1. Wilhelm S, Tavares AJ, Dai Q, Ohta S, Audet J, Dvorak HF, Chan WC. Analysis of nanoparticle delivery to tumours. Nat Rev Mater 2016; 1; 16014-16025.
2. Azad BB, Banerjee SR, Pullambhatla M, Lacerda S, Foss CA, Wang Y, Ivkov R, Pomper MG. Evaluation of a PSMA-targeted BNF nanoparticle construct. Nanoscale 2015; 7; 4432-4442.
3. Ngen EJ, Azad BB, Boinapally S, Lisok A, Brummet M, Jacob D, Pomper MG, Banerjee SR. MRI assessment of prostate-specific membrane antigen (PSMA) targeting by a PSMA-targeted magnetic nanoparticle: Potential for image-guided therapy. Mol Pharm 2019; 16; 2060-2068.
4. Kobayashi H, Choyke PL. Super enhanced permeability and retention (SUPR) effects in tumors following near infrared photoimmunotherapy. Nanoscale 2016; 8; 12504-12509.
5. Ngen EJ, Chen Y, Azad BB, Boinapally S, Jacob D, Lisok A, Shen C, Hossain MS, Jin J, Bhujwalla ZM, Pomper MG, Banerjee SR. Prostate-specific membrane antigen (PSMA)-targeted photodynamic therapy enhances the delivery of PSMA-targeted magnetic nanoparticles to PSMA-expressing prostate tumors. Nanotheranostics 2021; 5; 182-196.

Declarations

Conflict of Interest

The authors declare no competing interests.

021-Small Molecule MR Probes for Imaging Organ Fibrogenesis

Yingying Ning, Hua Ma, Iris Zhou, Mozhdeh Sojoodi, Kenneth Tanabe, Peter Caravan

Massachusetts General Hospital, Harvard Medical School, Boston, USA

Background

Fibrogenesis is the active production of extracellular matrix in response to tissue injury. In many chronic diseases persistent fibrogenesis results in the accumulation of scar tissue, which can lead to organ failure and death. However, no non-invasive technique exists to assess this key biological process. A universal feature of fibrogenesis is the oxidation of matrix proteins, chiefly collagen, by the lysyl-oxidase (LOX) family of enzymes. A prototype MR probe based on Gd-DOTA was shown to be able to detect fibrogenesis in rodent models 1. The purpose of this study was to design probes with improved reactivity (on-rate), affinity, off-rate, and relaxivity in order to enhance the sensitivity and dynamic range for quantitative MR imaging of fibrogenesis.

Methods and Materials

We synthesized a series of Gd3+- and Mn2+-based compounds that target LOX oxidized proteins, as well as structurally similar analogs as negative controls. The relaxivity (1.4T, 37 °C) was measured in PBS, in the presence of bovine serum albumin (BSA) and in oxidized BSA solution. Protein binding was also measured. On-rates and off-rates for binding to model compounds and oxidized protein were measured by HPLC or relaxivity. *In vivo* efficacy was assessed in mouse models of pulmonary (bleomycin injury) and hepatic (CCl4 injury and diet models) fibrosis, and in response to therapeutic interventions. Fibrosis and fibrogenesis were characterized by histological markers, pathological scoring, pro-fibrotic protein expression levels, biochemical quantification of hydroxyproline and allysine as measures of collagen and oxidized collagen, respectively.

Results

The molecular probes showed low relaxivity in PBS consistent with their molecular weight and little/no increase in the presence of BSA indicating very low non-specific binding. Relaxivity was increased 3-6-fold upon binding to oxidized BSA. Reactivity, off-rate, and affinity to oxidized BSA depended on type and orientation of targeting group. Improved *in vitro* properties translated to significantly larger changes in contrast to noise ratio (CNR) compared to prototype probes in disease models. Specificity was demonstrated using a 10-fold higher blocking dose of an Yb-analog. In a mouse model of non-alcoholic

steatohepatitis, the optimized fibrogenesis probe was shown to detect disease early, and be a sensitive marker of therapeutic response. In a lung injury model, the probe provided a non-invasive readout of treatment response with a novel antifibrotic therapy.

Conclusions

Rational molecular design results in MR probes with an order of magnitude higher *in vivo* performance compared to prototype probe, resulting in capability to detect and stage organ fibrogenesis noninvasively. This new family of contrast agents may have utility in chronic liver disease, pulmonary fibrosis, and any other fibroproliferative pathologies.

References

1. Chen HH, Waghorn PA, Wei L, Tapias LF, Schühle DT, Rotile NJ, Jones CM, Looby RJ, Zhao G, Elliott JM, Probst CK, Mino-Kenudson M, Lauwers GY, Tager AM, Tanabe KK, Lanuti M, Fuchs BC, Caravan P. Molecular imaging of oxidized collagen quantifies pulmonary and hepatic fibrogenesis. JCI Insight. 2017 Jun 2;2(11). pii: 91506

Declarations

Conflict of Interest

The authors declare no competing interests.

022-MRI Tracking of Magnetically Labeled Extracellular Vesicles Following Systemic Delivery

Zheng Han[1,2], Robert G. Weiss[1], Peter C.M. van Zijl[1,2], Jeff W.M. Bulte[1,2], Guanshu Liu[1,2]

[1]Johns Hopkins University School of Medicine, Baltimore, MD, USA
[2]Hugo W. Moser Institute, Kennedy Krieger Institute, Baltimore, USA

Background

The objective of this study is to develop an MRI tracking method to study the delivery and distribution of systemically administered EVs. Stem-cells-derived extracellular vesicles (EVs) have become a new class of therapeutics for cell-free regenerative medicine (1,2). Non-invasive tracking methods is of great importance for developing optimized EV-based therapies. Yet, MRI were only used for detecting locally administered EVs (3,4). Our overall aim was to develop a new EV labeling strategy to improve both labeling efficiency and magnetic EV purity for accurate *in vivo* MRI tracking of systemically injected EVs (5).

Methods and Materials

The new EV labeling strategy is outlined in Fig. 1A–C, where the surface His-tag is used to remove non-encapsulated superparamagnetic iron oxide nanoparticles (SPION) in solution. Histidine-tag-functionalized ("sticky") SPIONs was prepared from carboxyl-SPIONs (core size = 5 nm, Ocean Nanotech). Induced pluripotent stem cell (iPSC)-derived EVs were prepared from iPSC culture medium using an Amicon ultra-15 filter column and loaded with His-SPIONs (10 μg per 109 EVs) using electroporation (240V, 100A, 5s, Gene Pulser Xcell). Mice with injured kidneys or infarcted hearts were injected (i.v.) with approximately 109 EVs in 200 uL PBS and T2*-weighted images were intermittently acquired before and after injection for 30 min using a gradient echo sequence (TR=800 ms, TE=5.8 ms, matrix size=256×128, in plane resolution=0.167×0.280 mm2) using a 11.7T Biospec horizontal bore scanner.

Results

The His-SPION can be efficiently removed by an Ni-NTA column (> 97.4%), which allowed preparing highly purified SPION-loaded iPSC-derived EVs, which we termed magneto-EVs. The labeling efficiency is substantially higher than that by a traditional labeling strategy through parental cell loading (4) (*i.e.*, 95.87% vs. 19.32%). The detection limit was estimated to be 8.76× 107 EVs/mL, which is high enough for tracking therapeutic EVs *in vivo*. *In vivo* studies demonstrated the ability of MRI to monitor the dynamic uptake and distribution of intravenously injected magneto-EVs in the injured kidneys and infarcted myocardium (Fig. 1D–F). Compared to normal mice, the injured mice exhibited significantly higher uptake of magneto-EVs in the kidneys (Fig. 1D,E), indicating the innate homing ability of iPSC-EVs towards injured organs. The MRI findings correlated well with the histological assessment (Fig. 1D–F).

Conclusions

We developed an efficient platform technology for preparing magneto-EVs for *in vivo* MRI tracking. The magneto-EVs were free of non-encapsulated SPIOs, allowing accurate detection and interpretation of the spatiotemporal distribution of therapeutic EVs following intravenous injection.

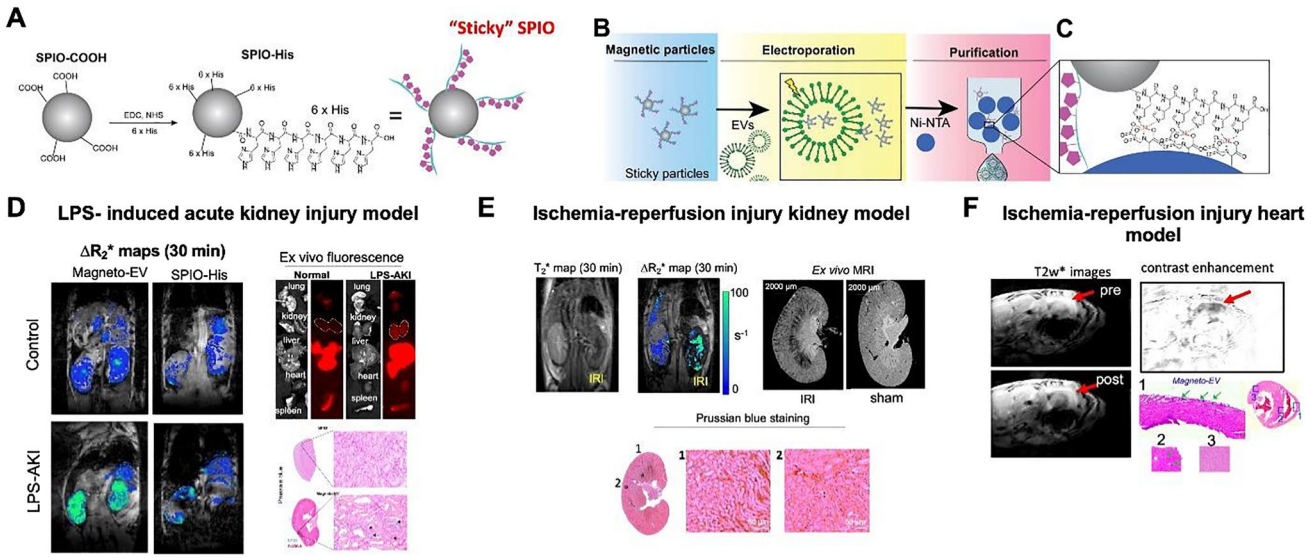

Fig. 1 Highly purified SPION-labeled EVs for MRI tracking of systemically injected iPSC derived EVs

References

1. Rani S, Ryan AE, Griffin MD, Ritter T. Mesenchymal Stem Cell-derived Extracellular Vesicles: Toward Cell-free Therapeutic Applications. Mol Ther 2015;23(5):812-823.
2. Marban E. The Secret Life of Exosomes: What Bees Can Teach Us About Next-Generation Therapeutics. J Am Coll Cardiol 2018;71(2):193-200.
3. Hu L, Wickline SA, Hood JL. Magnetic resonance imaging of melanoma exosomes in lymph nodes. Magnetic resonance in medicine 2015;74(1):266-271.
4. Busato A, Bonafede R, Bontempi P, Scambi I, Schiaffino L, Benati D, Malatesta M, Sbarbati A, Marzola P, Mariotti R. Magnetic resonance imaging of ultrasmall superparamagnetic iron oxide-labeled exosomes from stem cells: a new method to obtain labeled exosomes. International journal of nanomedicine 2016;11:2481-2490.
5. Han Z, Liu S, Pei Y, Ding Z, Li Y, Wang X, Zhan D, Xia S, Driedonks T, Witwer KW, Weiss RG, van Zijl PCM, Bulte JWM, Cheng L, Liu G. Highly efficient magnetic labelling allows MRI tracking of the homing of stem cell-derived extracellular vesicles following systemic delivery. J Extracell Vesicles 2021;10(3):e12054.

Declarations

Conflict of Interest

The authors declare no competing interests.

023-Early Detection and Staging Fibrosis and Inflammation by pMRI Using Targeted Protein Contrast Agents

Oluwatosin Y. Ibhagui[1], Zhonxiang Gui[1], Dongjun Li[1], Jingjuan Qiao[1,2], Mani Salarian[1], Shanshan Tan[2], Florence Reddish[2], Van Ha[2], Khan Hekmatyar[2], Jenny J. Yang[1,2]

[1]Georgia State University, Atlanta, GA, USA
[2]InLighta Biosciences, Atlanta, GA, USA

Background

Acute and chronic human diseases including liver and lung diseases, cancer, cardiovascular diseases and virus infection, share common key determinants including inflammation and fibrosis. In order to facilitate early detection, staging, and treatment responses, it is essential to develop a non-invasive imaging methodology that will allow us to longitudinally map and quantify the dynamic changes of inflammation biomarkers, such as chemokine receptors and collagen expression, during disease progression and upon treatment.

Methods and Materials

Here we report our recent breakthrough in optimization, characterization, formulation, and production of a set of novel human protein-based contrast agents (ProCA®s) pioneered by our team for both preclinical and clinical applications. We have developed a human collagen-targeted MRI contrast agent (hProCA32.collagen) with optimized binding fibrosis specificity. hProCA32.collagen exhibits 6.7-fold and 13.7-fold higher binding affinities for collagen type I over types III and IV, respectively.

Results
A manufacturing process has been established for large-scale production and formulation to optimize for solubility, homogeneity, and protein and metal stability to against metal dissociation and transmetallization. Our developed inflammation biomarker-targeted contrast agents specifically delineate activation of immune cells and can capture the pro-metastasis niche and fibrosis associated with fatty liver. We have also developed a new MR imaging methodology (precision imaging by MRI, pMRI), which takes advantage of high r1 and r2 relaxivities at both low and high magnetic fields, to achieve robust detection of early-stage liver and lung fibrosis, quantification of molecular biomarker changes for staging and monitoring treatment responses, and reduction of imaging time and motion artifacts to facilitate preclinical animal studies for drug development.

Conclusions
We are moving rapidly toward clinical applications in early detection, monitoring progression, image-guided intervention/treatment, and patient stratification against human diseases including NASH, ASH, IPF, COPD, and metastasis from multiple cancers.

References
1. Salarian M, Turaga RC, Xue S, Nezafati M, Hekmatyar K, Qiao J, Zhang Y, Tan S, Ibhagui OY, Hai Y, Li J, Mukkavilli R, Sharma M, Mittal P, Min X, Keilholz S, Yu L, Qin G, Farris AB, Liu ZR, Yang JJ. Early detection and staging of chronic liver diseases with a protein MRI contrast agent. Nat Commun. 2019;10(1):4777. Epub 2019/10/31. doi: 10.1038/s41467-019-11984-2. PubMed PMID: 31664017; PMCID: PMC6820552.
2. Tan S, Yang H, Xue S, Qiao J, Salarian M, Hekmatyar K, Meng Y, Mukkavilli R, Pu F, Odubade OY, Harris W, Hai Y, Yushak ML, Morales-Tirado VM, Mittal P, Sun PZ, Lawson D, Grossniklaus HE, Yang JJ. Chemokine receptor 4 targeted protein MRI contrast agent for early detection of liver metastases. Sci Adv. 2020;6(6):eaav7504. Epub 2020/02/23. doi: 10.1126/sciadv.aav7504. PubMed PMID: 32083172; PMCID: PMC7007242.
3. Xue S, Yang H, Qiao J, Pu F, Jiang J, Hubbard K, Hekmatyar K, Langley J, Salarian M, Long RC, Bryant RG, Hu XP, Grossniklaus HE, Liu ZR, Yang JJ. Protein MRI contrast agent with unprecedented metal selectivity and sensitivity for liver cancer imaging. Proceedings of the National Academy of Sciences of the United States of America. 2015;112(21):6607-12. doi: 10.1073/pnas.1423021112. PubMed PMID: 25971726; PMCID: 4450423.
4. Turaga RC, Yin L, Yang JJ, Lee H, Ivanov I, Yan C, Yang H, Grossniklaus HE, Wang S, Ma C, Sun L, Liu ZR. Rational design of a protein that binds integrin alphavbeta3 outside the ligand binding site. Nat Commun. 2016;7:11675. Epub 2016/06/01. doi: 10.1038/ncomms11675. PubMed PMID: 27241473; PMCID: PMC4895024.

Declarations

Conflict of Interest
Jenny J. Yang is the founder of InLighta Biosciences. The other authors disclosed no financial interest. The authors grant permission to publish this information or an appropriate summary thereof with the abstract.

024-A Systematic Review of the Incidence of Hypersensitivity Reactions and Post-contrast Acute Kidney Injury After Ioversol: Part 2-intra-arterial Administration

Ilona Dekkers[1], Aart van der Molen[1], Ibrahim Bedioune[2], Elisabeth Darmon-Kern[2]

[1]Leiden University Medical Center, Leiden, The Netherlands
[2]Roissy CDG Cedex, France

Background
To evaluate the incidence of adverse drug reactions (ADRs), including hypersensitivity reactions (HSRs) and post-contrast acute kidney injury (PC-AKI), after intra-arterial (IA) administration of ioversol.

Methods and Materials
A systematic literature search was performed (1980-2021) and studies documenting IA use of ioversol, and reporting safety outcomes were selected. Key information on study design, patients' characteristics, indication, dose, and type of safety outcome were extracted.

Results
Twenty-eight studies (including two pediatric studies) with 8373 patients exposed to IA ioversol were selected. Studies were highly heterogenous in terms of design, PC-AKI definition, and studied population. PC-AKI incidence after coronary angiography was 7.5–21.9% in a general population, 4.0–26.4% in diabetic patients, and 5.5–28.9% in patients with chronic kidney disease (CKD). PC-AKI requiring dialysis was rare and reported mainly in patients with severe CKD. No significant differences in PC-AKI rates were shown in studies comparing different iodinated contrast media (ICM). Based on seven studies of ioversol clinical development, the overall ADR incidence was 1.6%, comparable to that reported with other non-ionic ICM. Pediatric data were scarce with only one study reporting on PC-AKI incidence (12%), and one reporting on ADR incidence (0.09%), both after coronary angiography.

Conclusions
After ioversol IA administration, PC-AKI incidence was highly variable between studies, likely reflecting the heterogeneity of the included study populations, and appeared comparable to that reported with other ICM. The rate of other ADRs appears to be low. Well-designed studies are needed for a better comparison with other ICM.

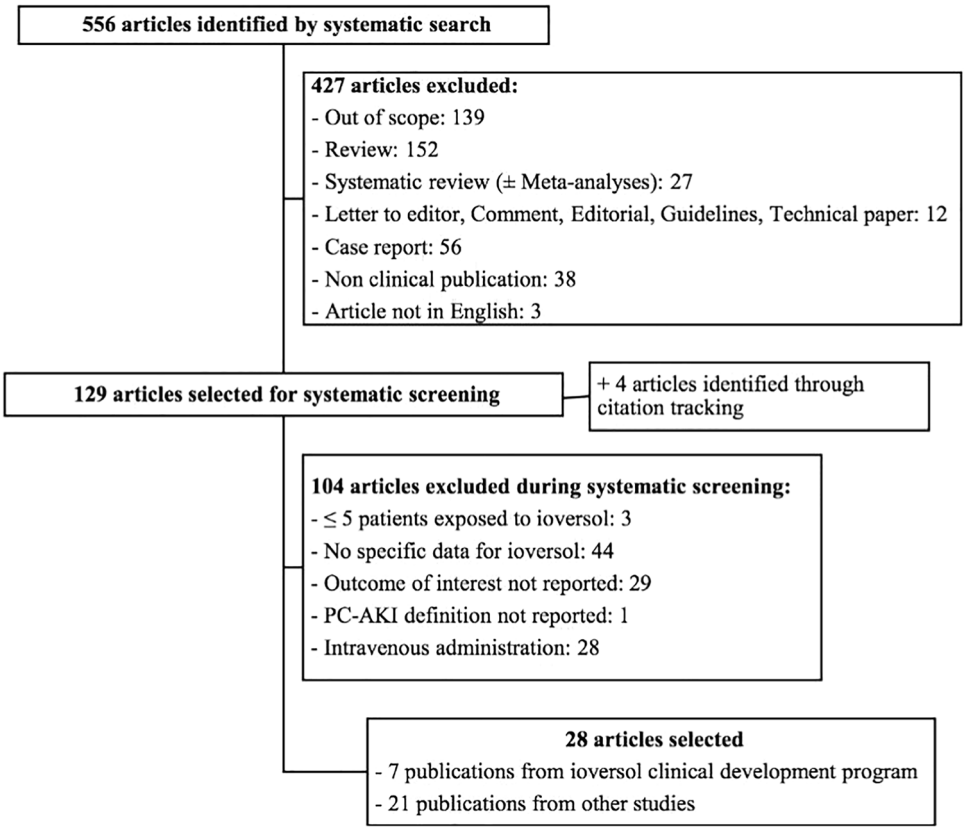

Fig. 1 Flow diagram of the search strategy and study selection

References
1. van der Molen AJ, Dekkers IA, Bedioune I, Darmon-Kern E. A systematic review of the incidence of hypersensitivity reactions and post-contrast acute kidney injury after ioversol: part 2-intra-arterial administration. Eur Radiol. 2022 Mar 21. doi: 10.1007/s00330-022-08637-2. Epub ahead of print. PMID: 35312791.

Declarations

Conflict of Interest
All authors of this publication would like to disclose a financial interest in this abstract.

025- OncoCiDia as a Dual Targeting Chemo-radial Theragnostics: Potential for Brain Metastasis

Shuncong Wang, Lei Chen, Yuanbo Feng, Ghislain Maheshe, Geert Maleux, Chantal Van Ongeval, Yue Li, Yicheng Ni

KU Leuven, Belgium

Background
As a dual-targeting chemo-radial cancer theragnostics, OncoCiDia has been derived from contrast media research [1]. Its safety and pan-anticancer efficacy have been evidenced by preclinical and clinical studies [2]. Brain metastasis often presents a culprit for cancer patient's death and

poses tremendous clinical challenges [3]. Inducing sufficient tumor necrosis using a vascular disrupting agent (VDA) proves crucial for the subsequent necrosis-targeting tumor radio-ablation [1]. Contrast enhancement of brain metastasis implies the broken blood-brain barrier (BBB) and the access of the VDA to the tumor. This ongoing study aims to explore the potential of OncoCiDia in the management of brain metastasis in order to help address such an unmet clinical need.

Methods and Materials

WAG/Rij rats (n=50) were implanted with rhabdomyosarcoma (R1) tissue in the frontal lobe of the brain to mimic a metastasis and scanned with MRI for monitoring tumor growth. When R1 reached 5 mm in diameter, the rat was randomized into either iv PBS control or VDA (20mg/kg CA4P) treated group. Gd-DOTA enhanced multiparametric MRI was performed at the baseline, and at 1h and 12h after the treatment, and compared between groups. Postmortem microangiography with 2D digital radiology and 3D nano-CT as well as histopathology were conducted to validate *in vivo* MRI findings, which were all statistically analyzed. Intra- and extra-cranial tumors were compared for VDA efficacy.

Results

Intracranial R1 implantation was of 100% success with tumor take rate >90%. All brain tumors (arrow or T) appeared hyper- and hypo-intense on T2 and T1 weighted precontrast MRI, respectively, and were enhanced by Gd-DOTA on post-contrast T1-MRI (Fig. 1), which were reflected by corresponding perfusion-weighted imaging (PWI) curves (Fig. 2), diffusion-weighted imaging (DWI) and apparent diffusion coefficient (ADC), T1 and T2 maps. CA4P caused massive or scattered brain tumor vascular shutdown and necrosis (N) as shown on MRI and ex vivo assays relative to controls (p<0.01), but with a lower response rate as compared to R1 tumors growing elsewhere [4] and craniofacially in this study (Fig. 2).

Conclusions

Brain tumors seem to be less responsive to VDA, as proven by comparison between intra- and extra-cranial tumors, which could be solved by interventional transarterial OncoCiDia [5].

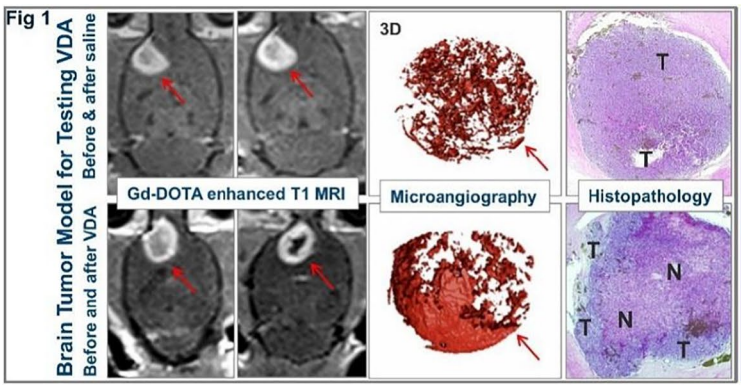

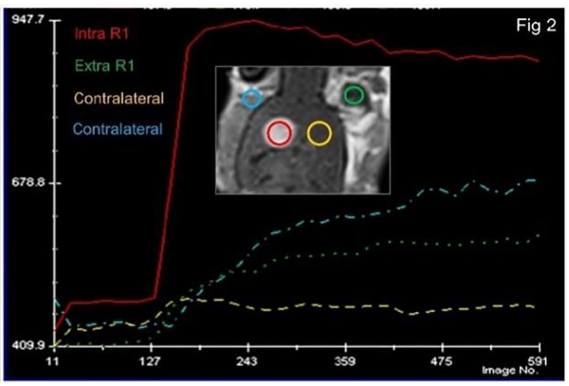

References

1. Li J, et al. A dual-targeting anticancer approach: soil and seed principle. Radiology 2011; 260: 799.
2. Wang SC, et al. A review on curability of cancers: more efforts for novel therapeutic options are needed. Cancers 2019; 11: 1782.
3. Boire A, et al. Brain metastasis. Nature Reviews Cancer 2020; 20: 4-11.
4. Liu Y, et al. Micro-HCCs in rats with liver cirrhosis: paradoxical targeting effects with vascular disrupting agent CA4P. Oncotarget 2017; 8: 55204. 5. He JT, et al. Pictorial imaging-histopathology…… International Journal of Medical Sciences 2020; 17: 2269-2275.

Declarations

Conflict of Interest

Yicheng Ni is one of the founders of the company OncoCiDia Ltd. UK. The other authors disclosed no financial interest.

026-MPI/MRI Cell Tracking of ALS Patient-Derived, Genome-Corrected iPSCs and iPSC-Derived Motor Neurons

Ali Shakeri-Zadeh[1], Mollie O'Brien[1], Alexandra Johns[1], Brice Tiret[2], Adnan Bibic[1,3], Nicholas Maragakis[1], Geoffrey Cotin[4], Delphine Felder-Flesch[4], Jeff W.M. Bulte[1,3]

[1]Johns Hopkins University School of Medicine, Baltimore, MD, USA
[2]Magnetic Insight Inc., Alameda, CA, USA
[3]Hugo W. Moser Institute, Kennedy Krieger Inc., Baltimore, MD, USA
[4]SuperBranche, Strasbourg, France

Background

Amyotrophic lateral sclerosis (ALS) is a progressive neurodegenerative disorder characterized by rapid and unremitting degeneration of motor neurons (MNs). Mutations in the gene superoxide dismutase 1 (SOD1) are the main causative factor for developing familial ALS, occurring in approximately 20% of patients. Isogenic induced pluripotent stem cell (iPSC)-based therapies aimed at restoring the presence of normal MNs in patients with ALS represents an attractive therapeutic approach, but patient-derived cells cannot be used until genetically corrected (1). When pursuing mutant SOD1-corrected iPSC cell therapy in patients, it is highly desirable to have non-invasive imaging techniques available that can report longitudinally on the fate of transplanted cells. In order to track mutant SOD1-corrected iPSCs *in vivo* with MPI and MRI, as part of the NIH somatic cell gene editing program (2), we have developed optimized magnetic labeling protocols for this purpose.

Methods and Materials

CS0002 and 39B2.5 iPSC lines were selected as normal and ALS patient-derived mutant SOD1-corrected iPSCs, respectively, and then differentiated into MNs through neural precursor cells (NPCs) as intermediate. Undifferentiated and differentiated cells were magnetically labeled with and without the transfection agent poly-L-lysine (PLL), using the commercial SPIO formulations Resovist? and dendronized SuperSPIO20® (3). Matrigel and laminin-coating of tissue culture plates, needed for structural support of iPSCs and MNs, was problematic as the coating absorbed near all SPIOs added to the medium. To overcome this obstacle, iPSCs or MNs were first collected and then incubated with 75 ?g Fe (with or without 1125 ng PLL) per ml of medium in 6-well ultra-low attachment plates for 6h. Prussian Blue staining and a Ferrozin-based spectrophotometric assay were used to assess intracellular iron uptake. T2-weighted MRI was performed at 11.7T using a horizontal bore Bruker Biospec scanner. MPI was performed at high-sensitivity mode using a Magnetic Insight Momentum scanner.

Results

SuperSPIO20 and Resovist labeled equally, but only when PLL was used for Resovist, whereas for SuperSPIO20 this was not required. The MPI performance of SuperSPIO20 was about 20% higher than that for Resovist. The lower limit of detection for MPI and MRI using SuperSPIO20 was 5x103 and 5x104 cells/500 ?l, respectively, with iron uptake levels between 9 and 13 pg Fe/cell. Viability of SuperSPIO20-labeled iPSCs and iPSC-derived MNs was 94–99%. The percentage of MN-positive cells (choline acetyl transferase-positive cells) was similar for both SuperSPIO20-labeled and unlabeled NPCs (Fig. 1).

Conclusions

Optimizing protocols is imperative for each cell specific cell type, in particular when using iPSCs. With our newly installed momentum MPI scanner, we are now performing *in vivo* tracking studies of genome-edited iPSC-derived cells in a transgenic mouse model of ALS.

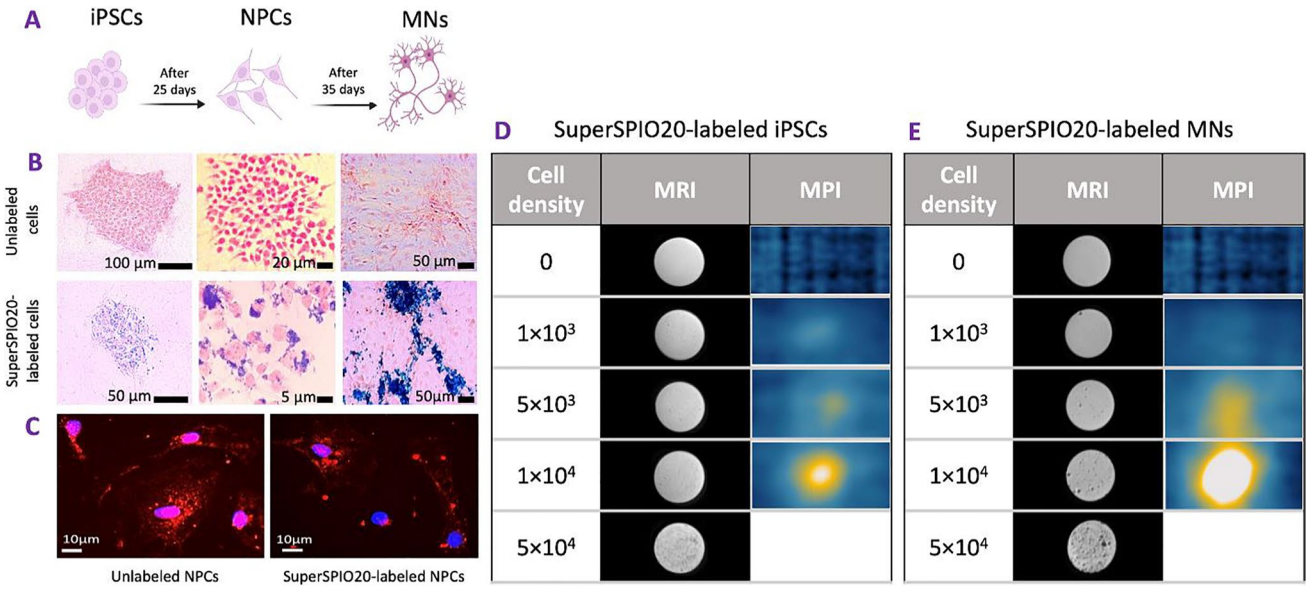

Figure caption: (A) Outline of cell differentiation and time frame. (B) Prussian Blue staining of SuperSPIO20-labeled cells. (C) Differentiation of NPCs into MNs for SuperSPIO20-labeled and unlabeled-NPCs. (D,E) MRI and MPI of SuperSPIO20-labeled iPSCs and MNs. Cell den

References

1. Kiskinis E, Sandoe J, Williams LA, Boulting GL, Moccia R, Wainger BJ, et al. Pathways Disrupted in Human ALS Motor Neurons Identified through Genetic Correction of Mutant SOD1. Cell Stem Cell. 2014;14(6):781-95.
2. Saha K, Sontheimer EJ, Brooks P, Dwinell MR, Gersbach CA, Liu DR, et al. The NIH somatic cell genome editing program. Nature. 2021;592(7853):195-204.
3. Cotin G, Blanco-Andujar C, Nguyen D, Affolter C, Boutry S, Boos A, et al. Dendron based antifouling, MRI and magnetic hyperthermia properties of different shaped iron oxide nanoparticles. Nanotechnology. 2019;30(37):374002.

Declarations

Conflict of Interest

The author Jeff Bulte has disclosed a financial interest in this abstract. The other authors disclosed no financial interest.

027- Gadolinium Labeled Macrophage-derived Exosome as a Magnetic Resonance Imaging Contrast Agent

Ramesh Marasini[1,2,3], Sagar Rayamajhi[1,2], Santosh Aryal[4*]

[1]Kansas State University, Manhattan, KS, USA
[2]Nanotechnology Innovation Center of Kansas State (NICKS), Kansas State University, Manhattan, KS, USA
[3]The Johns Hopkins University School of Medicine, Baltimore, MD, USA
[4]The University of Texas, Tyler, TX, USA

Background

During the last two decades, varieties of organic and inorganic nanomaterials have been extensively explored as a delivery vehicle for drugs and/or contrast agents in preclinical and clinical settings. These nanostructured agents rely on their surface chemistry to perform better in an in-vivo environment, for example, they can take advantage of leaky tumor vasculature to dislodge its cargo. While the advancement in nanotechnology has reached a different level yet possible clearance by the immune system as a foreign material limits its application. To tackles these problems, attention has been shifted towards the design of next-generation delivery vehicles that can deliver their payload while bypassing or collaborating with the biological barriers mimicking the way cells "talk." Henceforth, we selected immune cell-derived exosomes as a biological nanocarrier to deliver the payload. Exosomes are cell-released nanovesicles that are involved in the intercellular transportation of materials including protein, nucleic acid, and lipids. We hypothesize that exosomes derived from immune cells will accumulate within tumors, prolong the retention time for contrast enhancement, and have the potential for both tumor location or drug delivery owing to their endogenous functionality,

intrinsic targeting property, and ability to cooperate with a host defense mechanism.

Methods and Materials

Mouse macrophage (J J774A.1)-derived exosomes were labeled with gadolinium chelated lipid or near-infrared dye. The size, concentration, and morphology of exosomes before and after labeling were charactered by light scattering techniques and transmission electron microscopy, exosome markers were analyzed by western blot, and gadolinium was quantified by ICP-MS. The labeling efficacy, accumulation, and physiological effect of labeled exosomes on human and mouse osteosarcoma cell lines *in vitro* were examined by fluorescence resonance energy transfer, viability assay, confocal microscopy, and flow cytometry. Exosome accumulation within ectopic osteosarcoma tumor-bearing mice was determined by 3.0 T MRI or optical imaging after intravenous injection and compared with gadopentetate dimeglumine, Magnevist® (Bayer).

Results

Gadolinium-labeled exosome showed a preferential cellular interaction and accumulation towards cancer cells compared to non-cancer cells, both *in vitro* and *in vivo*. Gadolinium-labeled exosome showed a higher r1 relaxivity of 9.86 mM?1s?1 compared to 3.98 mM?1s?1 of Magnevist®. Importantly, labeled exosomes showed excellent contrast enhancement in the blood vasculature with a higher retention time compared to Magnevist®.

Conclusions

These results suggest that macrophage exosomes accumulate within tumor cells *in vitro* and *in vivo* after infusion. Therefore, gadolinium-labeled exosomes can help to reduce gadolinium dose and accelerate the development of safer MRI contrast agents.

Declarations

Conflict of Interest

The authors declare no competing interests.

028-Fluorescent ChoK? Inhibitor for Intraoperative Tumor Imaging in a Veterinary Clinical Trial

Sofya Osharovich, Michael Hart, Stefan Harmsen, Anatoily V. Popov, Jennifer Huck, Amy Durham, Sunil Singhal, David Holt, James Delikatny

University of Pennsylvania, Philadelphia, PA, USA

Background

Choline kinase ? (ChoK?), an enzyme overexpressed in 60% of human lung tumors, is associated with an aggressive phenotype, high histological tumor grade, and poor clinical outcome 1-2 . ChoK? catalyzes choline phosphorylation to generate phosphocholine, a precursor of phosphatidylcholine 3. We have developed JAS239, a novel near-infrared (NIR) fluorescent ChoK? inhibitor, which competitively inhibits ChoK?, decreasing phosphocholine production. Previously, we used JAS239 to image ChoK?-overexpressing breast and lung tumors in mice, as well as lung metastases 4,5 . We hypothesize that JAS239 can be used as a targeted NIR imaging agent for tumor resection guidance in ChoK?-overexpressing tumors. Here, we translate JAS239 into the veterinary clinic for intraoperative imaging in dogs with spontaneous lung adenocarcinomas.

Methods and Materials

An initial toxicology study was performed using five experimental dogs that received a single dose of JAS239 at 5× the imaging dose (5 mg/kg total). Dogs were observed for signs of toxicity, including lethargy, vomiting, and anorexia. Blood was collected at baseline, 0, 6, 12, 24, 48 h, and 5 days for pharmacokinetics, complete blood count-brief and blood chemistry. The dogs were adopted out at the end of the study. To date, three canine patients with operable lung adenocarcinomas have been recruited into an owner informed consent clinical trial. Patients received either 0.5 or 1 mg/kg JAS239 24h prior to intraoperative imaging using fluorescence guidance. After resection, the tumor was imaged from multiple sides, sections of the tumor were cut, and the borders of fluorescence were marked with sutures for pathological analysis. Excised pieces of the tumors and adjacent normal tissue were imaged using small-animal NIR imaging systems and submitted to Pathology for H&E and immunohistochemistry.

Results

Experimental dogs showed no signs of toxicity and blood results were within normal limits. Pharmacokinetics showed 80% probe elimination by 6h, further indicating low toxicity. Intraoperative imaging showed clear margin delineation with higher fluorescence in the tumor than in normal lung. Initial pathology results found no malignancies at the fluorescent border indicating clear margins.

Conclusions

The purpose of these studies is to establish optimal conditions for imaging JAS239 fluorescence in canine lung tumors. The clinical trial will recruit up to 30 patients to determine the efficacy of JAS239 for detecting tumor margins, identifying residual tumor deposits, lymph node involvement, and detection of micrometastases from lung or other cancers. The ultimate goal is translation of ChoK? sensors for fluorescence guidance during human lung tumor resections.

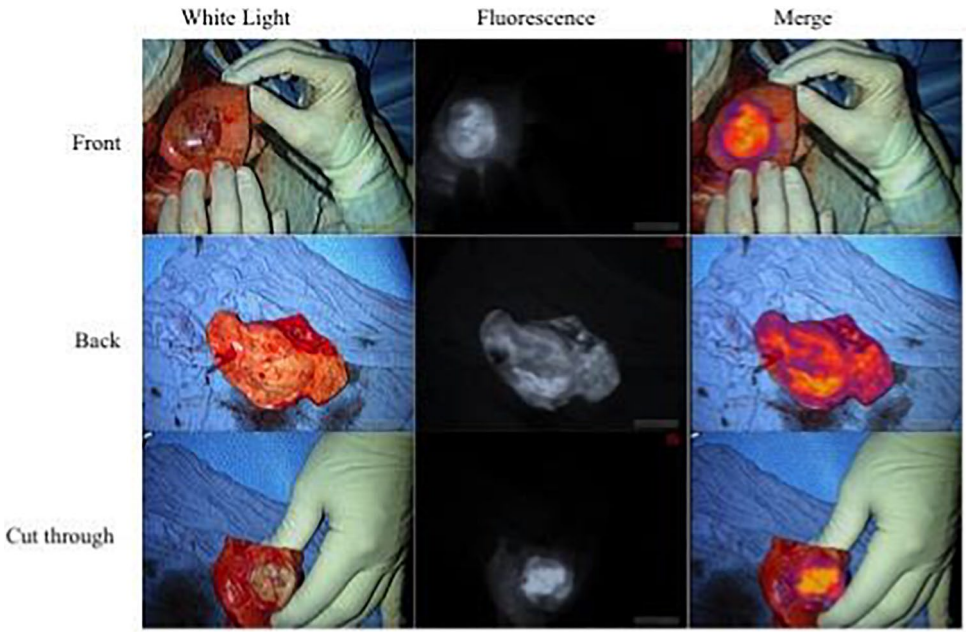

Figure caption: *In situ* and back table imaging of canine lung tumor. White light (left), fluorescent (middle), and merged (right) images of front (top), back (middle), and cut through (bottom) tumor from patient #1. Fluorescence imaging shows higher signal in the tumor t

References

1. Ramírez de Molina A, Sarmentero-Estrada J, Belda-Iniesta C, Tarón M, Ramírez de Molina V, Cejas P, Skrzypski M, Gallego-Ortega D, de Castro J, Casado E, García-Cabezas MA, Sánchez JJ, Nistal M, Rosell R, González-Barón M, Lacal JC. Expression of choline kinase alpha to predict outcome in patients with early-stage non-small-cell lung cancer: a retrospective study. The Lancet Oncology 2007; 8; 889-97. PMID: 17851129.
2. Ramírez de Molina A, Rodríguez-González A, Gutiérrez R, Martínez-Piñeiro L, Sánchez J, Bonilla F, Rosell R, Lacal J. Overexpression of choline kinase is a frequent feature in human tumor-derived cell lines and in lung, Prostate, and Colorectal Human Cancers. Biochemical and Biophysical Research Communications 2002; 296; 580-83. PMID: 12176020.
3. Arlauckas SP, Popov AV, Delikatny EJ. Choline kinase alpha-Putting the ChoK-hold on tumor metabolism. Progress in Lipid Research 2016; 63; 28-0. PMID: 27073147.
4. Arlauckas SP, Popov AV, Delikatny EJ. Direct inhibition of choline kinase by a near-infrared fluorescent carbocyanine. Molecular Cancer Therapeutics 2014; 13; 2149-2158. PMID: 25028471.
5. Arlauckas SP, Kumar M, Popov AV, Poptani H, Delikatny EJ. Near infrared fluorescent imaging of choline kinase alpha expression and inhibition in breast tumors. Oncotarget 2017; 8; 16518-16530. PMID: 28157707.

Declarations

Conflict of Interest

The authors declare no competing interests.

029-Iron-Chelate Based Redox Probe for MR Imaging of Aneurysmal Inflammation

Robert M. King, Eric J. Schmidt, Eric Gale*, Anita Leporati, Peter Caravan*, Matthew J. Gounis, Alexei A Bogdanov, Jr

University of Massachusetts Medical School, Worcester MA, USA
A. Martinos Center for Biomedical Imaging, Massachusetts General Hospital, Charlestown MA, USA

Background

Fe-PyC3A is a novel MR contrast agent that, in the presence of various biologically relevant oxidizers such as hydrogen peroxide, undergoes rapid transition from iron oxidative state 2+ to 3+ with simultaneous increase of molar relaxivity (r1,2) [1]. The transition leads to a rapid increase of T1-weighted MR signal intensity. We sought to perform

testing of Fe-PyC3A for imaging vascular inflammation in a recently developed model of in situ decellularized saccular aneurysm that exhibits characteristic aneurysmal expansion and sustained inflammation [2].

Methods and Materials

Aneurysm model was created by using elastinolysis of the right common carotid artery in rabbits (n=5). Aneurysmal inflammation was induced as in [2]. Dynamic MRI (T1-FFE, TR/TE 21/4ms, FA 20o) and respiratory gated MSDE (SR prepulse= 650 ms, TR/TE 2500/6ms, FA 90o V-enc= 1) were performed pre- and post- IV injection of 0.2 mmol Fe-PyC3A /kg, 0.1 mmol ascorbate/kg. A myeloperoxidase (MPO)-specific Gd-5HT-DOTAGA agent was used as a positive control [3]. MRI after gadobutrol injection (0.1 mmol Gd/kg) was performed 7d post Fe-PyC3A-assisted MRI. LPS-mediated inflammation was induced as in [4]. Distribution of MPO+ cells was imaged using Cy3-5HT substrate [5].

Results

The oxidation of Fe(II)PyC3A by H2O2 *in vitro* lead to a rapid increase of transverse molar relaxivity r2, which was attenuated by ascorbate. Dynamic MRI *in vivo* after the injection of Fe-PyC3A showed a strong increase of MR signal at the peak with ER=1.33±0.04 (Fig. 1B). The delayed enhancement of the aneurysmal wall was present on MSDE MRI (ER=1.24±0.06). Control injection of gadobutrol after a 3h delay resulted in significantly lower ER=1.07±0.03 on MSDE MRI (p<0.05). MPO-specific MRI resulted in overall higher ER=1.63±0.20, Fig. 1E. The colocalization of aneurysmal Fe-PyC3A MR signal and MPO marker enzyme expression was demonstrated by fluorescent microscopy of MPO enzymatic activity: 577±48 MPO positive cells/section were present in decellularized aneurysms vs. 17±6 in control ones (Fig. 1F).

Conclusions

1) Hydrogen peroxide-mediated Fe-PyC3A oxidation results in strong relaxivity increase; 2) dynamic and delayed contrast-assisted MRI showed that Fe-PyC3A results in MR signal enhancement coinciding with the presence of MPO, a marker of vascular inflammation; 3) the results of delayed MRI acquisitions suggests that Fe-PyC3A may potentially provide dynamic and delayed vascular inflammation MR sensing in clinical settings with few concerns related to metal toxicity.

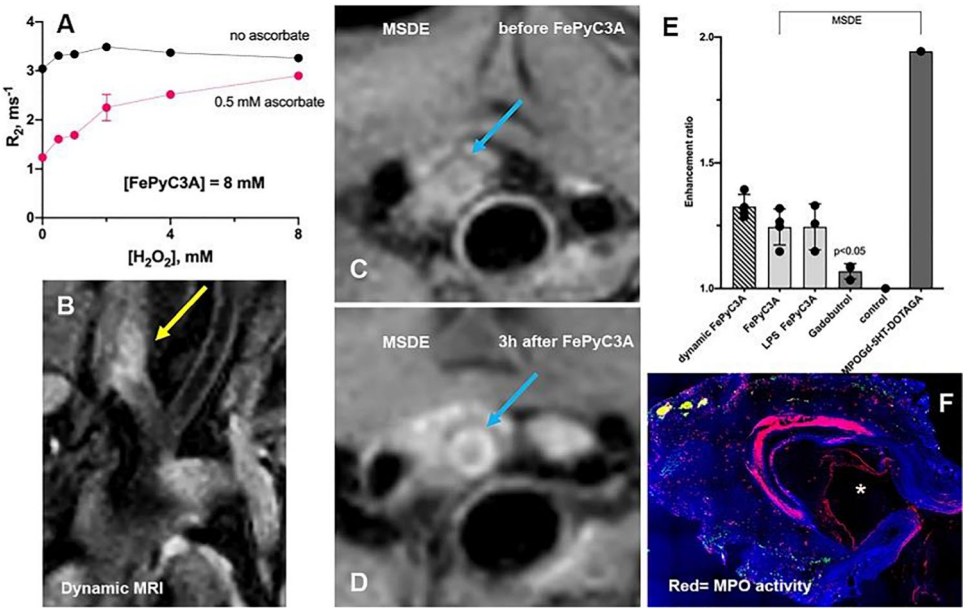

Figure caption: *In vitro* (A) and *in vivo* (B–E) testing of Fe-PyC3A with microscopy corroboration (F)

References
1. Wang H, Jordan VC, Ramsay IA, et al. Molecular Magnetic Resonance Imaging Using a Redox-Active Iron Complex. J Am Chem Soc 2019; 141; 5916-5925.
2. King RM, Caroff J, Langan ET, et al. In situ decellularization of a large animal saccular aneurysm model: sustained inflammation and active aneurysm wall remodeling. J Neurointerv Surg 2021; 13; 267-271.
3. Rodriguez-Rodriguez A, Shuvaev S, Rotile N, et al. Peroxidase Sensitive Amplifiable Probe for Molecular Magnetic Resonance Imaging of Pulmonary Inflammation. ACS Sens 2019; 4; 2412-2419.
4. DeLeo MJ, 3rd, Gounis MJ, Hong B, Ford JC, Wakhloo AK, Bogdanov AA, Jr. Carotid artery brain aneurysm model: *in vivo* molecular enzyme-specific MR imaging of active inflammation in a pilot study. Radiology 2009; 252; 696-703.
5. Wadghiri, Y.Z., Hoang, D.M., Leporati, A. et al. High-resolution imaging of myeloperoxidase activity sensors in human cerebrovascular disease. Sci Rep 2018; 8; 7687.

Declarations

Conflict of Interest
The authors Eric Gale and Peter Caravan have disclosed financial interest in this abstract. The other authors did not disclose any financial interest.

030-Detecting Zn(II) Secretion Using Mn(II)-Based Magnetic Resonance Imaging Contrast Agent Candidate

Enik Madarasi, Balázs Váradi, Richárd Botár, Enik Molnár, Zoltán Garda, András Zubor, György Trencsényi, János Kiss, Gerg Veres, Imre Tóth, Ferenc. K. Kálmán, Gyula Tircsó

University of Debrecen, Debrecen, Hungary

Background
The scientific community working on imaging probes is aware of the toxicity issues evidenced recently for certain Gd(III)-based Magnetic Resonance Imaging (MRI) contrast agents (CAs) (nephrogenic systemic fibrosis (NSF), Gd(III) accumulation in tissues etc.) and the urgent need for viable Mn(II)-based contrast agent (CA) alternatives [1,2]. Despite of the efforts made in the past decade, the task of finding Mn(II)-based Gd(III) alternatives remains very challenging because it is very difficult to achieve high inertness for Mn(II) complexes. What is more, Mn(II)-based responsive/smart probes (SCAs) capable of "sensing" various analytes (pH, metal ion concentration, pO2 etc.) are rare likely because the examples of such Gd(III)-based CA candidates often display the worsening of the kinetic properties of complexes upon converting general MRI CA structures into responsive/smart CA candidates (*i.e.*, ongoing form [Gd(DOTA)] to [Gd(DO3A)]-derivatives). Recently we have shown, that the pyclen-3,9-dicatate (3,9-PC2A) ligand form stable complex with Mn(II) endowed with acceptable relaxivity and it can be converted into SCA candidates capable of sensing pH (3,9-PC2A-EA) [3,4]. The aim of the current study is to synthesize a ligand possessing a Mn(II) binding platform (3,9-PC2A) linked to a DPA moiety as a potential Zn(II) responsive SCA candidate (3,9-PC2A-DPA, Figure 1).

Methods and Materials
Ligand was synthesized using standard chemical synthetic techniques, and metal complexes were isolated and characterized by high-pressure liquid chromatography (HPLC), mass spectrometry (MS), and 1H relaxometry. The thermodynamic stability of the Mn(II) complexes were determined by the combination of pH-potentiometry and 1H relaxometry, while solvent exchange kinetics was studied via variable temperature 17O NMR method. Dissociation kinetics of the complexes were studied by studying metal exchange reactions with essential (Cu(II) and Zn(II)) metal ions; and their serum stability was also evaluated by using commercially available human blood serum. T1 and T2-weighted images of phantoms and *in vivo* imaging were acquired at 25°C by using preclinical (Mediso NanoScan PET/MRI 1 T) and clinical (Siemens Magnetom Essenza 1.5 T and Philips Achivea 3T) MRI scanners.

Results
The current study shows that the 3,9-PC2A ligand forms a stable (log K[Mn(3,9-PC2A)] = 17.09, pMn = 8.64) complex with the Mn(II) ion, yet its dissociation remains relatively fast [3]. The attachment of a potential Zn(II) binding moiety (di-(2-picolyl)amine (DPA) unit) to the nitrogen atom being trans- to the pyridine nitrogen atom preserves the thermodynamic stability of the parent compound (log K[Mn(3,9-PC2A-DPA)] =15.87(6) which translates into pMn of 8.79) as well as improves notably the inertness of its Mn(II) complex (t1/2 at pH=6.0 is 64.5 h). The [Mn(3,9-PC2A-DPA)(H2O)] complex possess relatively low relaxivity (3.24 mM-1s-1 at 1.41 T and 37 oC) which is not affected by Zn(II) concentration directly, however in the co-presence of 0.7 mM Human Serum Albumin (HSA) relaxivity values (both r1p and r2p) increase significantly (12.14 and 26.89 mM-1s-1at 1.41 T and 37 oC) owing to the efficient binding of the complex to the HSA (log Kaff=3.5?0.1 M-1).

Conclusions
We have demonstrated that the PC2A platform can be used to build smart/responsible MRI CA's. The attachment of the DPA (Zn(II) binding) moiety to the parent 3,9-PC2A

returned a Mn(II) complex capable of visualizing the glucose stimulated Zn(II) secretion (GSZS) in the prostate of healthy mice as proved by MRI. With the Gd(III) alternative SCA candidate presented in this work, the field of functional Zn(II) MR imaging is receiving a potent tool to enable an essential progress.

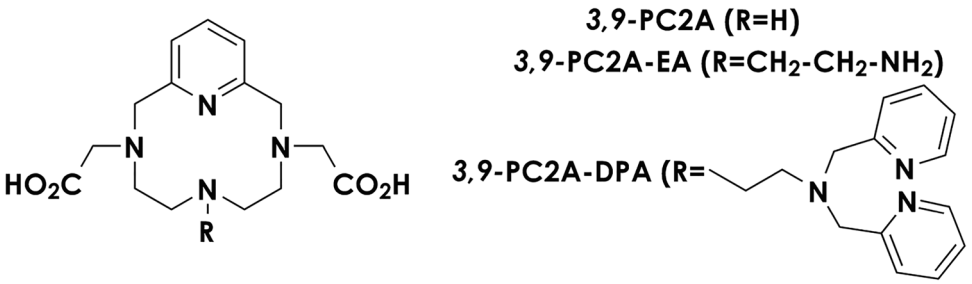

Fig. 1 Formulae of the 3,9-PC2A, 3,9-PC2A-EA, and 3,9-PC2A-DPA

References

1. Grobner T, Gadolinium - a specific trigger for the development of nephrogenic fibrosing dermopathy and nephrogenic systemic fibrosis? Nephrol. Dial. Transplant. 2006; 21; 1104-1108.
2. Kanda T, Ishii K, Kawaguchi H, Kitajima K, Takenaka D. High signal intensity in the dentate nucleus and globus pallidus on unenhanced T1-weighted MR images: relationship with increasing cumulative dose of a gadolinium-based contrast material. Radiology 2006; 270; 834-841.
3. Garda Z, Molnár E, Hamon N, Barriada JL, Esteban-Gómez D, Váradi B, Nagy V, Pota K, Kálmán FK, Tóth I, Lihi N, Platas-Iglesias C, Tóth É, Tripier R, Tircsó G. Complexation of Mn(II) by Rigid Pyclen Diacetates: Equilibrium, Kinetic, Relaxometric, Density Functional Theory, and Superoxide Dismutase Activity Studies. Inorg. Chem. 2021; 60(2); 1133-1148.
4. Botár R, Molnár E, Trencsényi G, Kiss J, Kálmán FK, Tircsó G. Stable and Inert Mn(II)-Based and pH-Responsive Contrast Agents. J. Am. Chem. Soc. 2020; 142(4); 1662-1666.

Declarations

Conflict of Interest

The authors declare no competing interests.

031-Elemental Imaging and Speciation Analysis of Gadoterate in Rat Kidney Samples

Mariane Le Fur[1], Iris Zhou[1], Alana Ross[1], Nicholas Rotile[1], Julie Ha[1], Pamela Pantazopoulos[1], Andrei Astashkin[2], Brian Jackson[3], Peter Caravan[1]

[1]Massachusetts General Hospital and Harvard Medical School, Charlestown, MA, USA
[2]University of Arizona, Tucson, AZ, USA
[3]Dartmouth College, Hanover, NH, USA

Background

Gadolinium-based contrast agents (GBCAs) are retained *in vivo* even in patients with normal renal function, but the long-term consequences remain unknown 1. Rodent studies of Gd retention consistently show that the organ with the highest Gd concentration is the kidney 2-4. Here we use MR imaging, elemental mapping, and electron paramagnetic resonance (EPR) spectroscopy to evaluate the pharmacokinetics, distribution, and speciation of gadoterate in rats.

Methods and Materials

Eight female Wistar rats (8-week-old) received 10 daily doses of gadoterate (Dotarem, Guerbet) at 2.0 mmol/kg. Age-matched naive rats were used as controls. 3D T1-weighted ultrashort echo time (UTE) images were acquired on a 4.7T scanner (Bruker) at 3, 17, 34, and 52 days after the last injection of gadoterate. The MR signal intensity (SI) of the kidney cortex was normalized to the SI of a phantom. Four rats per group were euthanized at the end of the scanning session at 3 and 52 days p.i. and the Gd concentrations in 18 organs and tissues were determined by inductively coupled plasma mass spectrometry (ICP-MS). The Gd distribution in the right kidney was determined by laser ablation ICP-MS. Gd speciation in the left kidney cortex was investigated using two EPR techniques: Electron Nuclear Double Resonance (ENDOR) and Electron Spin Echo Envelope Modulation (ESEEM).

Results

UTE MR images showed a significantly higher (except at 52 days p.i.) normalized SI in the cortex of gadoterate dosed animals compared to the control group (Fig. 1A). For the gadoterate group, the cortex SI decreased with time indicating a slow clearance of gadoterate (Figure 1B). Despite no significant SI enhancement at day 52, ICP-MS (CGd = 177 ± 39 nmol/g) and LA-ICP-MS clearly show high Gd levels remaining (Figure 1C). The ENDOR and ESEEM spectra of a rat kidney cortex harvested at 52 days p.i. are similar to the reference Gd-DOTA spectra (Fig. 1D) indicating that the majority of gadoterate is present in that organ in its chelated form.

Conclusions

The kidney cortex is the target organ for gadoterate in rats as revealed by ICP-MS, UTE MRI, and LA-ICP-MS. However, T1w MRI is not particularly sensitive to detecting retained Gd in the kidney. EPR spectroscopy shows that the majority of Gd is present as intact gadoterate over 7 weeks after the last administration.

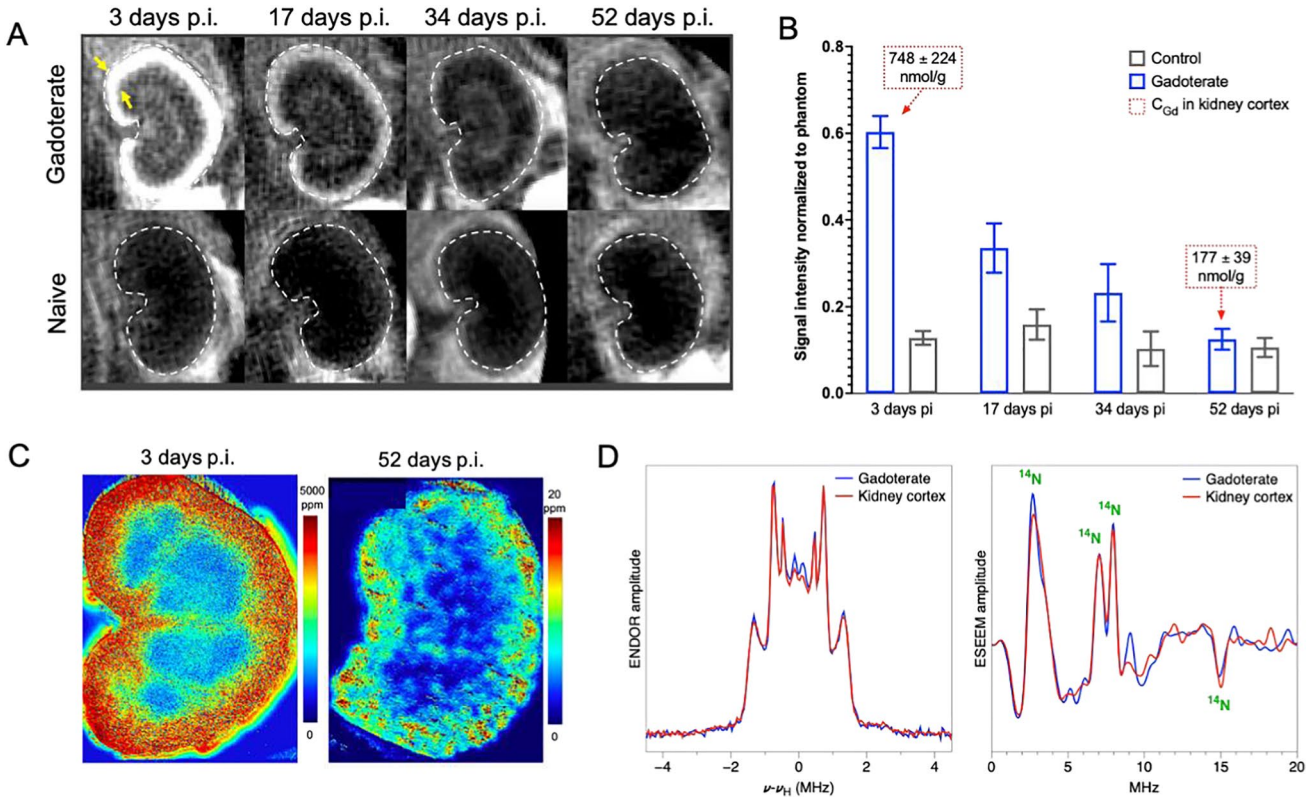

Figure caption: A) UTE MR images of rat kidneys at 3, 17, 34, and 52 days post injection of gadoterate, B) corresponding SI of the kidney cortex, C) Gd maps of sliced kidney from rats exposed to gadoterate, D) EPR spectra of the cortex (52 days pi) compared to Gd-DOTA

References

1. Le Fur M and Caravan P. The biological fate of gadolinium-based MRI contrast agents: a call to action for bioinorganic chemists. Metallomics 2019; 11; 240-254.
2. Bussi S, Coppo A, Botteron C, Fraimbault V, et al. Differences in gadolinium retention after repeated injections of macrocyclic MR contrast agents to rats. Journal of Magnetic Resonance Imaging 2018; 47; 746-752.
3. Bussi S, Coppo A, Celeste R, Fanizzi A, et al. Macrocyclic MR contrast agents: evaluation of multiple-organ gadolinium retention in healthy rats, Insights into Imaging 2020; 11; 11.
4. Mcdonald RJ, Mcdonald JS, Schroeder D, Jentoft ME, et al. Comparison of Gadolinium Concentrations within Multiple Rat Organs after Intravenous Administration of Linear versus Macrocyclic Gadolinium. Radiology 2017; 285; 536-545

Declarations

Conflict of Interest

The authors declare no competing interests.

032-Detection of D- and L-Lactate in Erythrocytes and Cancer Cells by Use of a Chiral NMR Shift Reagent

Eul Hyun Suh[1], Carlos F.G.C. Geraldes[2], Sarah Chirayil[1], Brandon Faubert[1], Raul Ayala[3], Ralph DeBerardinis[1], A. Dean Sherry[1,8*]

[1]University of Texas Southwestern Medical Center, Dallas, TX, USA
[2]University of Coimbra, Coimbra, Portugal
[3]School of Health Professions at Yvonne A. Ewell Townview Center, Dallas, TX, USA
[4]University of Texas at Dallas, Richardson, TX, USA

Background

Excessive lactate production, a hallmark of cancer, is largely formed by reduction of pyruvate via lactate dehydrogenase (LDH) to L-lactate. Although D-lactate can also be produced from glucose via the methylglyoxal pathway in small amounts, less is known about the amount of D-lactate produced in cancer cells [1, 2]. Since the stereoisomers of lactate cannot be distinguished by conventional 1H NMR spectroscopy, a chiral NMR shift reagent was used to fully resolve the 1H NMR resonances of D- and L-lactate [3]. Here, we demonstrated the feasibility of using Yb3 for enantiomeric discrimination of D- and L-lactate produced in Erythrocytes and cancer cells.

Methods and Materials

Production of L-lactate from glucose and D-lactate from methyl glyoxal was first demonstrated in freshly isolated red blood cells using the chiral NMR shift reagent, YbDO3A-trisamide. Then, two different cell lines with high GLO1 expression (H1648 and H 1395) were selected from a panel of over 80 well-characterized human NSCLC cell lines [4] and 3553T3 cells, grown to confluence in standard tissue culture media, washed with phosphate buffered saline, and exposed to glucose or methylglyoxal in basal media for 4 h. After 4 h, a small volume of extracellular fluid was collected and mixed with YbDO3A-trisamide for analysis by 1H NMR spectroscopy and CEST.

Results

A suspension of freshly isolated red blood cells exposed to 5 mM glucose produced L-lactate as expected but very little D-lactate. To evaluate the utility of the chiral NMR shift reagent, methylglyoxal was then added to red cells along with glucose to stimulate production of D-lactate via the methylglyoxal pathway. In this case, both D-lactate and L-lactate were produced and their NMR chemical shifts assigned. NSCLC cell lines with differing expression levels of GLO1 produced both L- and D-lactate after incubation with glucose and glutamine alone. A GLO1-deleted parental cell line (3553T3) showed no production of D-lactate from glucose while re-expression of GLO1 resulted in higher production of D-lactate.

Conclusions

The shift reagent aided NMR technique demonstrate that D-lactate is produced from glucose in NSCLC cells via the methylglyoxal pathway. The biological role of D-lactate is uncertain but a convenient method for monitoring D-lactate production could provide new insights into the biological roles of D- versus L-lactate in cancer metabolism. This NMR techniques could potentially be applied *in vivo* to image D- and L-lactate production in tumors using either magnetic resonance spectroscopy (MRS) or CEST.

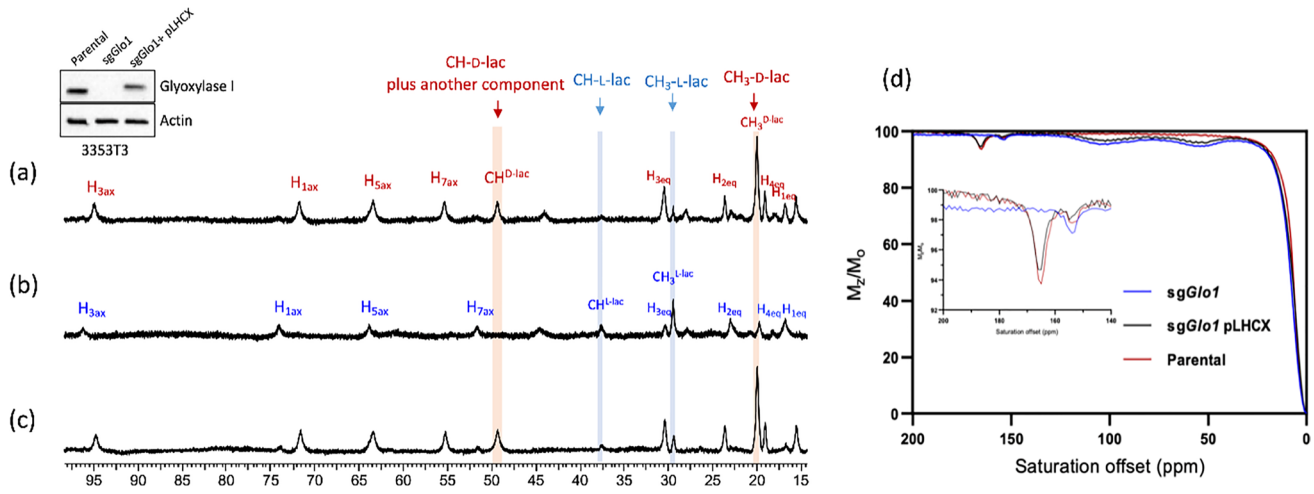

Figure caption: 1H NMR and CEST spectra of media collected from (a) sgGlo1 pLHCX (re-expressed GLO1 cells) (b) sgGlo1 (GLO1 deleted cells) and (c) parental 3353T3 cells (d) CEST using Yb3 after incubation with 5mM methylglyoxal (MG) in DMEM media for 4hr, 37°C

References
1. Thornalley PJ. The glyoxalase system: new developments towards functional characterization of a metabolic pathway fundamental to biological life. Biochem J.1990; 269(1); 1-11.
2. de Bari L, Moro L, Passarella S. Prostate cancer cells metabolize d-lactate inside mitochondria via a d-lactate dehydrogenase which is more active and highly expressed than in normal cells. FEBS Letters, 2013; 587(5); 467-473.
3. Zhang L., Martins AF, Zhao P, Tieu M, Esteban-Gómez D, McCandlesset GT, et al. Enantiomeric Recognition of d- and l-Lactate by CEST with the Aid of a Paramagnetic Shift Reagent. J. Am. Chem. Soc. 2017; 139(48); 17431-17437.
4. Chen PH, Cai L, Huffman K, Yang C, Kim J, Faubert B, et al. Metabolic Diversity in Human Non-Small Cell Lung Cancer Cells. Mol Cell, 2019; 76(5): 838-851.e5

Declarations

Conflict of Interest
Ralph J. DeBerardinis is advisor for Agios Pharmaceuticals and Vida Ventures. Other authors declare that they have no competing interests.

033-Building a Magnetosome-Like Nanoparticle for MRI Using Essential Bacterial Genes

Qin Sun[1,2], Prushoth Vivekanantha[1], Cécile Fradin[3], Terry Thompson[1,2], Frank S. Prato[1,2], Donna E. Goldhawk[1,2]

[1]Lawson Health Research Institute, London, Canada
[2]University of Western Ontario, London, Canada
[3]McMaster University, Hamilton, Canada

Background
With its superb spatial and temporal resolution, magnetic resonance imaging (MRI) has great potential to track cellular activities that define early stages of disease [1]. To improve molecular imaging techniques, we are developing MRI reporter gene expression based on the magnetosome. In magnetotactic bacteria (MTB), magnetosome formation compartmentalizes iron biominerals in membrane-enclosed vesicles [2]. Biosynthesis of magnetosome-like nanoparticles in mammalian cells would provide an endogenous magnetic resonance (MR) contrast agent under genetic control [3]. This patented technology would provide long-term molecular imaging for tracking cellular and molecular activities throughout the cell's life cycle. Hypothesis: Essential magnetosome proteins interact in any cell type to form rudimentary magnetosome-like nanoparticles, providing a genetically-controlled contrast agent for molecular MRI.

Methods and Materials
MTB genes mamE, mamB, mamI, and mamL were cloned from M. magneticum sp. AMB-1 genomic DNA by PCR and inserted into fluorescent vectors to create Mam fusion proteins then stably expressed in human MDA-MB-435 melanoma cells. Cines of fluorescent elements detected in intact cells were captured with confocal microscopy (Nikon A1R) and analyzed using the ImageJ Mosaic Particle Tracker 2D/3D plugin for Brownian motion and velocity. To obtain longitudinal and transverse relaxation rates, cells expressing GFP-MamE, Tomato-MamB, GFP-MamI, Tomato-MamL, or FLAG-MamL/GFP-MamI supplemented with 250 μM ferric nitrate, harvested, mounted in a gelatin phantom, and scanned at 3 Tesla (Biograph mMR) [4]. Statistical analyses were performed in GraphPad Prism 8.

Results
Tomato-MamL, Tomato-MamL/GFP-MamI, and Tomato-MamB all express punctate, mobile fluorescence, while GFP-MamE expresses punctate but immobile fluorescence. Analysis of motility revealed that velocity of Tomato-MamL/GFP-MamI particles was 3-fold greater than the velocity of Tomato-MamL alone (6.4 ± 2.2 vs 2.0 ± 0.7 μm/s; $p<0.01$). Tomato-MamB particles travel at 1.94 ± 0.7 μm/s, comparable to the velocity of Tomato-MamL alone. Relaxation rates (Fig. 1) of iron-supplemented cells expressing Tomato-MamB, GFP-MamI, or Tomato-MamL have significantly higher R^2 and R^2* than non-supplemented cells. Interestingly, iron-supplemented cells expressing GFP-MamE or co-expressing FLAG-MamL/GFP-MamI had relaxation rates comparable to unsupplemented cell types.

Conclusions
This is the first report characterizing essential magnetosome proteins MamE, MamB, MamI, and MamL in mammalian cells and demonstrating their effects on mammalian MR relaxation rates. Analysis of motion shows MamL and MamB travel at velocities comparable to transport kinesins when expressed alone, while co-expressed MamI-MamL particles travel at velocities comparable to myosin and axonemal dynein [5]. Expression of either MamB, MamI, or MamL increases transverse relaxation rates; however, co-expression of MamI and MamL reduces them again, suggesting a regulatory effect of magnetosome gene combinations. Future work will examine the potential of MamB and MamE to interact with the MamI-MamL particle and augment cellular MR parameters.

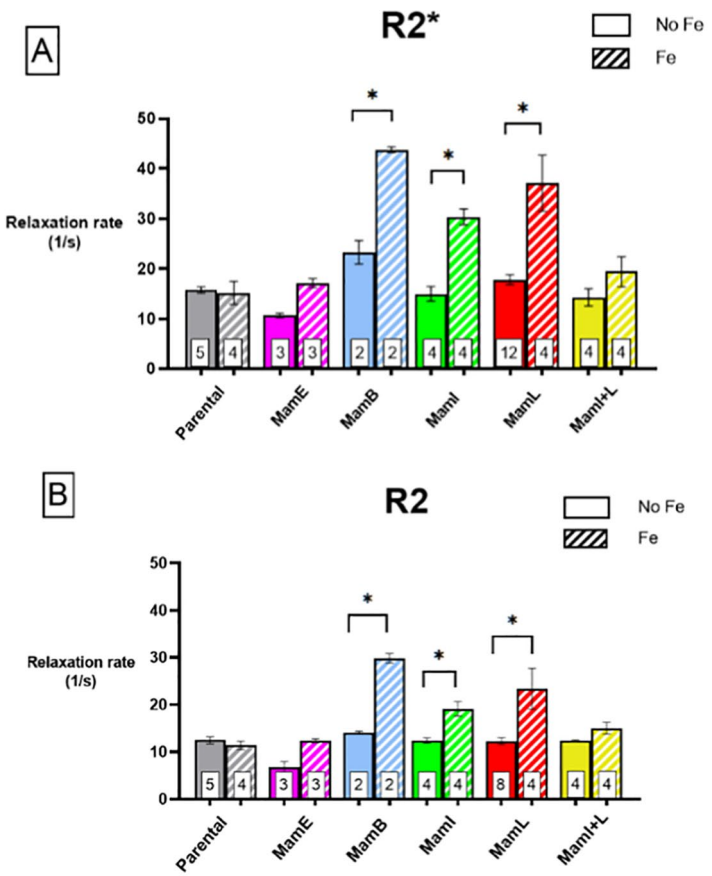

Figure 1. Transverse relaxation rates of essential magnetosome proteins expressed in mammalian cells. R2* **(A)** and R2 **(B)** relaxation rates of parental MDA-MB-435 cells, grown with and without iron supplement, are compared to those expressing GFP-MamE, Tomato-MamB, GFP-MamI, Tomato-MamL, and FLAG-MamL/GFP-MamI. Significant differences are denoted with an asterisk.

References

1. Goldhawk DE, Gelman N, Thompson RT, Prato FS. In: Design and Applications of Nanoparticles in Biomedical Imaging, Bulte JWM, Modo MMJ, Eds. Springer International Publishing, Cham, 2017; 187-293.
2. Uebe R, Schuler D. Magnetosome biogenesis in magnetotactic bacteria. Nat Rev Microbiol 2016; 14; 621-637.
3. Sun Q, Prato FS, Goldhawk DE. In: Bioimaging: Imaging by Light and Electromagnetics in Medicine and Biology, Ueno S, Ed. CRC Press & Taylor Francis Group, 2020; 201-214
4. Sengupta A, Quiaoit K, Thompson RT, Prato FS, Gelman N, Goldhawk DE. Biophysical features of MagA expression in mammalian cells: implications for MRI contrast. Front Microbiol 2014; 5; 1-9.
5. Howard J. In: Mechanics of Motor Proteins and the Cytoskeleton. Sinauer Associates: Sunderland, MA, 2001.

Declarations

Conflict of Interest

The authors declare no competing interests.

034- Precise and Noninvasive Detection of Liver Metastases and Progression by Protein MRI Contrast Agents

Jingjuan Qiao[1,2], Zongxiang Gui[1], Shanshan Tan[1], Hua Yang[3], Hans Grossniklaus[3], Nan Wang[4], Yiting, Xu[2], Oluwatosin Y. Ibhagui[1], Mani Salarian[1], Yuguang Meng[3], Philip Sun[3], Yibin Xie[4], Gregory Lesinski[3], Zhiren Liu[1], Debiao Li[4], Zhijun Wang[4], Eki Seki[4], Jenny Yang[1,2*]

[1]Georgia State University, Atlanta, GA, USA
[2]InLIghta Biosciences, Atlanta, GA, USA
[3]Emory University, Atlanta, GA, USA
[4]Cedars Sinai Medical Center, Los Angeles, CA, USA

Background

Liver is the most common organ for cancer metastasis, especially uveal melanoma (UM), ovarian cancer, colorectal cancer (CRC), and pancreatic ductal adenocarcinoma (PDAC). There is a pressing medical need to develop non-invasive imaging to detect early-stage metastases for optimal treatment. Here we report our development of severalprotein MRI contrast agents (ProCA32s) by engineering Gd3+ and Mn2+binding sites in a scaffold protein to enable precision imaging of various molecular biomarkers by MRI (pMRI)

Methods and Materials

Gd3+ and Mn2+ contrast agents targeted to Collagen, CXCR4 and CXCL12 (denoted as ProCA32.Collagen1, ProCA32.CXCR4 and ProCA32.CXCL12) were developed by engineering of the biomarker targeting moiety to novel protein contrast agent ProCA32 with created Gd3+ or Mn2+ binding sites. Their relaxivity were determined at 1.4 and 7T. UM models were developed by inoculating different UM cells with different CXCR4 expression levels into mouse eyes. Micrometastases in the mouse liver were expected in 4–6 weeks. CRC models were developed by inoculation of CRC cell line MC38 into the spleens of mice fed with high-fat diet (HFD) and low-fat diet (LFD) and cancer metastasized to livers in 1–2 weeks. UM mice were imaged with a 7T scanner using ProCA32.Collagen1, and ProCA32.CXCR4R4 using dual imaging methodology. The CRC mice were imaged at 3T human scanner using ProCA32.Collagen1and ProCA32.CXCL12 with the Multitasking technique.

Results

Sensitive detection of animal liver lesions can be achieved using multiple imaging methodologies taking advantage of the dual relaxation properties of ProCA32.collagen1 and ProCA32.CXCR4. Dual imaging and inversion recovery Gd3+-or Mn2+- ProCA32.collagen1 enable sensitive and early stage detection of hepatic micrometastasis as small as 0.144 mm2 with increased sensitivity and specificity. Gd3+- and Mn2+-and ProCA32.CXCR4 detect overall expressed CXCR4 at tumor microenvironment of small mouse liver metastasis from UM and ovarian cancer without trigger downstream signaling.

Conclusions

They are able to stage metastasis progression with differential liver growth patterns that have differential responses to therapeutic treatment. In contrast, these small hepatic metastases were invisible in using clinical contrast agent Eovist. Furthermore, the detailed vessel structure and fibrotic stroma and their changes under high fat condition during progression are well delineated by ProCA32.collagen and ProCA32.CXCL12 at 3T. All MRI results were confirmed by ex vivo correlation, histological analysis, and fluorescence microscopy. This combination of biomarker-targeted contrast agents and novel pMRI imaging methodology will provide non-invasive precise early detection of metastasis, improving our ability to predict progression, devise targeted therapy, and understand hepatic metastasis biology and survival rates.

References

1. Tan S, Yang H, Xue S, Qiao J, Salarian M, Hekmatyar K, Meng Y, Mukkavilli R, Pu F, Odubade OY, Harris W, Hai Y, Yushak ML, Morales-Tirado VM, Mittal P, Sun PZ, Lawson D, Grossniklaus HE, Yang JJ. Chemokine receptor 4 targeted protein MRI contrast agent for early detection of liver metastases. Sci Adv. 2020;6(6):eaav7504. Epub 2020/02/23. doi: 10.1126/sciadv.aav7504. PubMed PMID: 32083172; PMCID: PMC7007242.
2. Yang H, Tan S, Qiao J, Meng Y, Gui Z, Xu YN, Grossniklaus HE, Yang J. Precise and non-invasive detection of liver metastases via biomarker chemokine receptor 4. Submitted to Biomaterials. 2021.

Declarations

Conflict of Interest

Jenny J. Yang is the founder of InLighta Biosciences. The other authors declared no financial interest. The authors grant permission to publish this information or an appropriate summary thereof with the abstract.

035-PSMA-Targeted Microbubbles: a Potential Contrast Agent for Tumor Cell Imaging in Mosaic Vasculature

Matthew Wang[1], Arshad Ali Khan[1], Sangeeta Ray[2], Michael Tweedle[3], Martin Pomper[2], Anna Moore[4], Alexander L. Klibanov[1]

[1]University of Virginia, Charlottesville, USA
[2]Johns Hopkins University, Baltimore, USA
[3]Ohio State University, Columbus, USA
[4]Michigan State University, Michigan, USA

Background

An opinion exists that tumor cells are located alongside endothelium in tumors, creating “mosaic” vasculature. Evaluating vascular access of tumor cells will improve understanding tumor progression and metastatic seeding.

Published reports [1,2] suggest that tumors have up to 4% of total vasculature surface area represented by tumor cells. We hypothesize that exposed tumor cell biomarkers could be detectable by molecular ultrasound imaging with intravascular microbubble contrast agents targeted to tumor cell-specific receptors. We describe microbubbles decorated with PSMA-binding ligands and show *in vitro* and *ex vivo* selective adhesion of targeted microbubbles to PSMA-overexpressing cells. Contrast ultrasound *in vivo* is performed in the same model, after intravenous administration of microbubbles.

Methods and Materials

PSMA ligand, 2-(3-{5-[7-(5-amino-1-carboxy-pentylcarbamoyl)-heptanoylamino]-1-carboxy-pentyl}-ureido)-pentanedioic acid [3] was covalently coupled with amino-PEG-phosphatidylethanolamine. Ligand-lipid microbubbles were prepared as described for peptide-decorated ultrasound contrast [4]; ligand-free microbubbles served as controls. An *in vitro* microbubble binding study was performed in a flow chamber [4] with cultured PC3/PIP cells (overexpressing PSMA) or control PC3 cells, monitored by ultrasound imaging. Ex vivo targeting was tested by microbubble incubation with PC3/PIP tissue sections. Following repeated media rinses, microscopy was used to count retained microbubbles. To investigate PSMA vascular expression, *in vivo* ultrasound contrast imaging was performed in the same tumor-bearing mice, following intravenous administration of microbubbles.

Results

Selective adhesion of targeted microbubbles to cultured PSMA-expressing PC3/PIP cells was demonstrated in comparison with control bubbles (5.8-fold difference, $p<0.00001$). Likewise, targeted microbubbles demonstrated lower adhesion to control PC3 cells that did not express PSMA (3.1-fold, $p<0.0001$). *Ex vivo*, for PC3/PIP tumor sections, ligand-decorated microbubbles demonstrated targeting compared with control tumor (MC38 adenocarcinoma, 8.7-fold, $p<0.00001$) or control microbubbles (7.1-fold, $p<0.0001$). Conversely, intravenous administration did not result in a statistically significant enhanced accumulation of targeted microbubbles in the tumor vasculature, compared with control bubbles.

Conclusions

Microbubbles carrying a small molecule PSMA ligand were prepared by a simple translatable technique; they selectively adhered to PSMA-positive prostate cancer cells *in vitro* and *ex vivo*. However, following intravenous administration of targeted and control microbubbles to tumor-bearing mice, no statistically significant difference was observed. This points at low levels of expression of PSMA on the model tumor vasculature and implies undetectable levels of mosaic vasculature in the tumor model tested. Further studies in multiple tumor models are necessary; microbubbles targeted to tumor cell-specific biomarkers may become a non-invasive probe to prove lack or presence of noticeable levels of tumor cells exposed in tumor vasculature.

References

1. Chang YS, di Tomaso E, McDonald DM, Jones R, Jain RK, Munn LL. Mosaic blood vessels in tumors: frequency of cancer cells in contact with flowing blood. Proc Natl Acad Sci U S A. 2000;97;14608-13.
2. J Folkman. Can mosaic tumor vessels facilitate molecular diagnosis of cancer? Proc Natl Acad Sci U S A. 2001;98;398-400.
3. Chen Y, Dhara S, Banerjee SR, Byun Y, Pullambhatla M, Mease RC, Pomper MG. A low molecular weight PSMA-based fluorescent imaging agent for cancer. Biochem Biophys Res Commun. 2009;390;624-629.
4. Unnikrishnan S, Du Z, Diakova GB, Klibanov AL. Formation of microbubbles for targeted ultrasound contrast imaging: practical translation considerations. Langmuir. 2019;35;10034-10041.

Declarations

Conflict of Interest

The authors declare no competing interests.

036-Nodal Staging of Solid Tumors: USPIO-Enhanced MRI 2.0

Tom W.J. Scheenen[1,2]

[1]Radboud University Medical Center, Nijmegen, The Netherlands
[2]Erwin L. Hahn Institute for Magnetic Resonance Imaging, Essen, Germany

Background

Lymph node stage defines prognosis and treatment in patients with solid tumors. USPIO-enhanced MRI with Ferumoxtran-10 could alleviate the clinical need for reliable and non-invasive N-staging. Ferumoxtran-10 (Ferrotran, SPL Medical, Nijmegen, The Netherlands) has been reintroduced in clinical research and clinical care [1] and showed sensitivities up to 90% and specificities up to 96% for nodal involvement in several types of cancer [2]. With the newest developments in MR-methodology enabling the use of 3D USPIO-enhanced MRI at ultra-high magnetic field strength and in moving parts of the body like the upper abdomen or mediastinum [3], the accuracy of the technique should be re-evaluated and validated.

Methods and Materials
Fifty patients with one of four tumour types with high risk of nodal disease were included. Anatomical and T2*-weighted MR imaging was performed at 3T and in some cases at 7T (Siemens Healthcare, Erlangen, Germany), 24-36 hours after intravenous administration of Ferumoxtran?10. All studies were approved by the institutional review board and written informed consents were obtained from all patients. If patients underwent surgery, a workflow was developed to match *in vivo* annotated lymph nodes with *ex vivo* MRI of the resected specimen, which in turn was used for MR-guided histopathology ending up in a node-to-node correlation of histopathology and *in vivo* MRI. After anonymization and randomization all *in vivo* studies were radiologically reviewed. Lymph nodes were scored on a 5-point Level of Suspicion (LoS) scale depending on anatomical appearance and signal intensity on T2*-weighted MRI.

Results
In 10 patients with rectal cancer, node-to-node comparison was possible for 55 lymph nodes, of which 6 were metastatic on pathology [4]. Low true-positive rates (3/26) and high true negative rates were achieved (14/17). False positive lymph nodes appeared as inflammatory lymph nodes on histopathology. Twenty patients with prostate cancer were examined at both 3 and 7T with traditional LoS scoring. More, but on average not larger suspicious nodes were annotated on 7T versus 3T MRI by two readers, with less interobserver variability at 7T. In 10 patients with esophageal cancer the MRI examination was performed under general anesthesia (4-min apnea after hyperventilation to stop breathing motion [5]). Sensitivity and specificity for nodal staging on station level with LoS scoring were 0.63 and 0.84. Finally, in 10 patients with head and neck cancer we developed a new evaluation protocol on the basis of histopathology of resected nodes.

Conclusions
The latest 3D MRI technology at 3 and even 7T detects suspicious lymph nodes down to 1 mm in size. With two preliminary studies showing variable results for nodal staging with traditional LoS scoring, and one direct field strength comparison revealing unprecedented lymph node numbers and sizes *in vivo*, we concluded to revisit existing evaluation schemes and developed the first new radiological reading protocol for 3D high resolution USPIO-enhanced MRI.

References
1. Fortuin AS, Bruggemann R, van der Linden J, et al. Ultrasmall superparamagnetic iron oxides for metastatic lymph node detection: back on the block. Wiley Interdiscip Rev Nanomed Nanobiotechnol. 2018;10(1).
2. Wu L, Cao Y, Liao C, et al. Diagnostic performance of USPIO-enhanced MRI for lymph-node metastases in different body regions: a meta-analysis. Eur J Radiol. 2011;80(2):582-9.
3. Scheenen TWJ, Zamecnik P. The Role of Magnetic Resonance Imaging in (Future) Cancer Staging: Note the Nodes. Invest Radiol. 2021; 56: 42-49.
4. Stijns RCH, Philips BWJ, Nagtegaal ID, Polat F, de Wilt JHW, Wauters CAP, Zamecnik P, Fütterer JJ, Scheenen TWJ. USPIO-enhanced MRI of lymph nodes in rectal cancer: A node-to-node comparison with histopathology. Eur J Radiol. 2021; 138: 109636.
5. de Gouw DJJM, Maas MC, Slagt C, Mühling J, Nakamoto A, Klarenbeek BR, Rosman C, Hermans JJ, Scheenen TWJ. Controlled mechanical ventilation to detect regional lymph node metastases in esophageal cancer using USPIO-enhanced MRI; comparison of image quality. Magn Reson Imaging. 2020; 74: 258-265.

Declarations

Conflict of Interest
The author declares no competing interests.

037-Functionalized Fluorocarbon Nanoemulsions for Multimodal Imaging of Tumor-Associated Macrophages

Eric Ahrens, Chao Wang, Benjamin I. Leach, Deanne Lister, Stephen R. Adams

University of California San Diego, La Jolla, CA, USA

Background
Tumor-associated macrophages (TAMs) serve pro-tumoral functions including the expression of factors promoting growth and angiogenesis. The ability to image TAMs with high specificity would greatly enhance our ability to diagnose, stratify, and treat cancer. Importantly, high TAM burden in the tumor microenvironment is suspected to be associated with poor therapeutic outcomes. Fluorocarbon (FC) nanoemulsions (NE) have a proven safety profile and well-characterized pharmacokinetics. Intravenously delivered NE effectively labels macrophages in situ and enables 19F MRI inflammation "hot-spot" detection (1). However, FC inertness makes chemical modification challenging, and the high F-electronegativity makes dissolution of other molecules difficult. We have designed fluorous molecules, including chelators (2, 3) and fluorophores (4), that overcome FC solubility barriers and provide a platform for multimodal probe development. We demonstrate the use of functionalized NE for visualization of TAMs in mouse using 19F MRI, 89Zr PET and cryo-fluorescence tomography (CFT).

Methods and Materials

We synthesized the fluorous chelator tetrahydroxamate (FHOA) which is soluble in the 19F-rich nanoemulsion core. NE is formulated as a cold nanoemulsion, and before use, the NE is radiolabeled with 89Zr via simple premix and gel-filtration steps. Details concerning fluorous chelate syntheses and characterizations are described elsewhere (2). We prepared cohorts of orthotopically implanted syngeneic tumor bearing mice (4T1-Luc or MC38). At approximately 5 weeks, images were acquired 24 h after NE injection using PET/CT (Inveon, Siemens), 19F/1H MRI (11.7 T, Bruker), and CFT (Emit Imaging). Serial blood samples were collected to measure NE circulation time, and histology was used to confirm the macrophage internalization of FC NE.

Results

FHOA in NE binds 89Zr added to buffer within a few minutes at room temperature, with ~60% yield after purification (2). Pharmacokinetic studies showed that the NE has a blood circulation half-life of 14.5 h and high probe stability *in vivo* (2). A single NE dose enables 19F MRI and PET detection in the same subject (2) (Fig. 1a–c). Alternatively, fluorescent FC NE serves as an effective macrophage marker, enabling high-resolution, 3D CFT (Fig. 1d) and "ground truth" probe biodistribution visualization.

Conclusions

Oncology presents a key field of use for precise macrophage imaging. Synthesis of novel fluorous molecules, such as chelators and dyes, enables the stable functionalization of FC NE probes. A high degree of consistency is observed among PET, MRI, and CFT in the visualization of lesions and agent biodistribution.

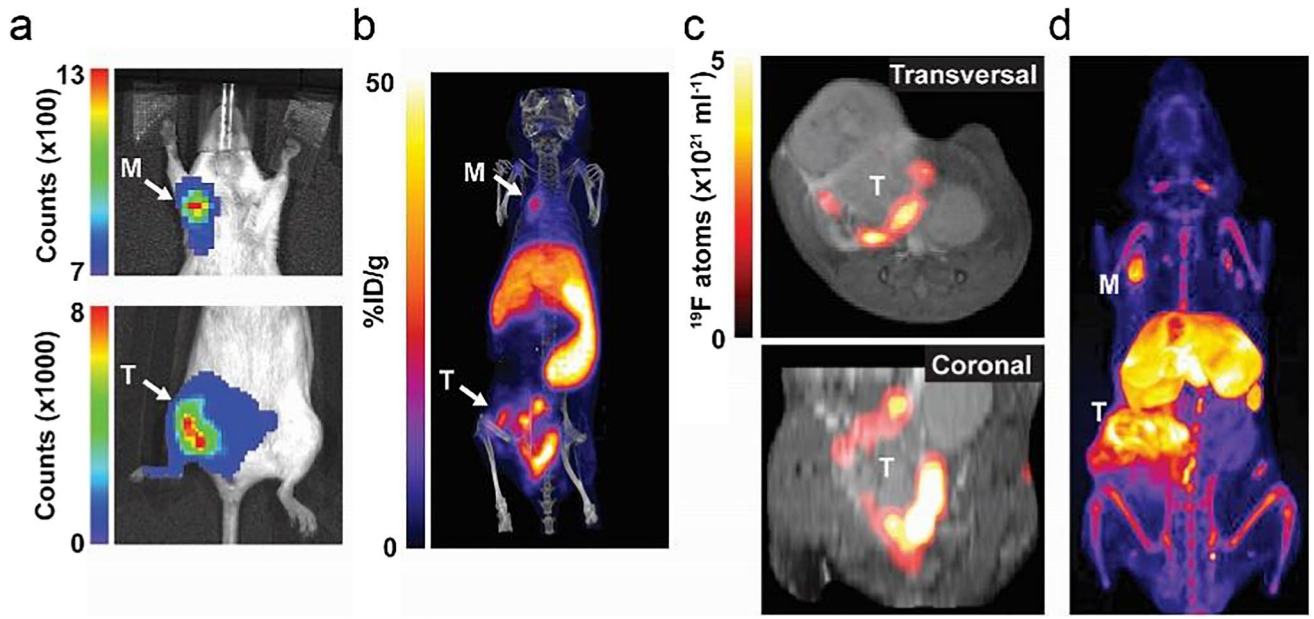

Figure caption: *In vivo* detection of TAMs using functionalized FC NE. (a)–(b) BLI and 89Zr-PET/CT, respectively. (c) 19F /1H MRI from mouse (a)–(b). (d) CFT with Alexa647 dye-conjugated NE (Dimant et al. 2018 WMIC abstract #174)

References

1. Ahrens ET, Zhong J. *In vivo* MRI cell tracking using perfluorocarbon probes and fluorine?19 detection. NMR Biomed 2013; 26(7); 860-871.
2. Wang C, Leach BI, Lister D, Adams SR, Xu H, Hoh CK, McConville P, Zhang J, Messer K, Ahrens E. Metallo-fluorocarbon nanoemulsion for inflammatory macrophage detection via PET and MRI. J Nucl Med 2020; jnumed.120.255273.
3. Kislukhin AA, Xu H, Adams SR, Narsinh KH, Tsien RY, Ahrens ET. Paramagnetic fluorinated nanoemulsions for sensitive cellular fluorine-19 magnetic resonance imaging. Nat Mater 2016; 15(6); 662-668.
4. Janjic JM, Srinivas M, Kadayakkara DK, Ahrens ET. Self-delivering nanoemulsions for dual fluorine-19 MRI and fluorescence detection. J Am Chem Soc 2008; 130(9); 2832-2841.

Declarations

Conflict of Interest
Eric Ahrens is a founder and shareholder of Celsense, Inc. The other authors have nothing to declare.

038-Long-Acting, APC Gd-Chelates for Tumor MR Imaging and Therapy

Christopher Choi, Ray Zhang, Christopher Massey, Reinier Hernandez, Justin Jeffery, Anatoly Pinchuk, Joseph Grudzinski, Jamey Weichert

University of Wisconsin-Madison, Madison, USA

Background
We have developed tumor-targeted alkylphosphocholines (APC) as broad-spectrum cancer imaging and therapy agents. Second-generation radioactive APC metal chelate analog, NM600, has shown selective uptake and prolonged tumor retention in over 30 preclinical cancer models. We previously described MR imaging characteristics of Gd-NM600 in over 8 preclinical tumor models. The aim of this work was to evaluate tissue retention and speciation properties of Gd-NM600 via high-resolution mass spectroscopy tissue imaging in xenograft and orthotopic tumor models. Based on its tumor uptake and retention properties, a secondary aim was to perform preliminary proof of concept studies to assess the therapeutic potential Gd-NM600 in combination with external beam radiotherapy (EBRT) and neutron capture therapy (NCT).

Methods and Materials
MALDI-MSI was used to characterize and map the biodistribution of the chemical species of Gd-NM600 in tissue. NM600 was exposed to 90-Gy of EBRT to determine the chemical stability of the agent in a high dose radiotherapy setting. Tumor uptake and retention values were used to determine the maximum tumor concentration of Gd to guide subsequent proof of concept EBRT and NCT modeling studies.

Results
Gd-NM600 exhibited excellent broad spectrum tumor uptake (4 % ID/g at 48 h), prolonged tumor retention (7 days) and MRI tumor conspicuity. Moreover, minimal tumor uptake saturability of Gd-NM600 was observed after 3 consecutive daily doses. Tissue mass spectrometry imaging successfully interrogated the spatial localization and chemical speciation of Gd compounds and also identified minor breakdown products of Gd species. NM-600 was also stable (97%) when exposed to high radiation doses of EBRT suggesting feasibility of use with MR guided EBRT. POC modeling results suggest that NM600 may afford potential for enhancing EBRT or NCT.

Conclusions
Gd-NM600 a new macrocyclic cancer-targeted Gd APC chelate that achieves broad-spectrum tumor uptake and prolonged retention demonstrated *in vivo* stability by ultra-high resolution MS tissue imaging. High tumor cell uptake of the agent accompanied by stability towards high dose EBRT suggests this agent is suitable for use in MR-guided EBRT and for therapeutic enhancement when used in combination with EBRT or NCT.

Declarations

Conflict of Interest
The authors declare no competing interests.

039-Novel Clathrin-Based Superparamagnetic Iron Oxide Nanoprobes for MRI of DAT in in Drug Addiction

Gordana Vitaliano[1], Christopher Adam[1], Gonzalo Zeballos[1], Michael Rohan[1], Kyoko Ohashi[1], Franco Vitaliano[2]

[1]McLean Hospital/Harvard Medical School, Belmont, MA, USA
[2]ExQor Technologies Inc., Boston, MA, USA

Background
MRI has high spatial resolution but poor sensitivity for visualization of molecular targets. Superparamagnetic iron oxide (SPIO) contrast agents along with antibodies are used to improve MRI sensitivity and molecular targeting, but they cannot cross an intact blood-brain barrier (BBB) limiting their use for CNS receptor/transporter imaging. Our goal was to enable MR imaging of dopamine transporters (DAT) in drug addiction using novel clathrin-nanoprobes (CNPs) carrying SPIO and anti-DAT-antibodies, which noninvasively pass a BBB and target DAT.

Methods and Materials
DAT-antagonists can be used for diagnosis and treatment of drug addiction, Parkinson's disease and ADHD. DAT-CNPs were synthesized by conjugating anti-DAT-antibody and SPIO (or NHS-Fluorescein) to clathrin using polyethylene glycols at 1:1:1 molar ratio. The size and uniformity of nanoprobe was determined by dynamic light scattering. C57BL/6J mice were given intraperitoneal injections of saline or neurotoxic dose of methamphetamine (METH, 30 mg/kg) 24h before MRI. Mice were then given saline or DAT-CNPs intranasally (68pmol, 50μL) 4h before *in*

vivo or *ex vivo* MRI. Voxel-wise R^2* relaxation rates were obtained at 9.4T using a series of gradient-echo images, and estimated in the striatum (STR), substantia nigra (SN) and visual cortex (vCTX), a control region with low DAT expression.

Results

DAT-CNPs remained immunoreactive after modifications. The iron stained brain slices showed an accumulation of DAT-CNPs in brain regions rich in DAT (*e.g.*, STR). Fluorescent microscopy demonstrated specific targeting of dopamine brain regions with DAT-CNPs. Confocal laser microscopy confirmed integrity of DAT-CNPs, as clathrin and DAT-antibody fluorescence co-localized in dopamine regions. MRI studies revealed that R^2* values were lower in STR (p=0.0077) and SN (p=0.0030) in METH vs. saline treated mice. R^2* values were significantly higher in the STR (p=0.0010) and SN (p=0.0007) compared to vCTX in animals that received DAT-CNPs, but not in saline treated animals. DAT-CNPs significantly increased R^2* in the STR (p<0.0001) and SN (p=0.0002) compared to saline without significantly altering R^2* in the vCTX.

Conclusions

DAT-CNPs successfully bypassed an intact BBB and noninvasively delivered SPIO contrast agents along with anti-DAT-antibody to the mouse brain, enabling MRI detection of decreased DAT levels in METH toxicity. Hence, clathrin appears to provide a highly efficient nanoplatform for targeted delivery of antibodies and SPIO to CNS. This nanotechnology strategy may lead to development of new neurotheranostics for imaging of molecular changes in brain disorders, for monitoring disease progression and recovery process, and for efficiently treating CNS disorders through targeted delivery of specific antibodies.

Declarations

Conflict of Interest

The authors Gordana Vitaliano, Michael Rohan, Kyoko Ohashi, and Franco Vitaliano have disclosed a financial interest in this abstract. The other authors have disclosed no financial interest.

040-Safety of Contrast Agents in Clinical Practice: Is There a Consensus Between Guidelines?

Olivier Clément

Université de Paris, Paris, France

Background

Contrast agents in radiology are drugs marketed to enhance the diagnostic performance of imaging procedures, not to treat a specific disease. Therefore, the risk/benefit ratio should be very low. Preclinical and clinical research on safety has been extensive other the last decades, and many papers and guidelines are published in different countries for iodinated, gadolinium based contrast agents and microbubbles. They often differ in terms of definition, risk factors or management, and updates are not synchronized. Contrast-induced nephropathy, diabetes, hypersensitivity reactions, pregnancy, and lactation are the main topics of daily questioning for the clinical radiologist who is often puzzled by contradictory messages. The objective of this work is to compare international guidelines on these issues and highlight common understanding and discrepancies.

Methods and Materials

Major American (ACR Manual On Contrast Media version 2021), European (Contrast Media Safety Committee of the ESUR) and national (UK, France,Germany, Japan, Korean) available guidelines and publications are compared. For contrast induced nephropathy and diabetes, the following items are reported: risk factors, age, renal function threshold for hydration, hydration protocol, metformin handling. For hypersensitivity reactions: mechanism (true or non-allergic hypersensivity), risk factor, use of skin testing, cross reactivity are compared. For pregnancy, lactation and breast feeding: contraindication for iodinated and gadolinium based agents, duration of interruption are compared.

Results

Contrast-induced nephropathy and diabetes: there are discrepancies between guidelines concerning the risks factors in terms of threshold values (age ranges from 60 to 70, renal function from 30 to 45 ml/min) and for the withholding of metformin depending on the renal status. For hypersensitivity reactions, CMSC, national European and Korean guidelines agree to use skin testing as a diagnostic tool to differentiate allergic and non-allergic hypersensitivities. Management of hypersensitivity patients differs between guidelines. Iodinated agents are not contra-indicated in pregnancy when there is a clinical indication. For gadolinium based agents, all guidelines agree with a stricter evaluation of the risk benefit ratio and to highlight the absolute need to inject the contrast agent. The use of macrocyclics is not very clearly exposed. For lactation and breast feeding, there is a general agreement.

Conclusions

Guidelines from learned societies are useful for daily clinical use. Their content varies over time and scientific knowledge, and it is difficult to compare guidelines that have been

written at different periods. In 2021, handling the risk of contrast induced nephropathy is very different from 20 years ago. There is a much more tolerant thresholds for renal function in intravenous injection, leading to less contra indications for contrast enhanced CT scanners. Recent safety crises with gadolinium chelates resulted in much more cautious guidelines for risk groups like pregant and breast feeding women. For hypersensitivity reactions, there is still a great need to share some common physiopathological mecanisms of allergic reactions in order to provide consistent guidelines.

Declarations

Conflict of Interest
The author declares no competing interests.

041-Interrogation of Tumor Microenvironment Using Nano-Radiomics

Zbigniew Starosolski[1], Laxman Devkota[1,2], Amy Courtney[1,2], Charlotte H. Rivas[2], Leonid Metelitsa[1,2], Ananth Annapragada[1], Robin Parihar[1,2], Ketan B. Ghaghada[1]

[1]Texas Children's Hospital/Baylor College of Medicine, Houston, TX, USA
[2]Baylor College of Medicine, Houston, TX, USA

Background
Myeloid-derived suppressor cells (MDSCs) and tumor-associated macrophages (TAMs), cellular components of tumor microenvironment (TME), play a central role in treatment resistance and disease relapse. Non-invasive imaging techniques for monitoring MDSC/TAM burden could enable TME profiling and aid in disease prognosis, a priori identification of treatment resistance and monitoring of tumor response to TME-directed immunotherapies. Nanoparticle contrast agents exhibit heterogenous distribution in solid tumors that is driven primarily by tumor architecture and TME. In this work, we investigated if radiomic analysis of nanoparticle contrast-enhanced images (nano-radiomics) would enable interrogation of TME.

Methods and Materials
In the first study, we investigated feasibility of nano-radiomics for detection of tumor response to MDSC-directed immunotherapy. Studies were performed in a humanized mouse model of neuroblastoma. Animals were randomized to tumor only (T), tumor+MDSC (T+M) and tumor +MDSCs+Immunotherapy (Therapy group). For Therapy group, MDSC-directed natural killer cells were administered 9 days prior to CT imaging. Nanoparticle contrast-enhanced CT (n-CECT) was performed 4 days after injection of a nanoparticle contrast agent (CT nanoprobe). In the second study, we investigated feasibility of nano-radiomics for classification of tumors based on TAM. Studies were performed in transgenic mouse models with low and high TAM burden. N-CECT was performed 4 days after administration of CT nanoprobe. In both studies, tumors were segmented in CT images and radiomic analysis was performed using PyRadiomics and machine learning algorithms.

Results
In the first study, CT-derived conventional tumor metrics (tumor volume or mean tumor attenuation) did not significantly differ between Therapy and non-Therapy (T+M) group. Nano-radiomic analysis identified 10 radiomic features (RFs) that differentiated ($p<0.05$) Therapy and non-Therapy group (T+M). Texture-based RFs were among the predominant features exhibiting high statistical power in differentiating therapy and non-therapy groups. In the second study, CT-derived conventional tumor metrics did not significantly differ between tumors in low and high TAM burden groups. However, nano-radiomic analysis revealed two RFs that differentiated ($p<0.05$) low TAM tumors from high TAM. The RFs were used to build a linear classifier that demonstrated 100% accuracy and further confirmed by 5-fold cross validation.

Conclusions
Our study shows that changes in tumor microenvironment causes subtle changes not effectively gauged by conventional imaging metrics but revealed by nano-radiomics.

Declarations

Conflict of Interest
The authors declare no competing interests.

042-Optimizing Imidazoles for Dynamic Contrast-Enhanced CEST MRI Urography

Shaowei Bo[1], Julia Stabinska[1], Yunkou Wu[1], KowsalyaDevi Pavuluri[1], Aruna Singh[1], Rehan Choudhry[1], Max Kates[1], Martin G. Pomper[1], Michael T McMahon[1,2]

[1]The Johns Hopkins University School of Medicine, Baltimore, MD, USA
[2]Kennedy Krieger Institute, Baltimore, MD, USA

Background
Urinary tract obstructions (UTOs) are blockages that inhibit the flow of urine through its normal path (the urinary tract) which may lead to kidney failure if left untreated. Chemical

exchange saturation transfer (CEST) MRI is a noninvasive molecular MRI technique which has shown promise for clinical applications. In this study, we prepared and tested a series of 4,5 disubstituted imidazoles CEST agents for discriminating between obstructed and unobstructed kidney kidneys and tested on a UTO mouse model.

Methods and Materials

Synthesis: A convenient synthesis of I45DCs was designed according to the published protcol.1 *In vitro* MRI: 20 mM of I45DCs were dissolved in PBS and titrated to 6.0, 6.3, 6.6, 6.9, 7.2, and 7.5. The CEST images were acquired on a Bruker 11.7 T MR scanner at 37 °C using a RARE sequence with a CW saturation pulse length = 3s, saturation field strengths (B1) from 1.2 ?T to 12.0 ?T. Other parameters were: TR=10 s, TE=4.5 ms, matrix size=64×64 and slice thickness = 1.2 mm, offsets between ±12 ppm. *In vivo* MRI: The left ureter of C57Bl/6 mice was sutured to obtain complete obstruction. These were anaesthetized and catheterized via the tail vein with 100 ?L of I45DCs (300 mM). High resolution T2W images were acquired using a RARE sequence. CEST images were acquired using a RARE sequence with centric encoding (saturation length = 3 s at B1 = 6 ?T) on a Bruker 11.7 T horizontal scanner. A two offset CEST protocol was used with offsets of 7.8 ppm and 4.5 ppm repeatedly after I45DCs administration with 8–10 pre-injection images for each offset. Other parameters were: TR/TE: 3.49/10000 ms, Matrix size: 48×48 and axial slice, thickness 1.5 mm. For CEST MRI data processing, mean pre-injection z-spectra were subtracted from all post-injection images. Twenty images were averaged using moving average filter to generate CEST contrast maps.

Results

Based on *in vitro* experiments on our I45DC agents, we selected diGlu and diAp as the most promising pH sensors for live animal studies. After injection into the UTO mice, a CEST contrast of 25% was obtained in the healthy kidney at peak contrast while only 10% is observed in the obstructed kidney. In addition, some fine structure was apparent in the contrast images including differentiation between inner and outer medulla. Furthermore, no adverse effects were observed on the mice due to administration.

Conclusions

The results demonstrate that imidazole CEST MRI agents can differentiate between obstructed and unobstructed kidneys in mice and provide pH maps which reveal functional changes. This technology has potential for clinical application.

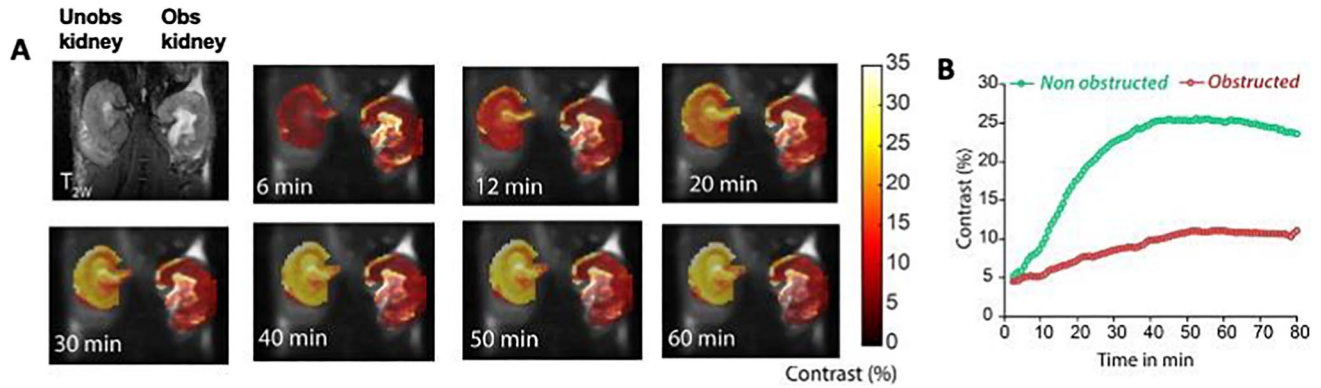

Figure caption: *In vivo* CEST MRI of UTO mice; (A) contrast images of kidney after administration of I45DC-diGlu overlayed on high resolution T2W anatomic images; (B) time course of CEST contrast for Non obstructed and obstructed kidneys

References

1. Saudi M, Zmurko J, Kaptein S, et al. Synthesis and evaluation of imidazole-4,5- and pyrazine-2,3-dicarboxamides targeting dengue and yellow fever virus. Eur J Med Chem. 2014; 87: 529-539.

Declarations

Conflict of Interest

The authors declare no competing interests.

043-Engineering Fluorinated Thermo-responsive Assembled Protein (F-TRAP) for Theranostic Applications in Glioblastoma Multiforme

Aparajita Bhattacharya[1,2], Orin Mishkit[4], James Tranos[4], Lucas Morales[1], Andrew Wang[1,2], Joshua Frenster[4], Devin Bready[4], Niklas Boess[4], Frances Lee[1], Youssef Wadghiri[4], Dimitris Placantonakis[4], Jin Kim Montclare[1,2,3,4,5]

[1]NYU Tandon School of Engineering, Brooklyn, NY, USA
[2]State University of New York Downstate Medical Center, Brooklyn, NY, USA
[3]New York University, New York, NY, USA
[4]New York University School of Medicine, New York, NY, USA
[5]NYU College of Dentistry, New York, NY, USA

Background

Gliomas account for roughly 27% of all brain tumors and there is an urgent need to develop new therapeutic modalities. A glioblastoma multiforme (GBM) prognosis signifies a survival time of 14-16 months with only 5% of patients surviving more than 5 years. (1) A significant challenge for traditional GBM drug delivery is the inability to: a) treat tumor cells with cytotoxic drugs due to their poor solubility and lack of blood brain barrier (BBB) permeation; b) specifically target tumor cells while avoiding normal tissue with such cytotoxic agents c) stimulate drug release; and d) monitor GBM status and therapy non-invasively. (2) Theranostic agents are being developed for their ability to diagnose disease and improve therapeutic delivery and can address these requirements because treatments specific to GBM do not currently exist. (3) While considerable efforts have been made in developing protein-based systems as drug-delivery carriers or as diagnostic agents (4), we are investigating a fundamental new insight that is helping us develop a single protein-based system combining drug delivery capabilities with the ability to cross the BBB and remain at cancer site due to the enhanced permeation and retention (EPR) effect. This biomaterial also incorporates functional groups detectable via magnetic resonance (MR) spectroscopy and imaging as well as near-infrared fluorescence (NIR) to enable visualization during chemotherapy. The protein-based theranostic agent we have engineered is called fluorinated thermo-responsive assembled protein (F-TRAP) that bears a non-canonical fluorinated amino acid (trifluoroleucine or TFL), can self-assemble into micellar structures, and encapsulate hydrophobic drugs.

Methods and Materials

Circular dichroism and dynamic light scattering have been performed to observe F-TRAP's secondary structure and micelle formation respectively (2). Additionally, 19F magnetic resonance imaging (MRI) has been carried out to visualize F-TRAP (5) and near infra-red fluorescence imaging (NIRF) has been utilized to determine its pharmacokinetic properties in a glioblastoma (GBM) mouse model.

Results

Results indicate that F-TRAP has an ?-helical secondary structure and forms micelles 30 nm in size. F-TRAP shows favorable pharmacokinetic data with a half-life of 123 minutes and high plasma retention. Importantly, animal data also reveals the ability of F-TRAP to cross the BBB and to be imaged inside the brain.

Conclusions

F-TRAP is capable of encapsulating small hydrophobic molecules, such as dox. It crosses the BBB and undergoes EPR effect allowing it to accumulate therein and be visualized NIRF imaging and is capable of undergoing MR imaging due to an appropriate half-life of about 123 min.

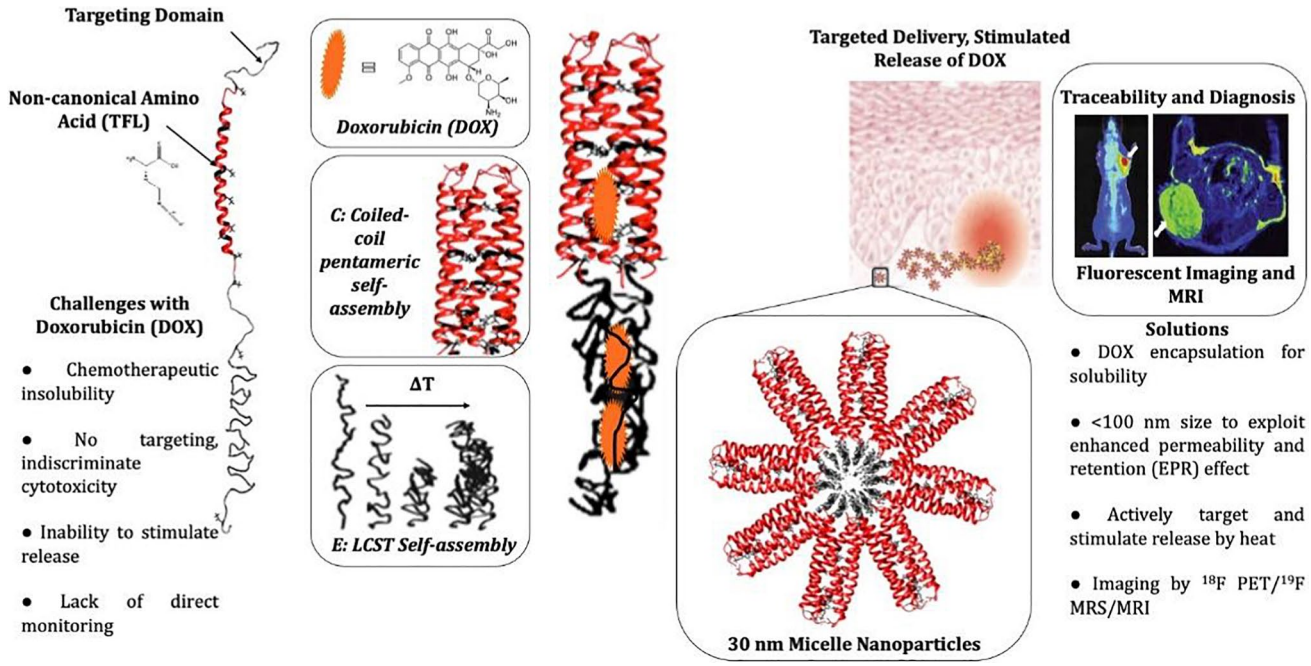

Figure caption: To address the challenges of drug solubility or breakdown, rapid clearance, non-specific killing of healthy cells, and the inability to directly monitor the impact of doxorubicin (DOX) on diseased cells, F-TRAP encapsulates the chemotherapeutic, prevents

References

1. Alexander, B. M.; Cloughesy, T. F., Adult Glioblastoma. Journal of Clinical Oncology 2017, 35 (21), 2402-2409.
2. Senapati, S.; Mahanta, A. K.; Kumar, S.; Maiti, P., Controlled drug delivery vehicles for cancer treatment and their performance. Signal Transduction and Targeted Therapy 2018, 3 (1), 7.
3. Zavaleta, C.; Ho, D.; Chung, E. J., Theranostic Nanoparticles for Tracking and Monitoring Disease State. SLAS Technol 2018, 23 (3), 281-293.
4. Desai, M. S.; Lee, S.-W., Protein-based functional nanomaterial design for bioengineering applications. WIREs Nanomedicine and Nanobiotechnology 2015, 7 (1), 69-97.
5. Hill, L. K.; Meleties, M.; Katyal, P.; Xie, X.; Delgado-Fukushima, E.; Jihad, T.; Liu, C.-F.; O'Neill, S.; Tu, R. S.; Renfrew, P. D.; Bonneau, R.; Wadghiri, Y. Z.; Montclare, J. K., Thermoresponsive Protein Engineered Coiled-Coil Hydrogel for Sustained Small Molecule Release. Biomacromolecules 2019, 20 (9), 3340-3351.

Declarations

Conflict of Interest

The authors declare no competing interests.

044-Preclinical Evaluations of a Targeted MRI Contrast Agent MT218 for Clinical Development

Yajuan Li[1,2,3*], Songqi Gao[1, 2,4], Hongfa Jiang[1,2], Michael F. Tweedle[1,2,5], Zheng-Rong Lu[1,2,3,4]

[1]Molecular Theranostics, LLC, Cleveland, USA
[2]US Motek, LLC, Cleveland, USA
[3]Jiangsu Ronghui Motek Pharmaceutical Technology Ltd Corp, Jiangsu, China
[4]Case Western Reserve University, Cleveland, USA
[5]Ohio State University, Columbus, USA

Background

We have recently developed a targeted MRI contrast agent, MT218, to target an oncoprotein, extradomain B fibronectin (EDB-FN), in tumor extracellular matrix for cancer molecular imaging with MRI. MT218 is a conjugate of gadoteridol and a small linear peptide, ZD2. EDB-FN is overexpressed in aggressive human cancers, including colon, breast, HNSCC, pancreatic, prostate, etal., and absent in normal tissues and low grade tumors. Preclinical assessments to support a Phase I trial were performed according to FDA guidelines: physicochemical properties, pharmacokinetics, clearance, safety, and tumor-specific MRI of MT218.

Methods and Materials

IND-enabling evaluations of the primary, secondary and safety pharmacology, pharmacokinetic, single and repeated dose toxicity, and genotoxicity studies of MT218 were performed *in vitro* and in mice, rats and dogs.

Results

At 1.4T, the r1 and r2 relaxivities of MT218 were 5.43 and 7.40 mM-1s-1 in pure water, 6.58 and 8.87 mM?1s-1 in PBS buffer, and 6.54 and 8.70 mM-1s-1 in human serum albumin, respectively. MT218 is stable at pH 7.4. MT218 is inert to DOTA, DTPA, HP-DO3A, Zn2+ and EDTA at pH 7.4. In human plasma, MT218's stability half-life is ~3 h. The average binding affinity constant (Kd) of MT218 to EDB is 3.45 μM. No MT218-related effect on parameters of central nervous system function was found following a single intravenous injection at doses of 0.1, 0.3 and 1.0 mmol/kg in Sprague-Dawley rats. No MT218-related effects were found on cardiovascular or respiratory systems at 0.07, 0.21, or 0.70 mmol/kg in conscious beagle dogs. MT218 showed low metabolism in incubation with hepatocytes. The major CYP enzymes and transporters were not involved in the primary metabolism. MT218 was cleared rapidly from circulation into urine with the mean plasma half-life (t1/2) of 0.31 and 0.70 h in rats and dogs, respectively. MT218 was mainly distributed in the kidney and prostate, with very low exposure in other tissues, especially in heart, muscle, and brain. No mortality or morbidity was noted in any rats or dogs in any dose group. In the repeated high dose groups (1.39 mmol/kg/day) in rats, vacuolation of tubular epithelial cells with some degenerative changes was observed at dose termination (Day 15) and at the end of recovery euthanization (Day 29). No such changes were observed for the low and medium repeated dosing groups. For dogs, a mild bilateral tubule degeneration of proximal and distal tubules was found in the single-dose group (0.70 mmol/kg). These changes were no longer evident on Day 15. For the repeated dose groups, there was reversible renal tubule degeneration in both sexes of medium (0.21 mmol/kg/day) and high dose (0.70 mmol/kg/day); there were no renal findings in low-dose dogs (0.07 mmol/kg/day). MT218 was not mutagenic.

Conclusions

MT218 is promising for further clinical development.

References

1. Vaidya, A., et al., Noninvasive assessment and therapeutic monitoring of drug-resistant colorectal cancer by MR molecular imaging of extradomain-B fibronectin. Theranostics, 2020. 10(24): p. 11127-11143.
2. Ayat, N.R., et al., Optimization of ZD2 Peptide Targeted Gd(HP-DO3A) for Detection and Risk-Stratification of Prostate Cancer with MRI. ACS Med Chem Lett, 2018. 9(7): p. 730-735.
3. Han, Z., et al., Targeted Contrast Agent Specific to an Oncoprotein in Tumor Microenvironment with the Potential for Detection and Risk Stratification of Prostate Cancer with MRI. Bioconjug Chem, 2017. 28(4): p. 1031-1040.
4. Li, Y., et al., Synthesis and Assessment of Peptide Gd-DOTA Conjugates Targeting Extradomain B Fibronectin for Magnetic Resonance Molecular Imaging of Prostate Cancer. Mol Pharm, 2017. 14(11): p. 3906-3915.
5. Han, Z., et al., EDB Fibronectin Specific Peptide for Prostate Cancer Targeting. Bioconjug Chem, 2015. 26(5): p. 830-8.

Declarations

Conflict of Interest

The authors declare no competing interests.

045-Encapsulation Techniques to Create Biocompatible Super-Resolution Tracers for Magnetic Particle Imaging

Benjamin D. Fellows, Chinmoy Saayujya, Jacob Bryan, Steven M. Conolly

University of California Berkeley, Berkeley, CA, USA

Background

MPI is a promising preclinical tracer imaging technique that has already been proven to compete on 3 of the 4 standard fundamentals for clinical imaging: dose-limited sensitivity, contrast and zero depth attenuation. Here, we aim to remove the final technical obstacle—weak spatial resolution—with an MPI super-resolution breakthrough, Superferromagnetic iron oxide (SFMIO) tracers. We believe that SFMIO MPI will soon demonstrate single-cell resolution, and be an enabling factor in the first affordable human MPI scanners. The investigation and rational design of nanoparticles for MPI is just now beginning to take hold in the magnetic nanoparticle community. First and foremost, it is of high importance that the critical parameters in MPI are understood by chemists as they differ from those desired by conventional magnetic hyperthermia or MRI contrast agents. The exploration on the effect of nano (composition, shape, etc.) and mesoscale (ordering, superlattice structure, etc.) is still in its infancy, and the effect of these properties has only recently been a subject of investigation in the MPI space.

Methods and Materials

Already, the Conolly lab has developed synthetic chemistry methods that exploit the unique mesoscale interactions of SPIOs to yield materials showing an order of magnitude increase in spatial resolution (below 100 microns) and MPI signal strength. This reproducible synthesis process uses a modified extended LaMer synthesis to produce highly interacting nanoparticles that exhibit "superferromagnetic" behavior yielding unprecedented magnetization flip times.

Results

This order of magnitude resolution increase may easily be furthered by the optimization of the reaction conditions, precursor composition, and selective particle filtration. However, with these new materials a new unique set of challenges arise, including maintaining critical concentration limits, aqueous dispersibility, and biocompatibility.

Conclusions

To this end, we have begun encapsulating the SFMIOs in a biocompatible, micrometer-scale capsule such that they retain their unique magnetic properties when exposed to biologics in an aqueous system. The encapsulation itself done in a surfactant free manner, allowing for mesoscale ordering of nanoparticles within the capsule. The interparticle interactions that arise from this ordering are necessary for obtaining superferromagnetic behavior. The surface of these capsules can be appropriately modified with small biomolecules to enable specific targeting of desired physiology and/or disease. We envision that these encapsulated tracers, when imaged in-vivo, will produce exquisite, high-resolution MPI images.

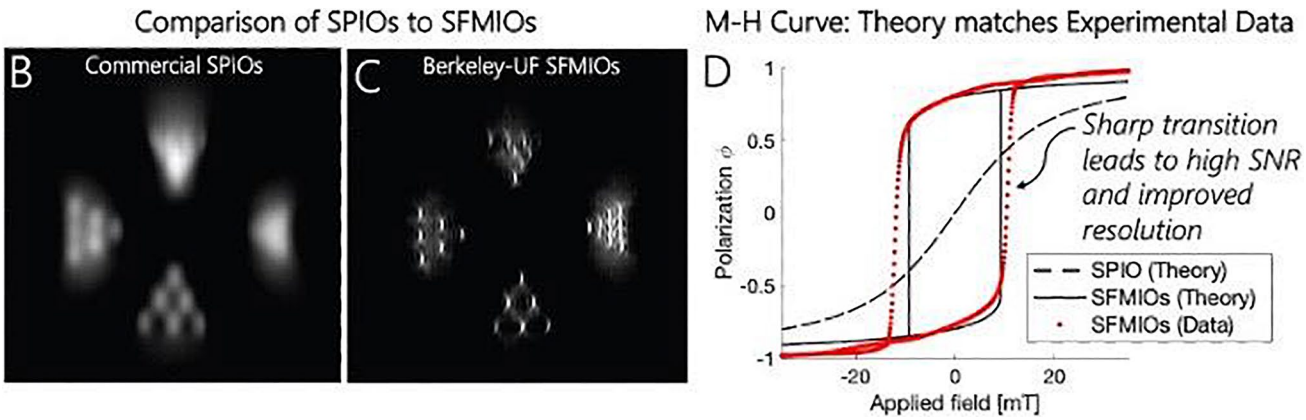

Figure caption: Cal SFMIO experiments show improved resolution and SNR. SFMIOs show a 10-fold improvement in resolution and 44-fold boost in SNR compared to commercial SPIOs. Experimental data from SFMIOs closely matches the M-H curve predicted by our nanoscale physics

Declarations

Conflict of Interest

The authors declare no competing interests.

046-PET/MRI Contrast Agents for Measuring Extracellular pH in the Tumor Microenvironment

Alyssa C. Pollard[1,2], Jorge de la Cerda[2], F. William Schuler[2], Tyler R. Pollard[3], Aikaterini Kotrotsou[2], Federica Pisaneschi[2], Mark D. Pagel[2*]

[1]Rice University, Houston, TX, USA
[2]MD Anderson Cancer Center, Houston, TX, USA
[3]Georgia Institute of Technology, Atlanta, GA, USA

Background

Acidosis is a useful biomarker for tumor diagnoses and for evaluating early response to anti-cancer treatments [1]. pH-responsive MRI contrast agents have been developed, but MRI contrast from the agent is also concentration-dependent. PET/MRI provides a unique opportunity to overcome this concentration dependence issue by using the PET component to report on the concentration of the pH-responsive MRI agent [2].

Methods and Materials

We synthesized our PET/MRI co-agents based on a pH-dependent MRI agent, Gd-(4-methoxyphenylsulfonamidylpropyl)-DO3A [3]. We chelated the agent with Gd(III) to develop the MRI co-agent and with gallium-68 to develop the PET co-agent. We correlated pH with the r1 relaxivity of the MRI agent. We also developed a procedure that uses PET radioactivity measurements and MRI R1 relaxation rate measurements to determine the r1 relaxivity of the MRI co-agent, which can then be converted to pH based on our r1-pH correlation. We used a NuPET insert (Cubresa, Inc.) within a Biospec 7T MRI instrument (Bruker Biospin, Inc.). We prepared phantoms ranging in pH from 6.2 to 7.4 units, and with 50-800 micromolar of the MRI co-agent spiked with 10-45 microCuries of the PET co-agent. We correlated pH measurements with our PET/MRI method vs. a standard benchtop pH meter. We then prepared a subcutaneous flank tumor model of MIA PaCa-2 pancreatic cancer. We simultaneously injected a mixture of 80 microliters of 120 microCuries PET co-agent and 170 microliters of 30 mM MRI co-agent i.v. We measured tumor pHe based on the simultaneous PET and MR images acquired after 8 min post-injection, allowing the co-agents some time to accumulate in tumor tissue.

Results

The co-agents were synthesized in 5 steps with a yield of 59% (MRI) and 30% (PET). The r1-pH calibration showed an outstanding dynamic range between 6.0 and 7.5 pH units, matching the physiological pHe range. Simultaneous PET/MRI accurately measured pH in phantoms, with a precision that depended on MRI agent concentration (standard error of 0.08 pH units at 800 micromolar, and 0.27 pH units at 50–800 micromolar). Our PET/MRI method measured an average pHe of 6.76 ± 0.12 in the MIA PACa-2 tumor model, which matched the tumor pHe measured in this model during previous studies using acidoCEST MRI [4,5].

Conclusions

Tumor acidosis can be evaluated with simultaneous PET/MRI.

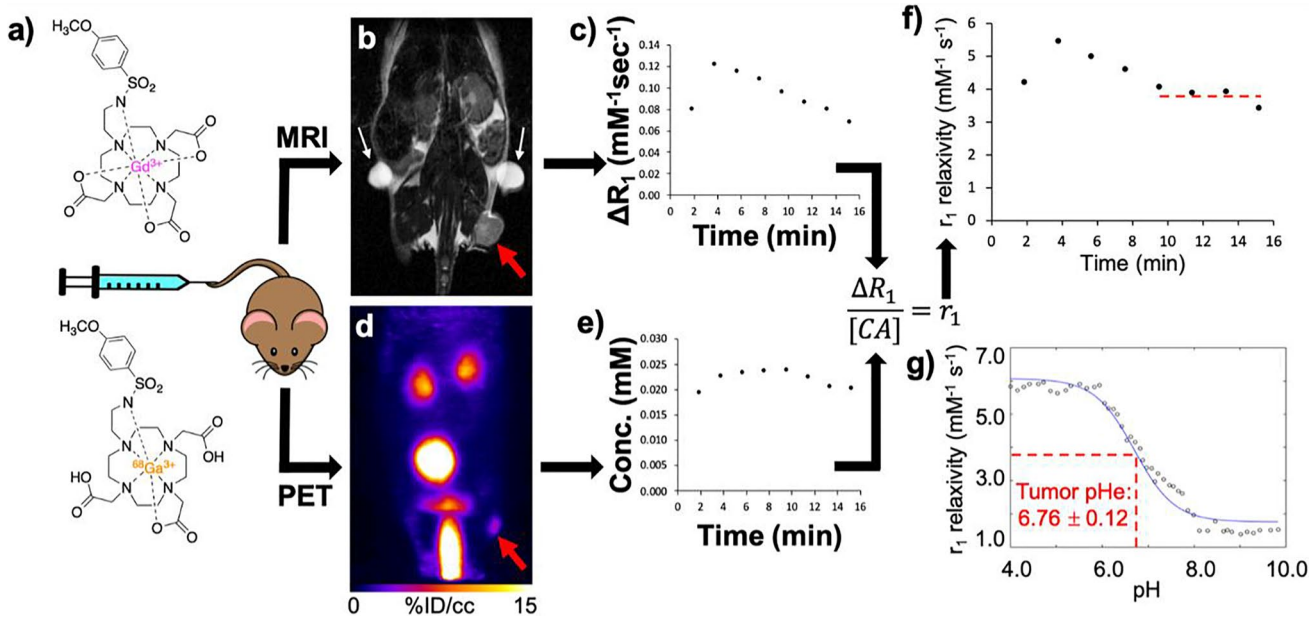

Figure caption: PET/MRI measures *in vivo* tumor pHe

References

1. Chen LQ, Pagel MD. Evaluating pH in the extracellular tumor microenvironment using CEST MRI and other imaging methods. Adv Radiol 2015; 2015; 206405.
2. Pollard AC, de la Cerda J, Schuler FW, Pollard TR, Aikaterini K, Pisaneschi FP, Pagel MD. Radiometal-based PET/MRI contrast agents for sensing tumor extracellular pH. Biosensors 2022; 12; 134.
3. Lowe MP, Parker D, Reany, Aime S, Botta M, Castellano G, Gianolio E, Pagliarin R. pH-dependent modulation of relaxivity and luminescence in macrocyclic gadolinium and europium complexes based on reversible intramolecular sulfonamide ligation. J Am Chem Soc 2001; 123; 7601-7609.
4. Lindeman LR, Randtke EA, High RA, Jones KM, Howison CM, Pagel MD. A comparison of exogenous and endogenous CEST MRI methods for evaluating *in vivo* pH. Magn Reson Med 2018; 79; 2766-2772.
5. Goldenberg JM, Cárdenas-Rodríguez J, Pagel MD. Preliminary results that assess metformin treatment in a preclinical model of pancreatic cancer using simultaneous [18F] FDG PET and acidoCEST MRI. Molec Imaging Biol 2018; 20; 575-583.

Declarations

Conflict of Interest
The authors declare no competing interests.

047- Skin Thickness of the Scalp in Multiple Sclerosis: Association with Linear Versus Macrocyclic Gadolinium-Based Contrast Agents Administration

Carlo Cosimo Quattrocchi[1,2], Marco Parillo[1,2], Federica Spani[1,2], Doriana Landi[1,2], Carlo Augusto Mallio[1,2]

[1]Fondazione Policlinico Universitario Campus Bio-Medico di Roma, Rome, Italy
[2]Fondazione Policlinico Tor Vergata, Rome, Italy

Background
Gadolinium-based contrast agents (GBCAs) are widely and repetitively used for diagnosis and monitoring of Multiple Sclerosis (MS). GBCAs are the source of minimum quantities of gadolinium that are retained and deposited into the brain and body tissues, including skin. The primary hypothesis is that patients with MS with normal renal function and history of multiple GBCAs administrations as well as the presence of dentate nuclei hyperintensity show detectable changes of skin thickness on clinical brain MRI scans. We also show skin histopathological data from one patient.

Methods and Materials
In this observational cross-sectional study, 71 patients with MS who underwent conventional brain MRI with an imaging protocol including enhanced 3D-Volumetric Interpolated Breath-hold examination (VIBE) T1-weighted with fat saturation were assessed. Patients with bilateral isointense dentate nucleus on unenhanced T1 weighted images were assigned to Group A (controls without MRI evidence of gadolinium deposition) and patients with visually hyperintense dentate nuclei were assigned to group B. Qualitative and quantitative assessment of the skin thickness were performed.

Results
Group A included 27 patients (median age, 33 years [IQR, 27–46]; 20 women) and Group B 44 patients (median age, 42 years [IQR, 35–53]; 29 women). Qualitative and quantitative assessment of the skin revealed significant differences between group A and group B. The average skin-to-scalp thickness ratios was significantly higher in group B than in group A (mean ± standard deviation = 0.52±0.02 in Group B vs. 0.41 ±0.02 in Group A, $p < 0.0001$) and showed a positive correlation with the total number of enhanced MRI scans ($r = 0.39$, 95% CI = 0.17–0.57, $p < 0.01$).

Conclusions
Brain MRI detects increased skin thickness of the scalp in patients with MS and dentate nucleus high signal intensity on enhanced T1-weighted images and shows positive association with previous exposures to linear GBCAs rather than macrocyclic GBCAs.

References
1. Quattrocchi CC, van der Molen AJ. Gadolinium Retention in the Body and Brain: Is It Time for an International Joint Research Effort? Radiology 2017; 282; 12-16.
2. Quattrocchi CC, Ramalho J, van der Molen AJ, Rovira À, Radbruch A. Standardized assessment of the signal intensity increase on unenhanced T1-weighted images in the brain: the European Gadolinium Retention Evaluation Consortium (GREC) Task Force position statement. European Radiology 2019; 29; 3959-3967.
3. Mallio CA, lo Vullo G, Messina L, Beomonte Zobel B, Parizel PM, Quattrocchi CC. Increased T1 Signal Intensity of the Anterior Pituitary Gland on Unenhanced Magnetic Resonance Images After Chronic Exposure to Gadodiamide. Investigative Radiology 2020; 55; 25-29.
4. Errante Y, Cirimele V, Mallio CA, Di Lazzaro V, Beomonte Zobel B, Quattrocchi CC. Progressive increase of T1 signal intensity of the dentate nucleus on unenhanced magnetic resonance images is associated with cumulative doses of intravenously administered gadodiamide in patients with normal renal function, suggesting dechelation. Investigative Radiology 2014; 49; 685-690.
5. Quattrocchi CC, Errante Y, Mallio CA, Marinelli L, Lo Vullo G, Giannotti G, Della Sala SW, van der Molen AJ, Beomonte Zobel B. Effect of Age on High T1 Signal Intensity of the Dentate Nucleus and Globus Pallidus in a Large Population Exposed to Gadodiamide. Investigative Radiology 2018; 53; 214-222.

Declarations

Conflict of Interest
The authors declare no competing interests.

048-Preparation and Characterizations of a Nanoplatform-Based MRI/OI Contrast Agent

Sarah Garifo[1], Dimitri Stanicki[1], Sébastien Boutry[2], Lionel Larbanoix[2], Indiana Ternad[1], Robert N. Muller[1,2], Sophie Laurent[1,2]

[1]University of Mons (UMONS), Mons, Belgium
[2]Center for Microscopy and Molecular Imaging (CMMI), Gosselies, Belgium

Background
The association of magnetic resonance imaging (MRI) with optical imaging (OI) presents several advantages in the preclinical imaging field owing to the high spatial resolution of the former and the high sensitivity of the latter. In this context, the objective of this project was to develop an efficient single MRI/OI probe by associating a gadolinium complex with a NIR-emitting compound within a nanoparticular matrix.

Methods and Materials
The preparation of the targeted systems required the following steps: (i) the development of paramagnetic silica nanoparticles (SiO2-Gd-NPs) by a one-pot reverse microemulsion process for the entrapment of a conventional Gd-complex (*i.e.*, Gd-HP-DO3A); (ii) The modification of the particle surface by PEG chains to ensure the colloidal stability; (iii) the demonstration of the covalent insertion of a carboxylic aryl diazirine photolinker on the outer coating corona; (iv) the grafting of fluorescent NIR-luminescent probes onto the carboxylated NPs using a classical EDC approach to obtain the desired fluorescent properties. At each step, spectroscopical techniques (UV, NMR,…) were used to validate the efficiency of different surface modifications.

Results
The confinement of Gd-complexes within SiO2-NPs resulted in a significant increase in longitudinal relaxivities (>500% at 20 MHz) in comparison with the free chelate, while the PEG-coating procedure has allowed a long-term stability in physiological conditions. In addition, the modification of the PEGylated-particles using a carboxylated diazirine linker by mean of photochemical treatment was considered for the easy post-derivatization with NIR-dye without affecting the colloidal stability. Preliminary imaging experiments complete this study.

Conclusions
Stable paramagnetic/fluorescent nanoparticles were successfully prepared and characterized. Preliminary biodistribution and elimination MRI/OI studies have been performed using this system and confirm the potential of the presented system for preclinical imaging experiments. In future development, the as-proposed system will be modified with biological vectors for molecular imaging applications.

Declarations

Conflict of Interest
The authors declare no competing interests.

049-Multimodality Detection and Treatment for Breast Cancer with a Biodegradable "One-For-All" Nanoparticle Contrast Agent

Jessica C. Hsu[1,2], Diego Barragan[1,2], Alex Tward[1,2], Maryam Hajfathalian[1,2], Yuxi C. Dong[1,2], Emma D. Cruz[1,2], Alexander Andrianov[1,2], Andrew D. A. Maidment[1,2], David P. Cormode[1,2]

[1]University of Pennsylvania, Philadelphia, USA
[2]Institute for Bioscience and Biotechnology Research, University of Maryland, Rockville, MD, USA

Background
Current screening and treatment standards for breast cancer may result in delayed diagnosis and incomplete tumor eradication, worsening the disease outcome and chance of survival. Herein, we synthesized ultrasmall, fluorescent silver sulfide nanoparticles (Ag2S-NP) for efficient renal clearance1 and encapsulated them in larger, biodegradable polymeric nanoparticles (AgPCPP) for improved tumor accumulation (A). AgPCPP have potent contrast properties for preoperative x-ray (DEM and CT)2 and optical (PA and NIRF) based detection modalities, as well as intraoperative NIRF image-guided surgical techniques (FLARE). Their remarkable photothermal conversion activity is suitable for postoperative anticancer therapy via localized thermal ablation. Importantly, we found that AgPCPP, or aggregated forms of Ag2S-NP, increased the absorption of NIR light, producing enhanced PA/NIRF signals and photothermal heating effects. Thus, we present a "one-for-all" theranostic agent that is multifunctional and gradually degrades into small components for swift elimination from the body.

Methods and Materials
AgPCPP were formed by encapsulating hydrophilic 2 nm Ag2S-NP in PCPP polymers with 10% PEGylated PCPP copolymers. The nanoparticles were characterized using TEM, fluorimetry, DLS, and SEM/EDX. Contrast production was evaluated via phantom imaging using clinical DEM and CT, as well as preclinical PA (VisualSonics), NIRF (IVIS Spectrum), and FLARE (Curadel) imaging systems. *In vitro* biocompatibility were examined using Renca, HepG2, and MDA-MB-231 cells. *In vitro* photothermal effects were investigated using an 808 nm laser. *In vivo* imaging, photothermal therapy, and biodistribution studies were performed in a murine model of breast cancer.

Results
The size of AgPCPP could be varied between 40-300 nm by adjusting the amount of PEG-PCPP copolymers used in the synthesis (B). For this study, we used AgPCPP formulation with an average core diameter of 95 nm. We found that both

Ag2S-NP and AgPCPP are biocompatible with all cell types. We also found that approximately 90% of Ag2S-NP payload was released within 7 days, indicating the biodegradability of AgPCPP. While Ag2S-NP and AgPCPP provide similar x-ray contrast, AgPCPP generate higher PA and NIRF signals (C,D) as well as greater photothermal killing compared to free Ag2S-NP due to increased NIR absorbance from aggregation induced red shift.3 Moreover, AgPCPP enhanced the tumor contrast as evidenced by *in vivo* NIRF imaging (E). AgPCPP further elevate tumor hyperthermia and reduce tumor growth post photothermal treatment (F). Biodistribution results indicate that more AgPCPP are found in the tumors than Ag2S-NP, suggesting that larger size is beneficial for increasing tumor accumulation.

Conclusions

AgPCPP possess more favorable optical properties than free Ag2S-NP. AgPCPP can fulfill diagnostic, surgical, and therapeutic tasks before gradually breaking down and releasing Ag2S-NP for renal excretion, thus providing good prospects for translation to clinical use.

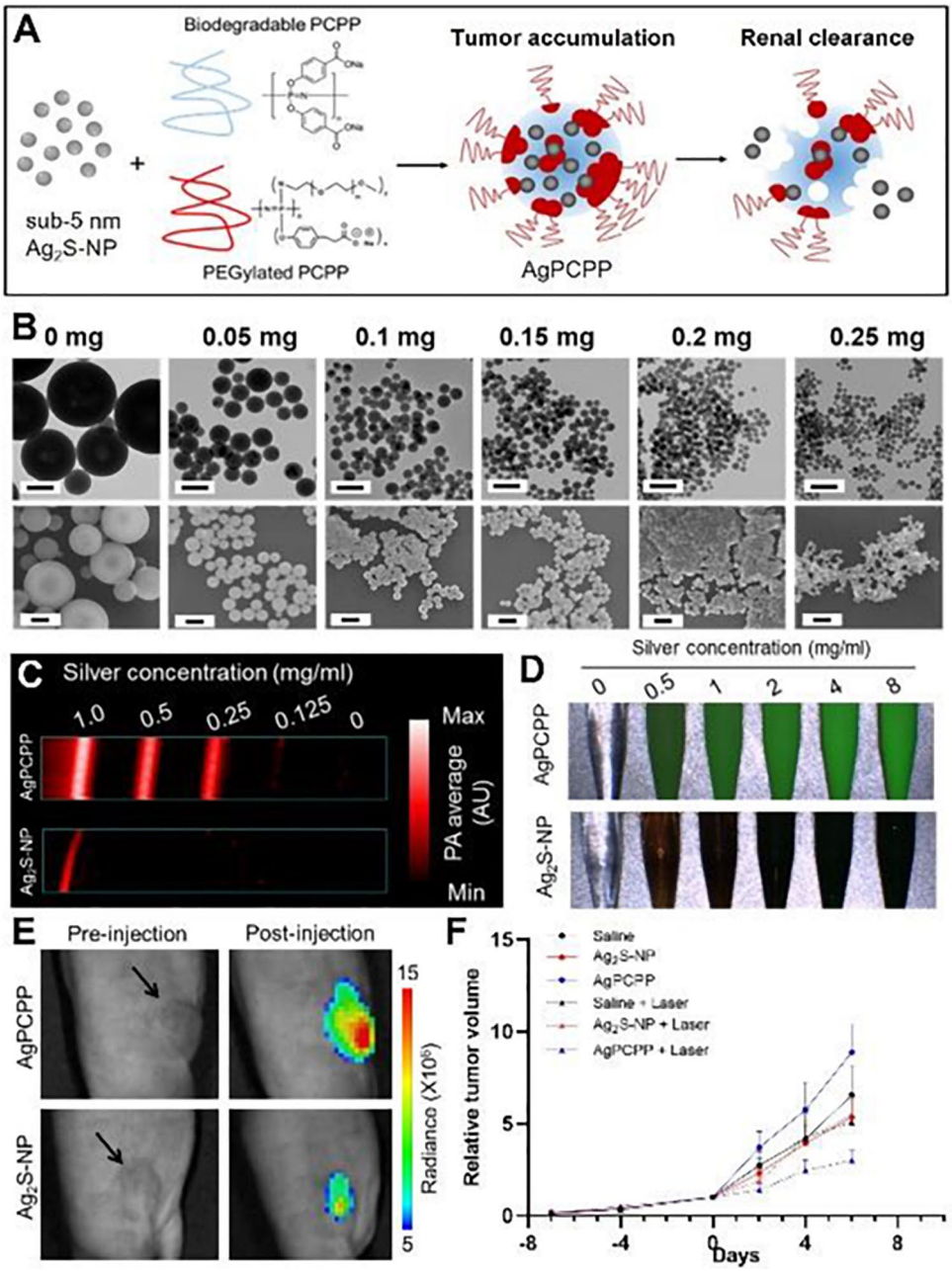

Figure caption: A) Schematic of AgPCPP synthesis. B) TEM and SEM of AgPCPP with varying amount of PEG-PCPP. C) Phantom imaging with PA. D) Phantom imaging with FLARE. E) Tumor imaging with IVIS Spectrum. F) Tumor growth after laser irradiation and nanoparticle treatment

References

1. Hsu JC, Cruz ED, Lau KC, Bouché M, Kim J, Maidment ADA, Cormode DP. Renally excretable and size-tunable silver sulfide nanoparticles for dual energy mammography or computed tomography. Chemistry of Materials. 2019. 31(19): 7845-7854.
2. Naha, P. C.; Lau, K. C.; Hsu, J., C.; Hajfathalian, M.; Mian, S.; Chhour, P.; Uppulari, L.; MacDonald, E. S.; Maidment, A. D. A.; Cormode, D. P. Gold silver alloy nanoparticles (GSAN): an imaging probe for breast cancer screening with dual-energy mammography or computed tomography. Nanoscale. 2016, 8, 13740-13754.
3. Cheheltani R, Ezzibdeh RM, Chhour P, Chandrika K, Jurcova M, Hsu JC, Blundell C, Litt HI, Ferrari VA, Allcock HA, Sehgal CM, Cormode DP. Tunable, biodegradable gold nanoparticles as contrast agents for computed tomography and photoacoustic imaging. Biomaterials. 2016. 102: 87-97.

Declarations

Conflict of Interest

The authors Andrew Maidment and David Cormode hold intellectual property on the agents discussed, and own stock in Daimroc Imaging, a company seeking to commercialize these agents. The other authors disclosed no financial interest.

050-Multinuclear Fe(III) Complexes as MRI Contrast Agents

Janet R. Morrow[1], Didar Asik[1], Greg Sokolow[1], Timothy R. Cook[1], Joseph A. Spernyak[2]

[1]University at Buffalo State University of New York, Amherst, NY, USA
[2]Roswell Park Comprehensive Cancer Center, Buffalo, NY, USA

Background

Transition metal-based MRI contrast agents or probes are under development as alternatives to gadolinium-based contrast agents (1). The use of iron may be advantageous given that it is the most abundant transition metal ion in the body, yet Fe(III) MRI probes have certain challenges to their development as T1 MRI contrast agents, including spin and oxidation state control and modulating water interactions for optimal proton relaxivity (2). Moreover, to produce probes that have more effective proton relaxivity, complexes with two or more metal ions are desirable. The linker connecting the two iron centers should be very rigid to increase rotational correlation times. To address these challenges, two different classes of Fe(III) coordination complexes will be presented.

Methods and Materials

Ligands and Fe(III) complexes were synthesized and characterized by NMR spectroscopy, mass spectrometry, magnetic susceptibility, pH potentiometric titrations, electrochemistry, and proton r1 and r2 relaxivity measurements over a range of field strengths including 1.4, 4.7, and 9.4 T. Complexes were injected into the tail vein of BALB/c mice at 25 μmol/kg or 50 μmol/kg for MRI studies on a Bruker preclinical 4.7 T MRI using a T1-weighted, 3D, spoiled-gradient echo scan. Both healthy mice and mice with subcutaneous ID8 ovarian cancer tumors were studied.

Results

Dinuclear Fe(III) complexes of 1,4,7-triazacyclononane with pendant hydroxypropyl groups show promising r1 proton relaxivity (r1 = 5.3 mM-1s-1 at 4.7 T, 37 °C) and also show enhanced contrast in mice.(3) This class of probe increases water proton relaxation largely through second-sphere water interactions as shown by variable temperature 17-O NMR studies. A second class of complexes has multiple Fe(III) centers deriving from a self-assembly approach by using catechol donors and aromatic linkers to form helical or tetrahedral shapes. Tetrahedral cages have four Fe(III) and no bound waters yet are effective proton relaxation agents (r1 = 8.7 mM-1s-1 or 21 mM-1s-1 with and without serum albumin, respectively). (4) Dinuclear self-assembled Fe(III) complexes show effective proton relaxation and contrast enhancement in mice. The Fe(III) MRI probes give distinct biodistribution and clearance kinetics depending on lipophilicity serum albumin binding strength.

Conclusions

Fe(III) centers can be linked together to produce new types of MRI probes. Complexes can be synthetically modified to give different classes of contrast agent including extracellular fluid and blood pool agents. Hydroxypropyl groups are effective for increasing proton relaxivity through second-sphere interactions and for controlling solution chemistry. Self-assembled Fe(III) agents have rigid connections that produce robust MRI probes with good relaxivity and tumor accumulation properties.

References
1. Gupta, A.; Caravan, P.; Price, W. S.; Platas-Iglesias, C.; Gale, E. M., Applications for transition-metal chemistry in contrast-enhanced magnetic resonance imaging. Inorg Chem 2020; 59; 6648-6678.
2. Kras, E. A.; Snyder, E. M.; Sokolow, G. E.; Morrow, J. R., The Distinct Coordination Chemistry of Fe(III)-based MRI Probes. Acc. Chem. Res. 2022: 55; in press.
3. Asik, D.; Abozeid, S. M.; Turowski, S. G.; Spernyak, J. A.; Morrow, J. R., Dinuclear Fe(III) Hydroxypropyl-Appended Macrocyclic Complexes as MRI Probes. Inorg Chem 2021; 60; 8651-8664.
4. Sokolow, G. E.; Crawley, M. R.; Morphet, D. R.; Asik, D.; Spernyak, J. A.; McGray, A. J. R.; Cook, T. R.; Morrow, J. R., Metal-Organic Polyhedron with Four Fe(III) Centers Producing Enhanced T1 Magnetic Resonance Imaging Contrast in Tumors. Inorg Chem 2022; 61; 2603-2611.

Declarations

Conflict of Interest
Janet Morrow has disclosed a financial interest in this abstract. The other authors have disclosed no financial interest.

051- VascuViz – a Multimodality and Multiscale Imaging Pipeline for Vascular Systems Biology

Akanksha Bhargava, Benjamin Monteagudo, Priyanka Kushwaha, Janaka Senarathna, Yunke Ren, Ryan C. Riddle, Manisha Aggarwal, Arvind P. Pathak
The Johns Hopkins University School of Medicine, Baltimore MD, USA

Background
Preclinical imaging has been instrumental in advancing our understanding of the role of vasculature in health and disease 1. However, integrating data on the vascular microenvironment (VME) across modalities and spatial scales for "image-based" systems biology applications remains a challenge 2 due to the lack of vascular contrast and the need to re-label the sample for each imaging technique. Therefore, we developed a multimodality contrast workflow 3 that achieves data integration and results in the generation of "vascular atlases" for systems and computational biology applications 4. We present prototype "vascular atlas" in a breast cancer model using multiscale data from MRI, CT, and optical microscopy.

Methods and Materials
We prepared a mixture 2 of radio-opaque BriteVu® with Galbumin^{TM}-Rhodamine contrast agent which is visible in MRI and optical imaging. MDA-MB-231 human breast cancer xenograft-bearing mice were perfused transcardially 2. Next, tissues were excised and imaged on a 9.4T MRI scanner using T1-weighted (T1W) and diffusion weighted (DW)5 MRI at 50 μm. Next, CT imaging was performed at 9 μm 2. Finally, the same sample was imaged using multiphoton microscopy (MPM) and second harmonic generation (SHG) imaging 2. Fractional anisotropy (FA) and apparent diffusion coefficient (ADC) maps were computed using DTIStudio 2. Vessel segmentation, image co-registration, and data visualization were performed 2 with Amira®.

Results
Our novel vascular contrast agent combination successfully enabled us to visualize the vasculature in *ex vivo* MRI, CT, and MPM images of the tumor xenograft and other organs. Moreover, it enabled creation of a multiscale "cancer atlas" facilitating integration and correlative analyses of MRI data with complementary contrasts from CT and optical imaging. This included soft tissue contrast from T1w-MRI (Fig. 1a), DW-MRI based 3D FA (Fig. 1b) and ADC maps (Fig. 1c), collagen (col) fiber maps from SHG imaging and green fluorescent protein (GFP) expression in cancer cells from MPM (Fig. 1d, g, h). Our co-registered SHG vs. FA data (Fig. i, k, m, o) indicated an overlap of high FA with high col fiber density (white contours). Similarly, co-registered GFP expression vs. ADC data (Fig. 1j, l, n, p) indicated overlap of necrotic regions with those exhibiting elevated ADC values (pink contours).

Conclusions
We successfully developed a novel multimodality contrast workflow and demonstrated its utility for integrating multiscale data in a breast cancer model from the cellular to whole-tumor spatial scales. We expect this vasculature-predicated approach to enable novel "image-based" systems biology applications in other preclinical disease models and healthy tissues.

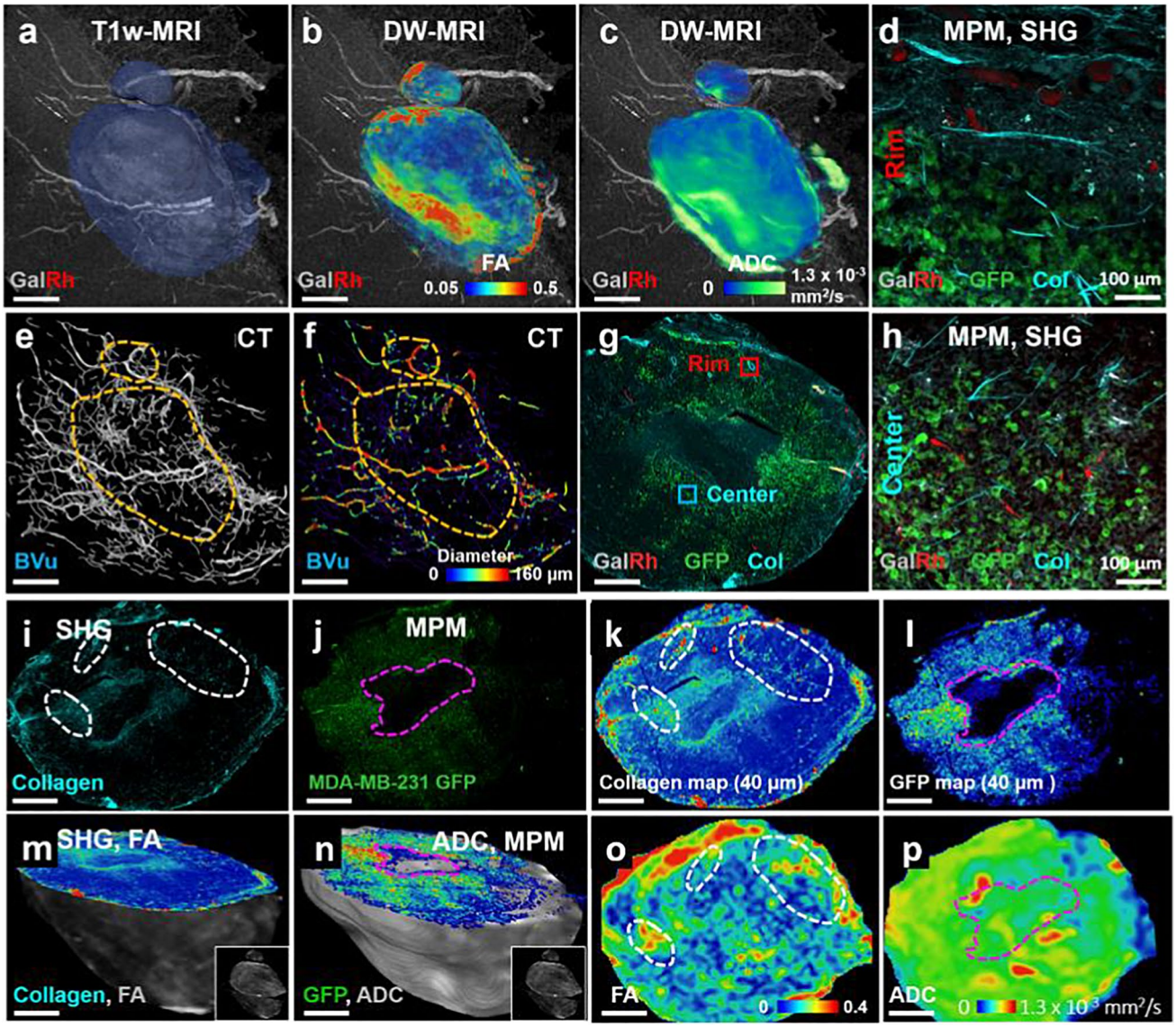

Figure caption: Creation of a multimodality, multiscale "cancer atlas"

References

1. McDonald DM and Choyke PL. Imaging of angiogenesis: from microscope to clinic. Nat Med 2003; 9; 713-725.
2. Kim E, Stamatelos S, Cebulla J, Bhujwalla ZM, Popel AS and Pathak AP. Multiscale Imaging and Computational Modeling of Blood Flow in the Tumor Vasculature. Ann Biomed Eng 2012; 40; 2425-2441.
3. Bhargava A, Monteagudo B, Kushwaha P, Senarathna J, Ren Y, Riddle RC, Aggarwal and Pathak AP. VascuViz: a multi-modality and multiscale imaging and visualization pipeline for vascular systems biology. Nat Methods 2022; 19; 242-254.
4. Stamatelos SK, Bhargava A, Kim E, Popel AS and Pathak AP. Tumor Ensemble-Based Modeling and Visualization of Emergent Angiogenic Heterogeneity in Breast Cancer. Sci Rep (2019); 9.
5. Aggarwal M, Mori S, Shimogori T, Blackshaw S and Zhang J. Three-dimensional diffusion tensor microimaging for anatomical characterization of the mouse brain. Magn Reson Med 2010; 64; 249-261.

Declarations

Conflict of Interest

The authors declare no competing interests.

052-MPI/CT Imaging of Stem Cell-Mediated Tumor Delivery of a Bimodal Superparamagnetic and Radiopaque Nanocomplex

Chao Wang[1,2], Ali Shakeri-Zadeh[1,2], Behnaz Ghaemi[1,2], Jeff W.M. Bulte[1,2*]

[1]Division of MR Research, Baltimore, MD, USA
[2]Institute for Cell Engineering, Baltimore, MD, USA

Background

Passive and active targeting of therapeutic nanoparticles (NPs) toward cancer cells have not been entirely efficient and efforts are being made to establish an effective targeting method for uniform distribution of the NPs within the tumor. The use of stem cells that have native trophic properties for homing to tumors has been proposed as a new approach for NP delivery to cancer cells (1, 2). It would be desirable to monitor the homing and intratumoral distribution of injected cells as well as off-target site biodistribution in the rest of the body. *In vivo* hybrid imaging has potential to meet this demand (3, 4). Here, we aimed to develop a bimodal cell tracking method using a novel superparamagnetic radiopaque nanocomplex that can be detected with magnetic particle imaging (MPI) and computed tomography (CT).

Methods and Materials

Through a step-by-step solvothermal decomposition method, a BBS nanocomplex composed of bovine serum albumin (BSA), radiopaque Bi2S3 nanoparticles and superparamagnetic iron oxide (SPIO) was fabricated. BBS nanocomplexes were characterized with different techniques. Human mesenchymal stem cells were labeled with poly-L-lysine as transfection agent and the BBS nanocomplexes for 24 h. Naked BBS or BBS-labeled hMSCs were injected intratumorally (i.t.) or intravenously (i.v.) in DU145 (human prostate cancer)-bearing mice. Thirty minutes and 48 h after injection, mice were imaged with MPI and CT. Two days after i.t. injection or 4 days after i.v. injection, mice were sacrificed and tumors were excised for *ex vivo* imaging.

Results

BBS nanocomplexes showed a spherical morphology with even distribution of bismuth, iron and sulfur across the spheres (size: 90 nm). *In vivo* MPI/CT images of mice receiving naked BBS nanocomplexes or BBS-hMSCs after i.t. injection are shown in Fig. 1A. I.t. injection of BBS-hMSCs demonstrated that labeled cells moved throughout the entire tumor while naked BBS nanocomplexes remaining as a focal point near the injection site. For i.v. injection, we observed homeing of cells to the lung 2 h after injection and in the liver 24 h later (Fig. 1B). No signal could be observed in the tumor for i.v. injection. *Ex vivo* imaging showed the highest amount of MPI signal intensity was obtained for i.t. injection of BBS-hMSCs (Fig. 1C).

Conclusions

We demonstrated the possibility of *in vivo* bimodal imaging of naked BBS and BBS-labeled hMSCs using CT and MPI. We are now developing protocols for MPI/CT-guided hyperthermal therapy using stem cell delivery of BBS nanocomplexes.

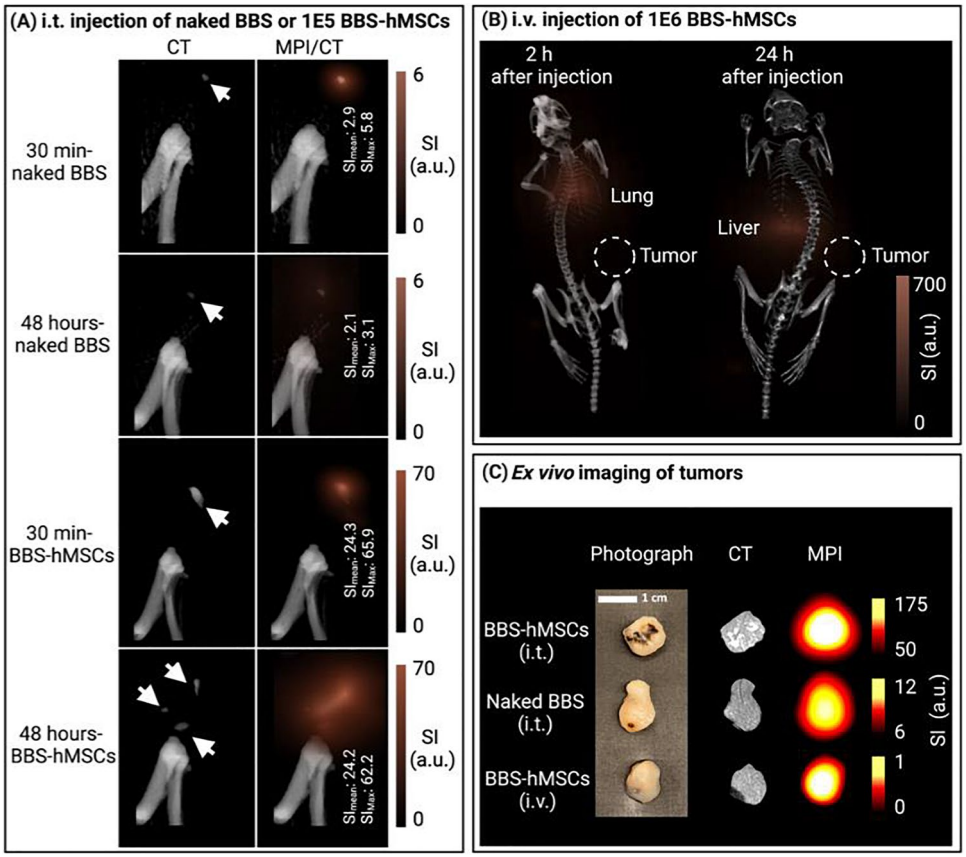

Fig. 1 *In vivo/ex vivo* MPI/CT data of DU145 human prostate tumor bearing mice at different time points after i.t. or i.v. injection of naked BBS or BBS-labeled hMSCs

References

1. Su Y, et al. Current advances and challenges of mesenchymal stem cells-based drug delivery system and their improvements. Int. J. Pharm. 2021; 600; 120477.
2. Cheng, S, Nethi, SK, Rathi, S, Layek, B & Prabha, S. Engineered mesenchymal stem cells for targeting solid tumors: therapeutic potential beyond regenerative therapy. J. Pharmacol. Exp. Ther. 2019; 370; 231.
3. Srivastava AK, et al. Seeing stem cells at work *in vivo*. Stem Cell Rev. Rep. 2014; 10; 127.
4. Bulte JWM, Superparamagnetic iron oxides as MPI tracers: A primer and review of early applications. Adv. Drug Deliv. Rev. 2019; 138; 293.

Declarations

Conflict of Interest

The author Jeff W. M. Bulte is a paid consultant for SuperBranche, which has been approved by JHU. The other authors disclosed no financial interest.

053- 4Iphf-d-HN17: a Novel Hybrid Small Molecule-Cell-Penetrating Peptide in HNSCC

Michael Tweedle[1,2], Shankaran Kothandaraman[2], Stacey Meeker[4], Reena Shakya[3], Reyjung Na[3], Li Gong[2], Arijit Ghosh[2], Adam Pippin[2], Krishan Kumar[2]

[1]CellSeek LLC, Columbus, OH, USA
[2]Wright Center of Innovation in Biomedical Imaging, The Ohio State University, Columbus, OH, USA

[3]Target Validation Services Resource, The Ohio State University, Columbus, OH, USA
[4]College of Veterinary Medicine, The Ohio State University, Columbus, OH, USA

Background
The first promising HNSCC (head and neck squamous cell carcinoma) targeted peptide, HN1, was discovered by phage display but was hampered by a slow (24 h) internalization process (1). HN1 has been labeled a cell-penetrating peptide (CPP) in literature due to its ability to internalize dye- and drug-conjugates into cell cytosol. 4lphf-l-HN17 (4Iph)(f) LPNSNHIKQGL (f=fmoc; 4Iph=4-iodophenyl) was developed to overcome the slow kinetics of HN1. d- and l- isomers of 4Iphf-HN17 were compared in both diagnostic and therapy in CDX (cell xenograft) and PDX (patient derived xenograft) mice models of HNSCC to assess efficacy and test the hypothesis that 4Iphf-HN17 molecules conformed to a specific class of CPP. Toxicity was also determined in normal mice.

Methods and Materials
Syntheses and chemical characterizations of d- and l-isomers of HN17 and conjugates used published methods (2). Cell experiments used CAL-27(HPV-), SCC-47(HPV+) cells from ATCC and Univ. Mich., respectively. Confocal microscopy was performed with Cy5 labeled peptides and animal tumor fluorescence optical imaging was performed after IV or IP administration of an S0456 conjugate emitting at 800 nm, using a Fluobeam imager. A human PDX (patient derived xenograft) model was created from a breeder mouse from Jackson Laboratories implanted with a live human HNSCC tissue, and extended in ASG mice. Toxicity was assessed in mice bearing no tumors. Cell tolerance IC50 of 4IphF-HN17 and cisplatin and in combination were assessed by MTT assay, and the studies were extended into PDX mice.

Results
Dye-labeled 4lphf-l-HN17 has 26 fold more Cal-27 cell uptake than dye-labeled HN1 in 1h, and has very rapid (visible in 5 min at 5 uM) cytosolic presence observed by confocal microscopy. It also maintains rapid uptake in live Cal-27 cells in the presence of endocytosis inhibitors, suggesting a complex uptake /internalization mechanism. In attempting to eliminate specific protein binding as a mechanism for internalization we synthesized 4Iphf-d-HN17 and studied uptake, internalization, IC50 cell killing, optical imaging, and therapeutic efficacy and toxicity. The d isomer of the dye conjugate showed faster cell uptake and brighter mice tumors in optical fluorescent imaging, but also little accumulation in cytosol microscopically compared to the l isomer. The l-isomer (not dye- nor drug-conjugated) also significantly potentiated cisplatin cell killing (>5 fold in IC50) and demonstrated pronounced potentiation of cisplatin tumor growth inhibition over 6 weeks in PDF mice, while the d isomer showed neither therapeutic effect.

Conclusions
Results are consistent with an unusual two-stage uptake mechanism where the first step, accumulation in the cell corona, is not observably isomer specific, like most CPP, while the second step, membrane penetration, shows preferential uptake of the l-isomer, probably through endocytosis, the finer details of which will require more extensive control experiments 3.

References
1. Hong FD, Clayman GL. Isolation of a peptide for targeted drug delivery into human head and neck solid tumors. Cancer Res. 2000, 60:6551-6.
2. Ding H, Kothandaraman S, Gong L, Wright C, Pan Q, Teknos T, Tweedle MF, Novel Peptide NIRF Optical Surgical Navigation Agents for HNSCC. Molecules 2019, 24. 10.3390/molecules24173070
3. Verduram WPR, Bovee-Geurts PH, Wadhwani P, Ulrich AS, Hallbrink M, KuppeveltTHV, Brock R, Preferential Uptake of L- versus D-Amino. Acid Cell-Penetrating Peptides in a Cell Type-dependent Manner. Chemistry & Biology 2011, 18:1000-1010.

Declarations

Conflict of Interest
The authors declare no competing interests.

054-Preclinical Profile of Gadoquatrane: a Novel Tetrameric, High Relaxivity, Macrocyclic Gadolinium-Based Contrast Agent for CE-MRI

Jessica Lohrke, Gregor Jost, Thomas Frenzel, Hubertus Pietsch

MR and CT Contrast Media Research, Bayer AG, Berlin, Germany

Background
The novel tetrameric, macrocyclic gadolinium (Gd)-based contrast agent (GBCA) gadoquatrane (BAY 1747846) features high stability and high relaxivity, a key property for use in contrast-enhanced MR-imaging. The present work investigates key physico-chemical characteristics and MR-Imaging features of the new Gd-chelate.

Methods and Materials

The complex stability was tested for Gd release in human plasma over 21 days. The T1-relaxivities in water and human plasma were measured at different field strengths (up to 4.7T). A 4D MR-angiography (MRA TWIST) study was performed with a clinical 1.5T scanner in healthy Goettingen minipigs. Two different doses of gadoquatrane (0.025 and 0.03 mmol Gd/kg) were compared to the standard dose (0.1 mmol Gd/kg) of gadoterate meglumine and gadobutrol.

Results

The tetrameric gadoquatrane showed high kinetic inertness and no Gd release over 21 days in human plasma under physiological conditions. Compared to clinically available GBCAs, highly pronounced T1-relaxivities were observed in water and human plasma at field strengths used in clinical practice (r1: 47.2 mM-1·s-1 per molecule corresponding to 11.8 mM-1·s-1 per Gd at 1.41T in human plasma1). In the 4D-MRA study similar signal enhancement profiles were observed for gadoquatrane at approximately 70% reduced Gd dose compared to the standard dose of marketed macrocyclic GBCAs (gadoterate meglumine and gadobutrol).

Conclusions

The novel tetrameric Gd-chelate combines high stability and high relaxivity. The high relaxivity of gadoquatrane offers the opportunity of a substantially lower Gd dose, while reaching the same MR signal enhancement compared to the marketed GBCAs gadoterate meglumine and gadobutrol at a standard dose.

References

1. Lohrke J , Berger B, Frenzel T, Hilger CS, Jost G, Panknin O, Bauser M, Ebert W, Pietsch H. Preclinical Profile of Gadoquatrane: A Novel Tetrameric, Macrocyclic High Relaxivity Gadolinium-Based Contrast Agent. Invest Radiol 2022, online ahead of print.

Declarations

Conflict of Interest

All authors are employees of Bayer AG, Berlin, Germany.